Treatment of epistemic uncertainty in conjunction analysis with Dempster-Shafer theory

Luis Sánchez [a], Massimiliano Vasile [a,*], Silvia Sanvido [b], Klaus Merz [c], Christophe Taillan [d]

[a] *Aerospace Centre of Excellence, University of Strathclyde, Glasgow, United Kingdom*
[b] *IMS Space Consultancy GmbH, Darmstadt, Germany*
[c] *Space Debris Office, ESA/ESOC, Darmstadt, Germany*
[d] *Space Security, Safety and Sustainability Office, CNES, Toulouse, France*

Abstract

The paper presents an approach to the modelling of epistemic uncertainty in Conjunction Data Messages (CDM) and the classification of conjunction events according to the confidence in the probability of collision. The approach proposed in this paper is based on Dempster-Shafer Theory (DSt) of evidence and starts from the assumption that the observed CDMs are drawn from a family of unknown distributions. The Dvoretzky–Kiefer–Wolfowitz (DKW) inequality is used to construct robust bounds on such a family of unknown distributions starting from a time series of CDMs. A DSt structure is then derived from the probability boxes constructed with DKW inequality. The DSt structure encapsulates the uncertainty in the CDMs at every point along the time series and allows the computation of the belief and plausibility in the realisation of a given probability of collision. The methodology proposed in this paper is tested on a number of real events and compared against existing practices in the European and French Space Agencies. We will show that the classification system proposed in this paper is more conservative than the approach taken by the European Space Agency but provides an added quantification of uncertainty in the probability of collision.

1. Introduction

The close encounter of two space objects, also known as a conjunction between a chaser and a target, can lead to a collision if the relative position of the two objects is not properly controlled. The Probability of Collision (PoC) to happen depends on the probability that each of the two objects occupies a given position in space. This probability can be derived from the knowledge of the orbit of the two objects and the associated uncertainty.

It is customary to assume that the distribution of possible positions of the two objects at the time of closest encounter follows a multivariate Gaussian with a given mean and covariance matrix, see Merz et al. (2017, 2019). This assumption is limited by three sources of uncertainty: the uncertainty in the dynamic model used to propagate the orbit from the last available observation to the time of closest approach, the uncertainty in the actual distribution at the time of closest approach, and the uncertainty in the last observed state before closest approach. We argue that all three forms of uncertainty are epistemic in nature since

* Corresponding author at: James Weir Building, 75 Montrose St., G1 1XJ, Glasgow, United Kingdom.
E-mail address: massimiliano.vasile@strah.ac.uk (M. Vasile).

Nomenclature

AI	Artificial Intelligence
Bel	Belief
bpa	basic probability assignment
CAM	Collision Avoidance Manoeuvre
CARA	Conjunction Assessment Risk Analysis
CDF	Cumulative Distribution Function
CDM	Conjunction Data Message
CNES	Centre National d'Etudes Spatiales
DKW	Dvoretzky–Kiefer–Wolfowitz
DoU	Degree of Uncertainty
DSt	Dempster-Shafer theory of evidence
eCDF	empirical Cumulative Distribution Function
ESA	European Space Agency
ESOC	European Space Operations Centre
FE	Focal Element
FN	False Negative
FP	False Positive
FPR	False Positive Rate
HBR	Hard-Body Radius
IDSS	Intelligent Decision Support System
JAC	Java for Assessment of Conjunctions
KS	Kolmogorov–Smirnov
LEO	Low Earth Orbit
ML	Machine Learning
mWSM	modified Weighted Sum Method
Pl	Plausibility
PoC	Probability of Collision
ROC	Receiver Operating Characteristic
SEM	Space Environment Management
SDO	Space Debris Office
sPoC	scaled Probability of Collision
STM	Space Traffic Management
TCA	Time of Closest Approach
TN	True Negative
TOPSIS	Technique for Order of Preference by Similarity to Ideal Solution
TP	True Positive
TPR	True Positive Rate
WPM	Weighted Product Method
WSM	Weighted Sum Method

they derive from a lack of knowledge of the model, distribution and error in the observations.

The information on a given close encounter is generally available in the form of a Conjunction Data Message (CDM), which contains the means and covariances of the two objects at Time of Closest Approach (TCA), see CCSDS (2013). Thus, in this paper, we start from the assumption that the mean and covariance in each CDM are affected by epistemic uncertainty, which is reflected in an uncertainty in the correct value of the PoC.

The general attempt to compensate for the uncertainty in the CDMs is to improve the realism of the covariance matrix by improving its propagation, Aristoff et al. (2014), or by some form of updating of the dynamic model, Cano et al. (2023). These approaches are all very valuable but require direct access to the post-observation data. Other methods based solely on the available CDMs tried to predict the next CDMs using machine learning starting from an available time series, see Pinto et al. (2020, 2021, 2022, 2023), or increased the last covariance under the assumption that the series of CDMs should follow a given distribution, Laporte (2014a,b). This last approach does not modify the mean value or miss distance.

So far, only a limited number of authors have directly addressed epistemic uncertainty in conjunction analysis, see for example Tardioli and Vasile (2015, 2018, 2019, 2021). In Sánchez and Vasile (2021, 2022,) the authors proposed a robust approach to conjunction analysis and collision avoidance planning based on Dempster-Shafer theory of evidence (DSt). DSt allows making decisions informed by the degree of confidence in the correctness of a value

rather then by the value itself, Helton et al. (2005). However, the available information to build the frame of discernment that is needed in DSt is often limited in a sequence of CDMs. CDMs contain little information on the three forms of uncertainty listed above and essentially only provide covariance and mean value of the miss distance. Thus, one key question is how to translate the time series of CDMs into the frame of discernment used in DSt. The underlying assumption in this work is that the CDMs are observables drawn from an unknown family of distributions defined within some bounds. In fact the actual distribution of possible states at time of closest approach is not known and the CDMs can be considered to contain only an approximation of the first two statistical moments of that unknown distribution. The actual distribution depends on the uncertainty in the propagation model, in the observations and orbit determination process. However, that uncertainty, which is epistemic in nature, can only by quantified by observing the time series of CDMs. Furthermore, we assumed that the CDMs computed from observations acquired close to the TCA were less affected by model and distribution uncertainty. This is reasonable as the propagation time is shorter and thus both nonlinearities and model errors have a lower impact on the propagation of the distribution of the possible states.

The paper introduces a methodology, based on the Dvoretzky–Kiefer–Wolfowitz (DKW) inequality, Dvoretzky et al. (1956), to derive a DSt structure capturing the epistemic uncertainty in a given sequence of CDMs. From the DSt structures, one can compute the Belief (*Bel*) and Plausibility (*Pl*) that the value of the PoC is

correct and an upper and lower bound on its value. The paper then proposes a classification system that exploits the use of *Bel* and *Pl* to differentiate between events that are uncertain from events that can lead to a collision. The overall methodology is tested on a number of real conjunction scenarios with known sequences of CDMs and compared against current practices in the European Space Agency (ESA) and Centre National d'Etudes Spatiales (CNES).

The rest of the paper is structured as follows. Section 2 briefly introduces a methodology previously presented by the authors to deal with epistemic uncertainty for risk assessment in space encounters. Section 3 extends this methodology to deal with a sequence of CDMs. In Section 4, some numerical cases are presented showing the operation of the proposed method and comparing the approach with the procedure followed by real operators. Finally, Section 5 concludes the paper with the final remarks and future work.

2. Conjunction analysis with Dempster-Shafer structures

This section briefly introduces the basic idea of DSt applied to Conjunction Assessment Risk Analysis (CARA). It also includes the DSt-based conjunction classification system already introduced by the authors in previous works. More details on DSt can be found in Shafer (1976), and more details on its application to space conjunction assessment can be found in Sánchez and Vasile (2021, 2022,).

In this paper, we consider only fast encounters between two objects: object 1 and object 2. Under the typical modelling assumptions of fast encounters, see Serra et al. (2016), the PoC can be defined as:

$$PoC = \frac{1}{2\pi\sqrt{\|\Sigma\|}} \int_{\mathscr{B}((0,0),R)} e^{-\frac{1}{2}\left((\mathbf{b}-\boldsymbol{\mu})^T \Sigma^{-1} (\mathbf{b}-\boldsymbol{\mu})\right)} d\xi d\zeta \quad (1)$$

where, without loss of generality, object 2 is at the centre of the coordinate system of the impact plane at the time of closest approach (TCA), $\mathbf{b} = [\xi, \zeta]^T$ is the position vector of object 1 with respect to object 2 projected onto the impact plane, Σ is the 2×2 combined covariance matrix of the position of the two objects in the impact plane ($\Sigma = \Sigma_1 + \Sigma_2$, with Σ_1 and Σ_2 the individual covariance matrices of object 1 and 2 respectively) and $\boldsymbol{\mu} = [\mu_\xi, \mu_\zeta]^T$ is the expected position vector of object 1 with respect to object 2 projected onto the impact plane. In the remainder of the paper $\boldsymbol{\mu}$ is called miss distance. The integration region $\mathscr{B}((0,0),R)$, or Hard-Body Radius (HBR), is a disk with radius R centred at the origin of the impact plane.

When the covariance Σ and miss distance $\boldsymbol{\mu}$ are not precisely known the PoC is affected by a degree of uncertainty. This lack of knowledge translates into an epistemic uncertainty in the exact value of Σ and $\boldsymbol{\mu}$. The epistemic uncertainty in covariance Σ and miss distance $\boldsymbol{\mu}$ can come from incertitude in the sources of information, from poor knowledge of the measurements or propagation model or

from an approximation of the actual distribution on the impact plane at TCA. As shown in Sánchez and Vasile (2021) and Sánchez and Vasile (2022), this epistemic uncertainty can be modelled with DSt.

The idea proposed in Sánchez and Vasile (2021), was to use DSt to compute the level of confidence in the correctness of the value of the PoC, given the available evidence on the sources of information. Each component of the combined covariance matrix in the impact plane, $[\sigma_\xi^2, \sigma_\zeta^2, \sigma_{\xi\zeta}]$, was modelled with one or more intervals and so was the miss distance $[\mu_\xi, \mu_\zeta]$. A basic probability assignment (*bpa*) was then associated with each interval. The intervals and the associated *bpa* can be derived, for example, directly from the raw observations, Greco et al. (2021,), or from a time series of CDMs, CCSDS (2013), as explained later in this paper. Note that in the case in which raw observation data are available, one could directly compute the confidence on the miss distance, see Greco et al. (2021). However, in the following we will consider the CDMs as the observable quantities and the PoC, computed from the CDMs, to be the quantity of interest.

Given the intervals and associated *bpa*, one can compute the cross-product of all the intervals under the assumption of epistemic independence. Each product of intervals with non-zero *bpa* constitutes a Focal Element (FE), γ_i, whose joint *bpa* is the product of the *bpa*s of the individual intervals. When computing the PoC, each FE defines a family of bi-variate Gaussian distributions on the impact plane. In the following, the collection of all focal elements forms the uncertainty space U, and the uncertain parameter vector is $\mathbf{u} = [\mu_\xi, \mu_\zeta, \sigma_\xi^2, \sigma_\zeta^2, \sigma_{\xi\zeta}]^T$ so that $\mathbf{u} \in U$.

Given the set $\Phi = \{PoC | PoC \geqslant PoC_0\}$ and $\Omega = \{\mathbf{u} \in U | PoC(\mathbf{u}) \in \Phi\}$ the *Pl* and *Bel* that the *PoC* is larger than a given threshold PoC_0 given the available evidence are:

$$Bel(\Omega) = \sum_{\gamma_i \subset \Omega} bpa(\gamma_i) \quad (2a)$$

$$Pl(\Omega) = \sum_{\gamma_i \cap \Omega \neq \varnothing} bpa(\gamma_i) \quad (2b)$$

For different values PoC_0, Eqs. 2a, define two curves (see the example in Fig. 1). The area between the curves, $A_{Pl,Bel}$, in logarithmic scale, is:

$$A_{Pl,Bel} = A_{Pl} - A_{Bel}$$

$$= \int_{\log(\underline{PoC})}^{0} Pl(\Omega) \, d(\log(PoC))$$

$$- \int_{\log(\underline{PoC})}^{0} Bel(\Omega) \, d(\log(PoC)), \quad (3)$$

where A_{Pl} and A_{Bel} are the areas below the *Pl* and *Bel* curves, respectively, for $PoC \in [\underline{PoC}, 1]$.

$Bel(\Omega)$ is a lower bound on the probability that $PoC \geqslant PoC_0$. Its value is computed by adding up all the FEs fully supporting the hypothesis $PoC \geqslant PoC_0$. $Pl(\Omega)$ is
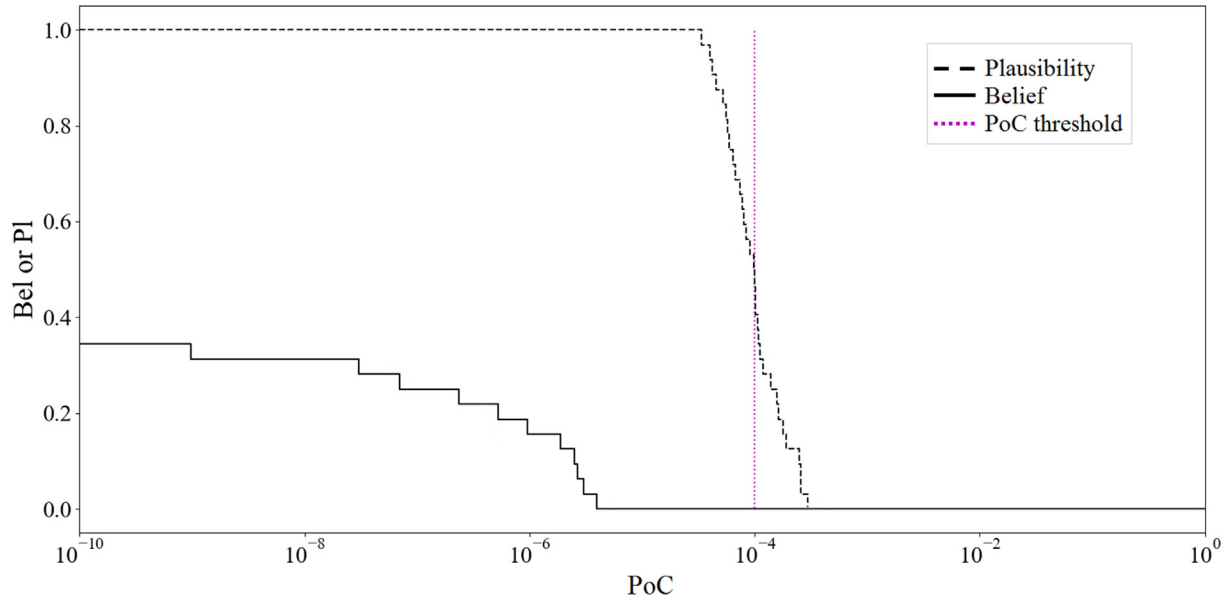
Fig. 1. Support to the value of *PoC* being greater than a given value: *Bel* -black solid line; *Pl* - black dashed line. The dotted purple line represents a possible PoC_0.

an upper bound on the probability that $PoC \geqslant PoC_0$. Its value is computed by adding up all the FEs only partially supporting the hypothesis $PoC \geqslant PoC_0$. The area $A_{Pl,Bel}$ quantifies the amount of uncertainty on the probability that $PoC \geqslant PoC_0$, i.e. if no epistemic uncertainty is present, both curves would reduced to the same Cumulative Distribution Function (CDF). Thus, for a given value of PoC_0, a large value of Pl associated with a small value of $A_{Pl,Bel}$ suggests that there is a lot of support to the hypothesis $PoC \geqslant PoC_0$ given the available information. On the contrary a large value of Pl associated to a large value of $A_{Pl,Bel}$ suggests that the hypothesis $PoC \geqslant PoC_0$ is very plausible to be true but with a high degree of uncertainty.

Sánchez and Vasile (2021) proposed a DSt-based classification system to decide whether, for a given conjunction event, a Collision Avoidance Manoeuvre (CAM) was required or not. In this paper, we propose a revised version of the classification approach proposed Sánchez and Vasile (2021). A given conjunction event is classified according to: i) the value of the *Pl* at $PoC = PoC_0$ or $Pl(PoC_0)$, ii) the time of closest approach *t2TCA* and iii) the area $A_{Pl,Bel}$. We introduced five thresholds: two time thresholds indicating the proximity of the event, T_1 and T_2, the maximum admissible *PoC*, or PoC_0, the level of *Pl*, Pl_0, above which there is sufficient support to the hypothesis $PoC \geqslant PoC_0$, and the value of area A_0, above which the information is considered to be uncertain. Three of the five thresholds, T_1, T_2 and PoC_0, are decided by the operators and depend on operational constraints, the other two Pl_0 and A_0 need to be tuned under evidence-based criteria, as it will be explained in the remainder of the paper.

We then introduce the following six classes, see Table 1, each defined by a combination of $Pl(PoC_0), t2TCA$ and $A_{Pl,Bel}$:

- *Class 0*: there is enough evidence supporting the fact that $PoC \geqslant PoC_0$ is plausible but is accompanied by a high degree of uncertainty and no time to acquire new measurements, due to the proximity of the event, hence a CAM is suggested. In other words, most pieces of evidence are saying that there is a non-zero probability that the value of the *PoC* is correct, however the actual probability that the value of the *PoC* is correct could be very low. Given the degree of uncertainty on the correctness of the *PoC* and the short time before TCA a CAM is suggested as a worst case solution.
- *Class 1*: there is full support to the hypothesis $PoC \geqslant PoC_0$, with limited uncertainty, and short *t2TCA*, hence a CAM is required.
- *Class 2*: there is full support to the hypothesis $PoC \geqslant PoC_0$, with limited uncertainty, preparing a CAM is recommended, but a CAM is not executed yet due to the available time before the encounter.
- *Class 3*: there is enough evidence supporting $PoC \geqslant PoC_0$ but is accompanied by a high degree of uncertainty with sufficient time to acquire new measurements, hence more measurements are recommended. Note that the underlying assumption is that the new measurements are of sufficient quality to reduce the uncertainty. On the other hand if subsequent measurements do not reduce the uncertainty the class changes naturally from 3 to 0 as the *t2TCA* reduces below T_1.
- *Class 4*: there is insufficient evidence supporting $PoC \geqslant PoC_0$ and sufficient time to acquire new measurements.
- *Class 5*: no action is implemented, since *t2TCA* is too short and there is insufficient evidence supporting $PoC \geqslant PoC_0$.

Table 1
Conjunction risk assessment evidence-based classification criterion.

Time to TCA	Pl at PoC_0	Area between curves	Class
$t2TCA \leqslant T_1$	$Pl(PoC_0) < Pl_0$	-	5
	$Pl(PoC_0) \geqslant Pl_0$	$A_{Pl,Bel} < A_0$	1
		$A_{Pl,Bel} \geqslant A_0$	0
$T_1 < t2TCAt2TCA \leqslant T_2$	$Pl(PoC_0) < Pl_0$	-	4
	$Pl(PoC_0) \geqslant Pl_0$	$A_{Pl,Bel} < A_0$	2
		$A_{Pl,Bel} \geqslant A_0$	3
$t2TCA > T_2$	-	-	3

Note that for $t2TCA > T_2$ all events are classified as *Class 3* because the required action is to acquire more measurements. Also, it has to be noted that the level of confidence that one has in the computed value of the *PoC* depends only on Pl_0. If Pl_0 is set to zero it means that one accepts even a single piece of partial evidence that $PoC \geqslant PoC_0$ to escalate the *Class* from 5, to 0 or 1, or from 4 to 2 or 3.

3. Modelling epistemic uncertainty in conjunction data messages

The use of DSt to model epistemic uncertainty does not require any assumption on the probability of an event and also captures rare events with low probability. On the other hand with no direct information on measurements and dynamic model, one can only rely on the CDMs to define the FEs and associated probability masses.

This section presents a methodology to associate one of the six classes introduced in the previous section to a given sequence of CDMs. The first step is to derive the FEs from the time series of miss distances and covariance matrices in the CDMs. In accordance with DSt, we make no prior assumption on the underlying distribution of the CDMs and, instead, we consider that each CDM is drawn from an unknown set of probability distributions. The assumption is that the value of the uncertain vector **u** in each CDMs is a sample drawn from the set of unknown distributions. We make use of the DKW inequality, Dvoretzky et al. (1956), to build an upper and lower bound to the set starting from the empirical Cumulative Distribution Function (eCDF) derived from the sequence of CDMs.

Given a sequence of CDMs and the eCDF of each of the components of the uncertain vector **u**, the DKW inequality defines the following upper and a lower bounds

$$F_n(x) - \sqrt{\frac{\ln\frac{2}{\delta}}{2n}} \leqslant \mathscr{F}(x) \leqslant F_n(x) + \sqrt{\frac{\ln\frac{2}{\delta}}{2n}} \quad (4)$$

around the eCDF $F_n(x)$ (dashed green lines in Fig. 2b), given n CDMs and the confidence level $1 - \delta$ that the exact distribution $\mathscr{F}(x) \in F_n(x) \pm \varepsilon$, where $\varepsilon = \sqrt{\frac{\ln\frac{2}{\delta}}{2n}}$.

Note that expression Eq. (4) implies that for an infinite number of observations $\mathscr{F}(x) = F_n(x)$. However, in the following, we will show that in real sequences not all CDMs follow the same distribution. Convergence to a single distribution is, therefore, plausible for a single sequence with consistent measurements and propagation model. Furthermore, $F_n(x)$ would converge to a delta function if each observation returned the same mean and covariance and the propagation model would not introduce any variability or nonlinearity.

From the confidence region defined by the DKW bands, it is possible to build a probability box, or p-box, Ferson et al. (2023, 2007, 2017), for each of the components of **u**. A p-box is a set of all CDFs compatible with the data, that is, the bounded region containing all distributions from where the set of samples may have been drawn, Ferson et al. (2007). The upper and lower bounds of the p-box are monotonic non-decreasing functions, ranging from 0 and 1, so that $\underline{\mathscr{F}}(x) \leqslant \mathscr{F}(x) \leqslant \overline{\mathscr{F}}(x)$, with $\underline{\mathscr{F}}(x)$ and $\overline{\mathscr{F}}(x)$ the upper and lower bounds of the p-box for a given variable x, Ferson et al. (2023).

In this work, the p-box bounds are computed from the CDF of a weighted sum of univariate Gaussians, each one centred at one of the samples. More formally the assumption is that $\mathscr{F}(x)$ can be approximated by:

$$\mathscr{F}(x) \sim \mathscr{P}(x) = \int_{-\inf}^{\inf} \sum_i^n w_i \mathscr{N}(x_i, \sigma_i)(x)\, dx, \quad (5)$$

with x_i the realisations of the uncertain variable x, w_i a weight associated with each sample, and σ_i the variance of the Gaussian distribution associated with the ith-sample. See Fig. 2a for an illustrative example. Implicitly, it implies that each sample presents some uncertainty which is modelled with a Gaussian distribution (grey lines in Fig. 2a). This distribution represents the confidence in the sample's value. By doing so, we admit that when we observe a sequence of CDM we cannot tell from which exact distribution that sequence is drawn. This is consistent with the available sequences of real CDMs and the approach adopted by CNES to model the uncertainty in the covariance realism (see Section 4.2.2).

In order to define the limits of the p-box, the two free parameters on each Gaussian distribution on the weighted sum, w_i and σ_i, must be computed by solving the optimisation problems:
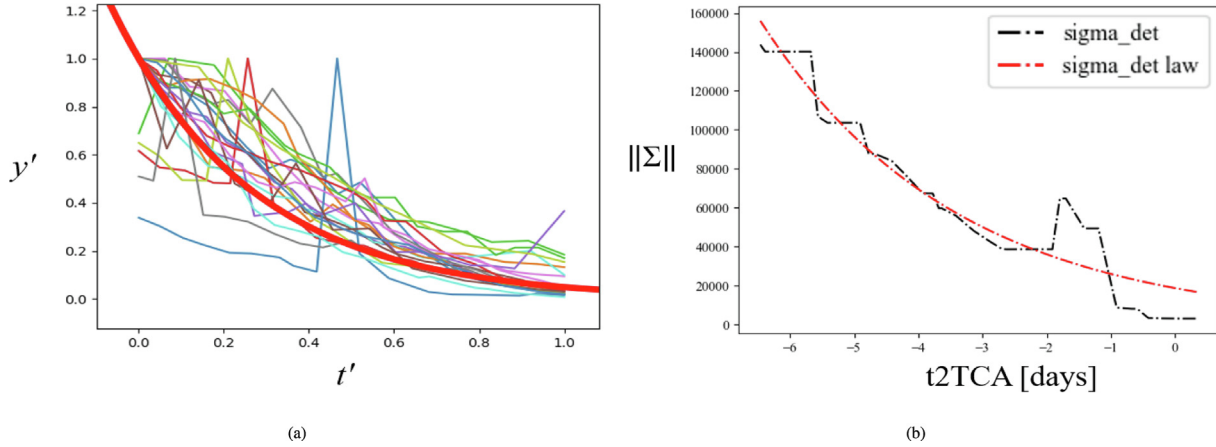
Fig. 2. Example of intervals derivation form the eCDF. (a) eCDF (solid blue), individual sample's Gaussian pdf distributions (solid grey), pdf of the sum of Gaussians distributions for the eCDF fit (solid orange) (b) eCDF (solid blue), DKW bands (dashed green), fitted eCDF with weighted sum of Gaussian distributions (dashed-pointed orange). (c) eCDF (solid blue), DKW bands (dashed green), p-box optimising the weighted sum of Gaussian distributions (dashed-pointed red), 1% and 99% percentiles (vertical pointed black lines). (d) eCDF (solid blue), p-box (dashed-pointed red), 1 α-cut 2 intervals' Pl and Bel (dashed blue), 7 α-cuts 8 intervals' Pl and Bel (dashed black). Dotted thin horizontal lines for the α-cuts: light blue at 0.5 for the 2 intervals partition, grey lines spaced 0.125 for the 8 intervals partition. (For interpretation of the references to colour in this figure legend, the reader is referred to the web version of this article.)

$$\begin{cases} \overline{\mathscr{P}}(x) = \max_{w_i,\sigma_i} \mathscr{P}(x; w_i, \sigma_i) \\ \underline{\mathscr{P}}(x) = \min_{w_i,\sigma_i} \mathscr{P}(x; w_i, \sigma_i) \end{cases} s.t. \begin{cases} \overline{\mathscr{P}}(x) \leqslant \min(1, F_n(x) + \varepsilon) \\ \underline{\mathscr{P}}(x) \geqslant \max(0, F_n(x) - \epsilon) \end{cases},$$

(6)

where $\overline{\mathscr{P}}(x), \underline{\mathscr{P}}(x)$ are the upper and lower bounds of the p-box, respectively (red dashed-pointed line in Fig. 2c). An approximation to $\overline{\mathscr{P}}(x), \underline{\mathscr{P}}(x)$ can be computed by finding the values of w_i and σ_i in Eq. (5) that best fit the upper and lower DKW bands:

$$\begin{cases} \overline{\mathscr{P}}(x) \approx \overline{P}(x) = \text{fit}_{w_i,\sigma_i}(F_n(x) + \epsilon) \\ \underline{\mathscr{P}}(x) \approx \underline{P}(x) = \text{fit}_{w_i,\sigma_i}(F_n(x) - \epsilon) \end{cases}.$$

(7)

Eq. (7) gives the upper and lower bounds on the probability of realising a particular value of the uncertain vector **u** but the definition of a set of intervals for each component of **u** requires first the definition of the range of each component. Eq. (5) suggests that each p-box has infinite support. However, this would lead to an inconvenient infinite range for variance and miss distance. Instead, in the following we define the more practical interval $[\underline{x}, \overline{x}]$ such that:

$$\int_{\underline{x}}^{\infty} w_1 \mathcal{N}(x_1, \sigma_1; x)\, dx = 0.99, \quad \int_{-\infty}^{\overline{x}} w_n \mathcal{N}(x_n, \sigma_i; x)\, dx$$
$$= 0.99.$$

(8)

Note that this confidence interval is independent of the δ introduced above and is used to define the range of variability of x when constructing the focal elements.

It is important to note that the assumption is that the miss distance and each component of the covariance can be treated independently. This is generally not the case, but the independence assumption in this paper leads to a more conservative set of focal elements that covers the space of realisations of the uncertainty vector. Although this can lead to over-conservative decisions, it is deemed to be acceptable in the case of high-risk events with little available information. However, in order to reduce the number of collision avoidance manoeuvres without compromising the quantification of the uncertainty in the probability of a collision, dependencies should be properly accounted for. This will be the subject of future developments.

3.1. Scaling of the CDMs

The approach described in previous sections assumes that every CDM has the same relative importance and no additional source of information is available to qualify each individual CDM. However, as the *t2TCA* decreases, so does the effect of the uncertainty on the true shape of the distribution on the impact plane and the effect of model uncertainty in the propagation. Fig. 3a shows the normalised determinant of multiple sequences of covariance matrices taken from the database of the ESA's Collision Avoidance Kelvins Challenge, ESA (2019, 2022). The database contains 13,152 sequences of CDMs of some of the Low Earth Orbit (LEO) satellites monitored by the ESA Space Debris Office (SDO). The figure shows that one can fit the simple exponential law $y\prime = e^{-3t\prime}$ to the magnitude of the determinant (red line in the figure). However, one cannot simply trust later CDMs due to large uncertainty in each individual sequence. Thus, we propose the following fit for each individual sequence:

$$y\prime = \frac{\|\Sigma\|}{\max_{CDMs}(\|\Sigma\|)}$$

(9a)
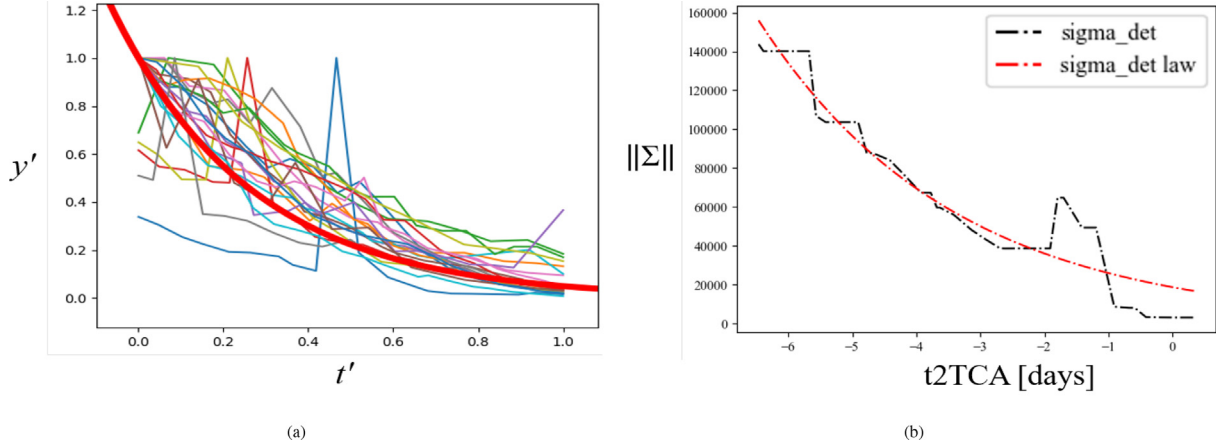
Fig. 3. Fitting law: (a) $y\prime = e^{-3t\prime}$ (thick red line) and the dimensionless covariance determinant for a number of sequences of CDMs (thinner lines), (b) Fitted law (dashed-pointed red) of a single CDM sequence (dashed-pointed black). (For interpretation of the references to colour in this figure legend, the reader is referred to the web version of this article.)

$$y\prime = Ce^{At\prime} + B A, B, C \geqslant 0, \tag{9b}$$

$$t\prime = \frac{\left(1 - \max_{CDMs}(t2TCA)\right)}{\left(\min_{CDMs}(t2TCA) - max_{CDMs}t2TCA\right)} \tag{9c}$$

, where $\|\mathbf{\Sigma}\|$ is the determinant of the combined covariance matrix.

Once the parameters A, B and C are fitted to the samples from a given sequence, the following weight is associated with each CDM in that sequence:

$$w_{CDM_i} = \frac{1}{y\prime(t2TCA_{CDM_i})} \tag{10}$$

The weight is applied to each sample in the eCDF used to compute the DKW bounds: the probability mass associated with each sample is re-scaled by a factor w_{CDM_i}. See Fig. 4 where the eCDF of μ_ξ for an example with 5 obser-
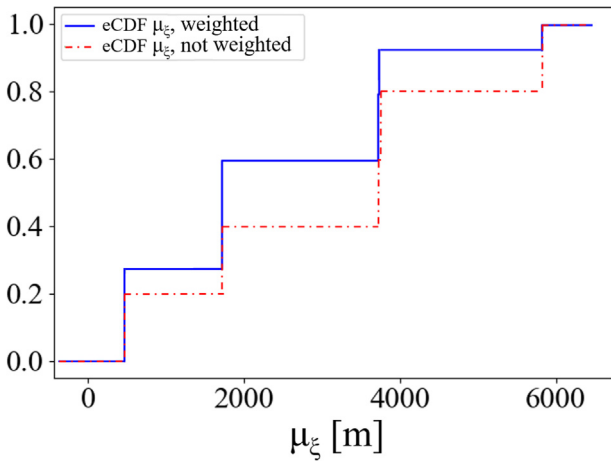
Fig. 4. eCDF for μ_ξ weighing the samples (blue) and with samples equally weighted (dashed red). (For interpretation of the references to colour in this figure legend, the reader is referred to the web version of this article.)

vations is shown both with samples equally weighted (dashed red) or having applied the weighting law described above (blue). This approach results in a scaling of the probability mass associated with the CDMs but still allows the quantification of highly uncertain CDMs since there is no filtering process. The reason is that, with no information on trusted sources or individual CDMs, one cannot make any assumption on which CDM is more credible.

3.2. α-cuts and DSt Structures

Once a p-box is defined, the intervals for each component of **u** are derived from a series of equally spaced α-cuts, light blue and grey dotted horizontal thin lines in Fig. 2d. Each α-cut creates interval, He et al. (2015, 2007):

$$[x_\alpha, x^\alpha] = \{x \mid \mathcal{F}(x) \geqslant \alpha\}. \tag{11}$$

The intersection with the upper bounds in the p-box defines the lower limit of the interval, and the intersections with the lower bound define the upper limit of the interval. The number of intervals is equal to the number of cuts plus one, and the *bpa* associated with each interval, assuming the cuts are evenly spaced, is equal to the inverse of the number of cuts. The intervals and their *bpa* will define an envelope around the p-box (blue and black dashed lines in Fig. 2d). The greater the number of α-cuts, the closer the envelope will be to the p-box, but the more computationally expensive is the computation of *Bel* and *Pl*. From the intervals associated with each component of **u** one can compute the FE γ_i and their associated $bpa(\gamma_i)$ by performing the Cartesian product of all the intervals and associated *bpa*s. Once the FE and *bpa*s are computed, the *Pl, Bel* of $PoC \geqslant PoC_0$ are computed with Eq. (2) (see Fig. 5) and the conjunction event is classified according to Table 1.

Even in this case, we implicitly maintained the assumption that variables are independent, although it is not true that the components of the miss distance and of the covariance are all independent. Approaches to address dependen-
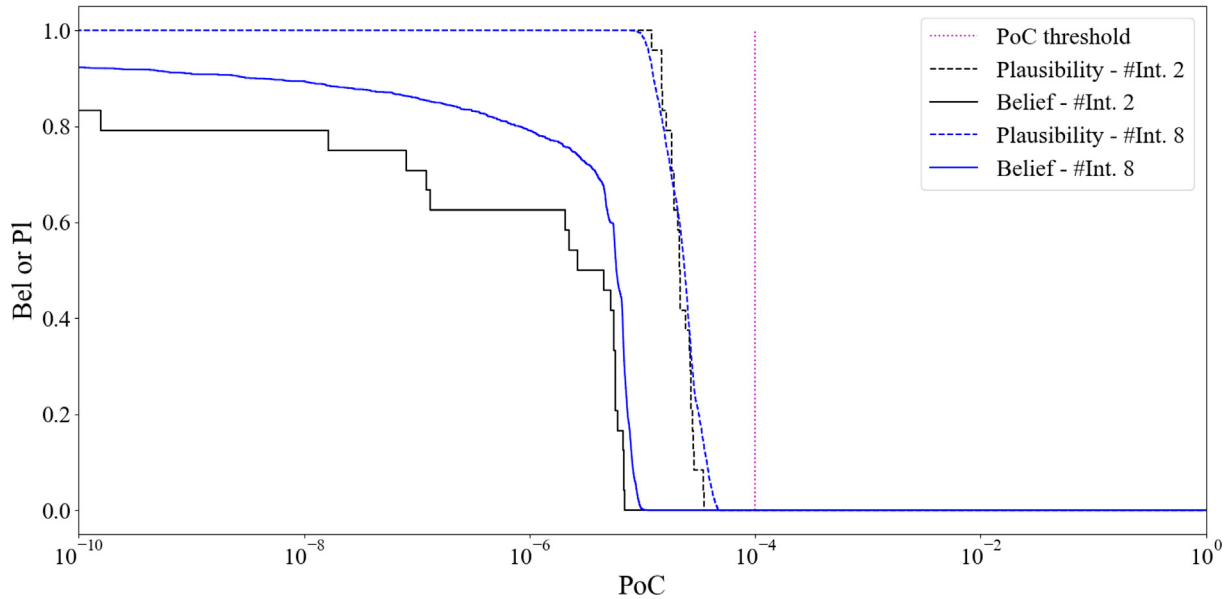
Fig. 5. Plausibility and Belief of $PoC \geqslant PoC_0$. Black: 1 α-cut (two intervals) per variable, 32 FEs. Blue: 7 α-cut (eight intervals) per variable, 32768 FEs. Solid lines: belief. Dashed lines: plausibility. Dotted purple vertical line: PoC_0. (For interpretation of the references to colour in this figure legend, the reader is referred to the web version of this article.)

cies already exist in the literature, see Ferson et al. (2004), and will be considered in future works. The independence assumption has two implications: i) the uncertainty space U is an outer approximation of the space of all distributions of **u** and ii) some focal elements might not contain any sample of **u**. The combination of the two generally leads to over-conservative results. Thus, in order to partially recover the interdependence between uncertain quantities, yet coherent with DSt, a $bpa = 0$ is assigned to all empty FEs and their bpa, coming from the Cartesian product, is evenly distributed to the rest of FEs so that $\sum_i bpa(\gamma_i) = 1$.

4. Numerical experiments

In this section, some numerical tests are presented. The aim is to show the applicability of the methodology presented in previous sections and compare its outcome to the decisions made in past real cases by actual satellite operators: European Space Operations Centre (ESOC) and CNES.

4.1. Parameter Tuning

The methodology proposed in this paper requires the prior definition of the values of two thresholds: Pl_0 and A_0. These two thresholds should be tuned by analysing a large dataset of conjunction events with known outcomes. However, in every database of CDMs available to the authors, the number of provable *Class 1* and *2* conjunctions is very small or zero.

Since A_0 does not affect *Class 4* and *5*, which depend only on Pl_0, but influences the number of True Positives

(TPs) (actual collisions) and False Positives (FPs) (no-collisions believed to be collisions), one can define Pl_0 first and then use A_0 to quantify the degree of uncertainty in the class associated to an event. According to the classification in Table 1, the expected outcome is that low values of Pl_0 would increase the number of events classified as *Class 1* or *2*, reducing, at the same time, the number of False Negatives (FNs) (collisions believed to be no-collisions) and increasing the amount of TPs (detected real collision or high-risk events). If this is combined with high values of A_0, the chances of detecting all high-risk events are high, but at the cost of increasing the number of FPs (low-risk encounters wrongly classified as high-risk). If instead, A_0 is low, more events will be classified as uncertain (*Class 0* and *3*). On the contrary, a higher value of Pl_0 would reduce the false alerts, FPs, but at the risk of increasing the number of FNs. Table 2 contains the definition of TPs, True Negatives (TNs), FPs and FNs.

This paper used the DSt structure to set a value for Pl_0. If there is at least one FE supporting $PoC > PoC_0$, it means that there exists at least one piece of evidence suggesting that the PoC can be correct. This piece of evidence may correspond to an extreme event with low probability. Following this idea, we propose the value $Pl_0 = \min_i(bpa(\gamma_i))$. This implies that even a PoC that corresponds to a rare event in the generation of a CDM is considered to be plau-

Table 2
Definition of TP, TN, FP and FP.

	Class 1/2	Class 0/3	Class 4/5
Collision	TP	Unc.	FN
No Collision	FP	Unc.	TN

sible. The value of A_0 is selected by balancing the number of TPs and FPs. The idea is to try to reduce the number of FPs by reclassifying them as uncertain cases and presenting the level of such uncertainty to the operator. A low value of A_0 implies that the operator accepts very little uncertainty in the sequence of CDM, which reduces the number of FPs but potentially classifies some TPs as uncertain. On the other hand, a greater value of A_0 implies that the operator is very conservative and accepts to treat a number of FPs as TPs. Thus, the decision to execute a CAM is related to the confidence of the operator in the quality of the CDMs. For highly uncertain sequences of CDMs, a low A_0 is recommended, but if the quality of the CDMs is high, a higher A_0 should be used.

In the following, rather than selecting the value of the area threshold A_0, we select the value of the normalised area $A_0^* = \{0, 0.05, 0.1, 0.15, \ldots, 0.95, 1\}$, where A_0^* is the fraction of the maximum possible area between the *Bel* and *Pl* curves, that is, when *Bel* drops to zero at the minimum value of PoC, $\underline{PoC}$, and *Pl* remains equal to one until $PoC = 1$. In this tuning exercise the area is computed by taking the lower limit $\underline{PoC} = 10^{-30}$ for the PoC as this is the lowest value computed from all the sequences of CDMs in our database. For all the first four tests in this paper, we will use a value of $A_0^* = 0.1$ that allows one to clearly differentiate Event 1 from Events 3 and 4 in the following section. In the last test, we will present the sensitivity of the number of recommended CAMs to the value of A_0^*.

4.2. Comparison Against SDO and CNES

The results in this section will show a comparison between the CARA performed with the proposed evidence-based method and the decisions made by real operators in a selected number of real cases. The two operators considered in this study are the ESA's SDO and CNES. Each of them has a different approach to conjunction analysis. Four real conjunction events are analysed and the different operational approaches are compared.

For all examples the values of the thresholds are reported in Table 3. The evolution of the normalised area gap between the *Pl* and *Bel* curves, or $A_{Pl,Brel}$, over time, for all four cases can be found in Fig. 6, where $A_{Pl,Bel}^* = A_{Pl,Bel}/max(A_{Pl,Bel})$ is the normalised area between curves, $A_{Pl,Bel}$, defined in Eq. (3). The Figure confirms that an $A_0^* = 0.1$ is appropriate to differentiate between cases

Table 3
Threshold values.

Threshold	Units	Value
T_1	days	3
T_2	days	5
PoC_0	-	10^{-4}
Pl_0	-	$1/\#FE$
A_0^*	-	0.1
$\underline{PoC}$	-	10^{-30}

like Event 1 from cases like Event 3 and 4. All four cases are presented in more detail in the following subsections.

4.2.1. Space debris office conjunction risk assessment

The approach followed by the ESA SDO is probability-based, relying mainly on the value of the PoC computed with the information from the CDMs, or the PoC included in the CDM. The following quote may summarise the conjunction risk assessment process adopted by the SDO: "For a given close approach the last obtained CDM, including the computed risk, can be assumed to be the best knowledge we have about the potential collision and the state of the two objects in question. In most cases, the Space Debris Office will alarm control teams and start thinking about a potential avoidance manoeuvre 2 days prior to the close approach in order to avoid the risk of collision, to then make a final decision 1 day prior", ESA (2019). Nevertheless, each mission monitored by the SDO has specific operational constraints (i.e. the time needed to prepare and execute the manoeuvre) and will have its own risk and time thresholds, PoC_0 and T_1. The time threshold T_1 is generally 2 or 3 days away from TCA. At that point the mission team is informed about the possible collision, and a final decision is usually made (when possible) 1 day from TCA, ESA (2019). The risk threshold PoC_0 is determined statistically based on the overall collision risk and the annual frequency of close approaches, trading off the ignored risk and the avoided risk by selecting the risk threshold at the cost of an expected number of annual manoeuvres, see Merz et al. (2017). Generally, for missions in the LEO regime, a threshold of $PoC_0 = 10^{-4}$ leads to a risk reduction of around 90% at the expense of 1 to 3 manoeuvres per year, with current levels of traffic. However, a lower threshold, around 10^{-5}, may be considered to ensure sufficient time to prepare a collision avoidance manoeuvre in the case of escalated events, Merz et al. (2017).

Following this approach, the SDO escalates an event when the PoC of the last CDM is bigger than the threshold. Escalating an event means that further and more detailed analyses are required. If the risk is still above the threshold at the decision time, a CAM is designed in cooperation with the mission team, whose final decision will be made based on the value of PoC included in the last CDM received before the go/no-go decision time. More detailed information on the CARA process of the SDO can be found in Merz et al. (2017). For the first three events in this subsection, only CDMss from the MiniCat database were considered.

4.2.1.1. Event #1.
This event represents a high-risk scenario provided by the ESA SDO. The uncertain geometry in the impact plane, with the whole sequence of CDMs and the PoC evolution are displayed in Fig. 7. Events with PoC above the threshold for times to TCA greater than T_1 make the event escalate, that is, they are further analysed
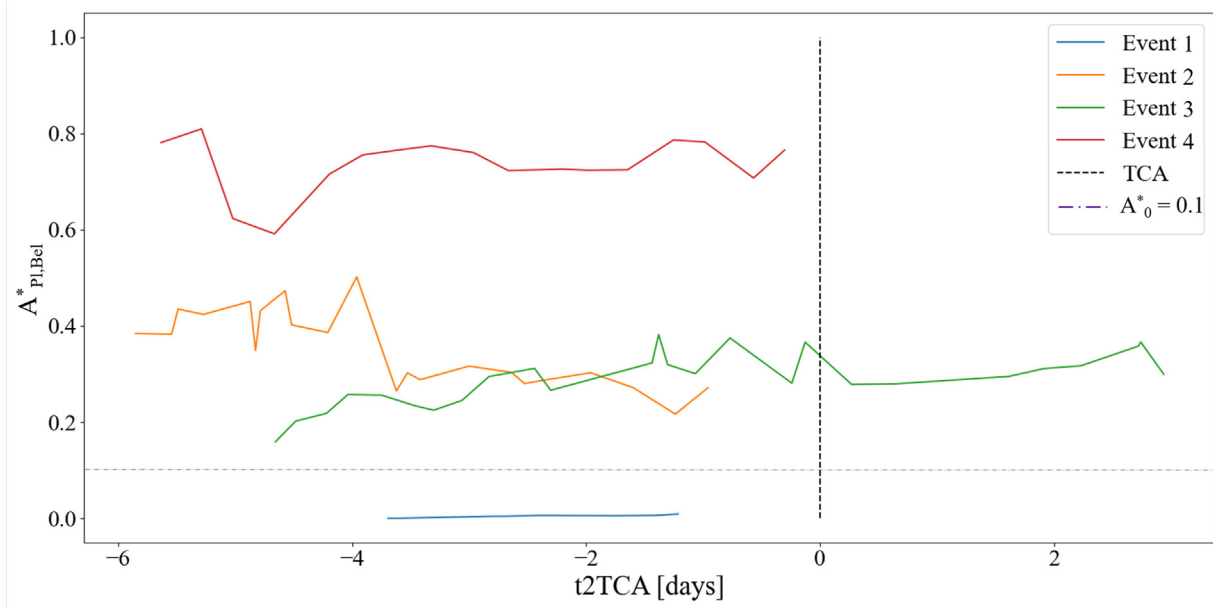
Fig. 6. Evolution of the normalised $A_{Pl,Bel}$ over time, for Events 1 to 4.

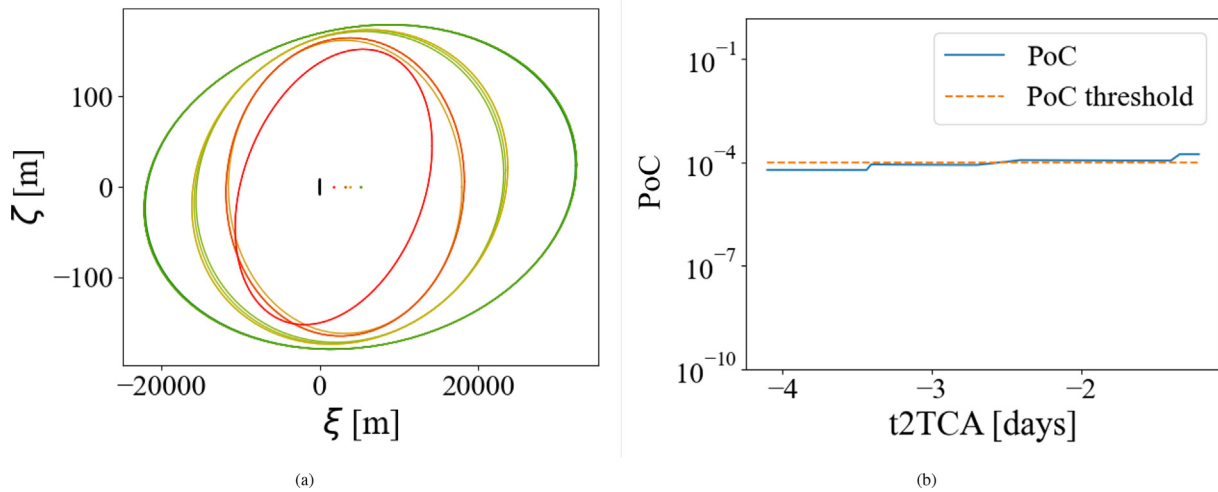(a)   (b)

Fig. 7. CDM information for example in Event #1: High-risk event. (a) Uncertain ellipses in the sequence of CDMs. Green ellipses correspond to earlier CDMs, and red ellipses to later CDMs. (b) Evolution of the PoC in the CDMs with the time to the TCA. Blue solid line: PoC; orange dashed line: PoC threshold. (For interpretation of the references to colour in this figure legend, the reader is referred to the web version of this article.)

and possible alerts to the mission's team can be triggered, while high-risk CDMs received in the last 72 h trigger a CAM procedure.

From Fig. 7b, one can see that the PoC remains high along the whole sequence. Even if at the beginning it was below the threshold, its proximity to PoC_0 along with the upward trend made the operator escalate the event. The PoC threshold was violated within the last few days before TCA, which led to a CAM execution to reduce the risk of the event.

We applied our evidence-based methodology to this case by following the approach presented in Section 3. The DKW bands were computed assuming a confidence inter-

val $\delta = 0.5$. This value was chosen after some tests as a compromise between the confidence in the sequence of CDMs and their variability. Indeed the choice of this parameter, as the choice of the number of α-cuts later on, defines how conservative a decision maker wants to be. In this and the following cases, it was found that a smaller δ, down to 0.1, is only marginally changing the size of the focal elements and thus is not significantly affecting the decision. The CDMs were weighted according to the exponential law in Eq. (9). Fig. 8 shows the fitting law after having received all the CDMs (red) along with the value of the combined covariance matrix determinant, for the whole sequence (black). For the fitting law in Fig. 8b, the value of
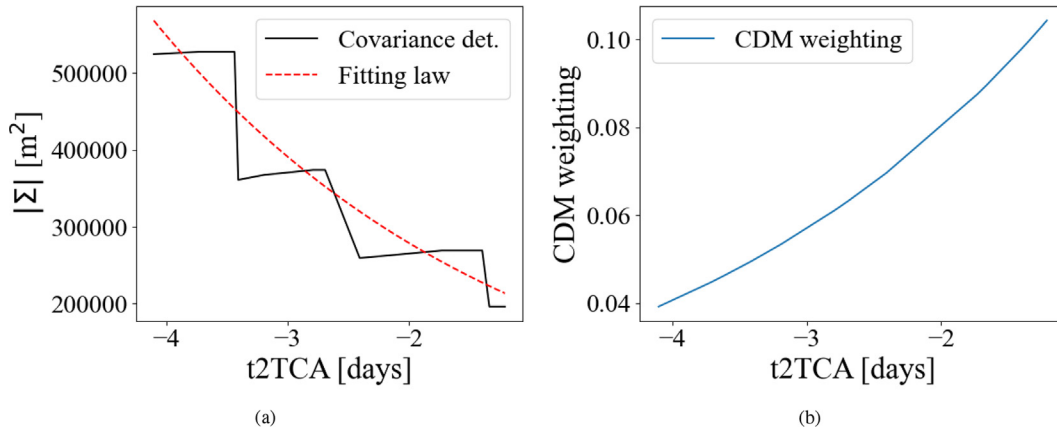
Fig. 8. Fitting law to weight the CDMs after having received the whole sequence in Event #1: High-risk event. (a) Solid black line: value of the determinant from the CDMs, dashed red line: fitting law of the covariance matrix determinant. (b) Weight of the CDMs as a function of the time to the TCA.

the dimensionless parameters in Eq. (9b) after having received the whole sequence are: $A = 1.0752, B = 0.9811$, $C = 0.001716$. Note that the value of the parameters varies with the number of CDMs received to better fit the covariance determinant evolution up to that time.

We repeated the same analysis with different numbers of α-cuts per uncertain variable: $\#\alpha - cuts = \{1, 2, 3, 4, 5, 7\}$. These cuts led to a number of intervals per variable equal to $\#intervals = \{2, 3, 4, 5, 6, 8\}$, which translated into a number of FEs $\#FE = \{32, 243, 1024, 3125, 7776, 16807\}$, respectively. The *Pl* and *Bel* curves for the PoC, for each number of cuts, is presented in Fig. 9, after having received the whole sequence of CDMs.

Fig. 9 shows that, although the increasing number of α-cuts provides a more refined set of curves, their shape and

values varies only slightly. In this case, the *Bel* and *Pl* curves overlap for most values of PoC except for a small interval around the PoC_0, as it could be expected both, from the uncertainty geometry in Fig. 7a and the values of the PoC in Fig. 7b. Since the information in the CDM is coherent across the whole sequence, the gap between the *Pl* and *Bel* curves is small.

Fig. 10 shows the classification, purple solid line, as a function of the time to the TCA from the last received CDM. The figure shows also the PoC directly computed from the CDM.

Initially, the event is classified as *Class 4* and rapidly falls to *Class 5*, since there is little evidence supporting a higher PoC. However, at 2.5 days from TCA, the PoC consistently grows above the threshold. Given the little uncer-
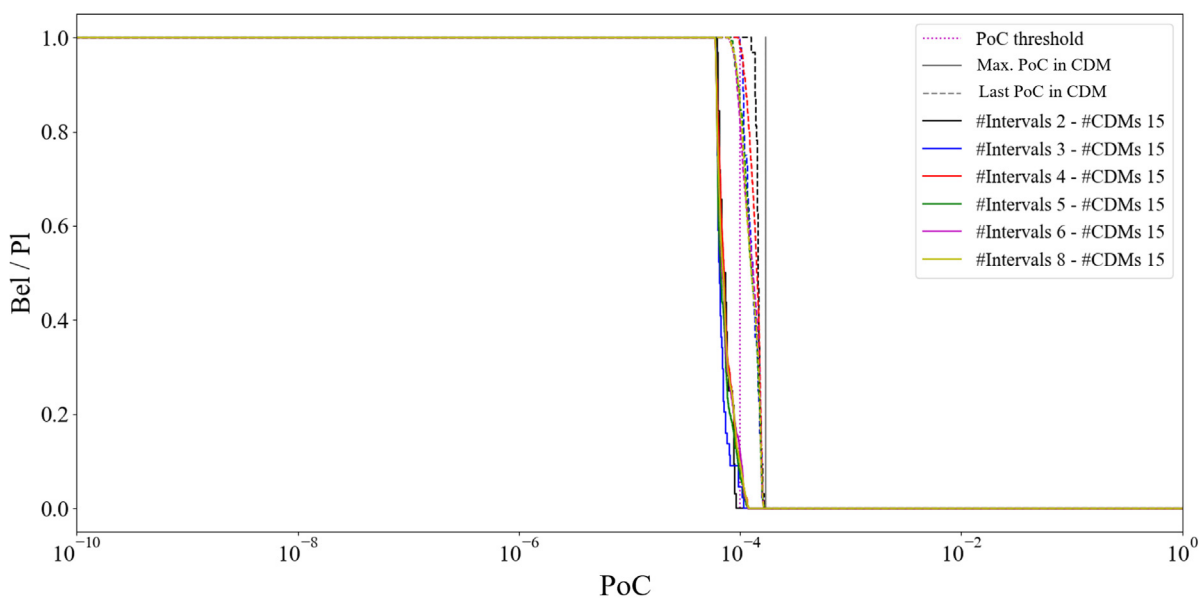
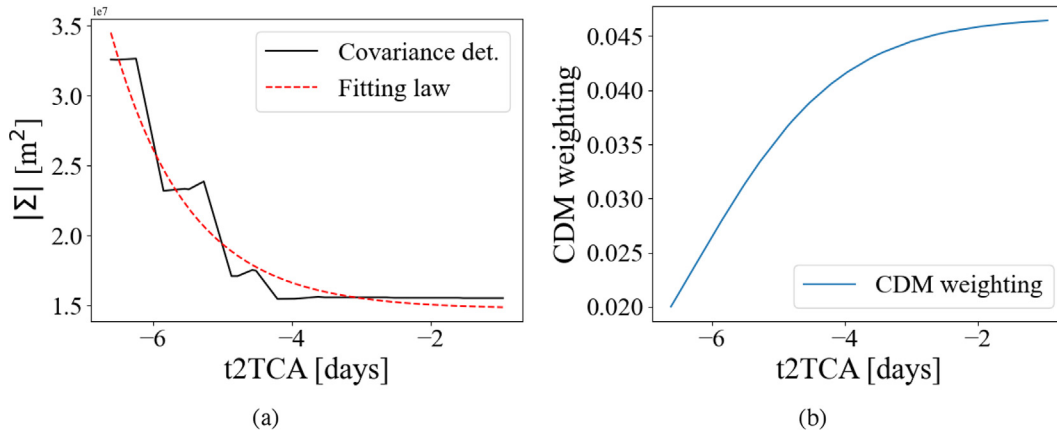Fig. 9. *Pl* and *Bel* of the PoC after having received the whole sequence of CDMs Event #1: High-risk event. Solid vertical grey line: maximum PoC in the sequence, dashed vertical grey line: PoC of last CDM, pointed purple line: PoC threshold. For the rest of the colours: Belief in solid lines and Plausibility in dashed lines. Black: 1 α-cut per variable (2 intervals per variable, 32 FEs), blue: 2 α-cuts, red: 3 α-cuts, green: 4 α-cuts, purple: 5 α-cuts, yellow: 7α-cuts.
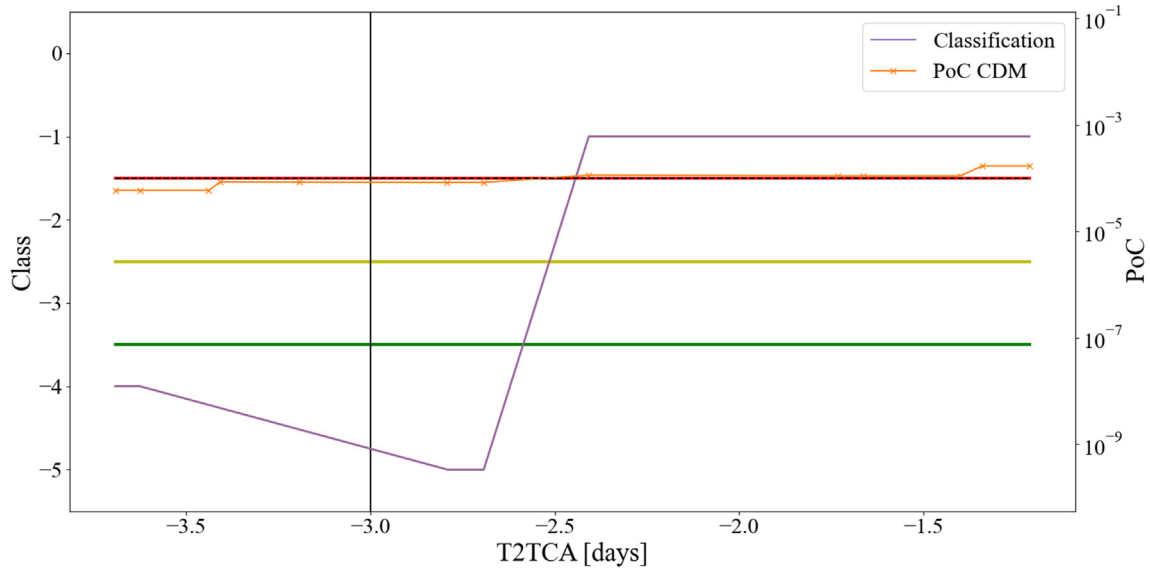
Fig. 10. Collision risk assessment for Event #1: High-risk event. Solid narrow lines: evidence-based classification with different number of α-cuts: $\#\alpha - cuts = \{1, 2, 3, 4, 5, 7\}$ (note that they overlap each other, so only $\#\alpha - cuts = 7$ is visible in solid purple). Crossed-solid line: PoC in the CDMs used by SDO for assessment. Horizontal thick lines: evidence approach safety bands: green, low risk-uncertain boundary; yellow, uncertain–high risk boundary; red, mid term high risk-long term high risk boundary. Dashed black line: Risk threshold (overlapping evidence-based high-risk boundary). Vertical black line: decision time threshold T_1. (For interpretation of the references to colour in this figure legend, the reader is referred to the web version of this article.)

tainty in the sequence of CDMs the event is reclassified as *Class 1* and a CAM is recommended.

This is the same decision finally taken by the SDO. As seen in Fig. 9, the support for a high value of PoC is high and the gap between the curves (level of uncertainty) is very small. Thus, the recommended action in the last days prior to the encounter would be to implement a manoeuvre to reduce the risk of a collision.

4.2.1.2. Event #2. A similar analysis was done for the Low-risk conjunction event illustrated in Fig. 11, also provided by the ESA SDO. Opposite to the previous event, in this case, the PoC remains well below the threshold, so no alert is required to be triggered and no CAM is required to be designed or executed.

The evidence-based analysis was performed using the same parameters as before: $\delta = 0.5$ for the DKW bands, with a different number of α-cuts: $\#\alpha - cuts = \{1, 2, 3, 4, 5, 7\}$ per variable. The final set of CDMs was weighted with the exponential fitting law Eq. (9b) using the following parameters: $A = 0.6049, B = 5.0896, C = 0.4518$. The fitting law (red) and the combined covariance matrix determinant in the CDMs (black) appear in Fig. 12. Note the convergence in the second half of the sequence.

In Fig. 13, the corresponding *Pl* and *Bel* curves on the value of PoC after having received all the CDMs of the event are shown. Again, increasing the number of α-cuts makes the curves smoother and shows a converging trend, but does not change the overall confidence in the value PoC. The maximum value of PoC with some supporting

(a)   (b)
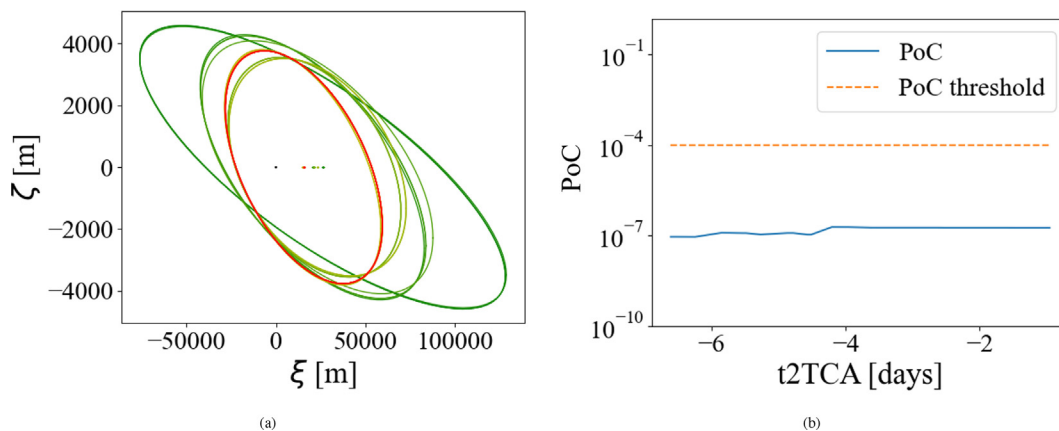
Fig. 11. CDM information for example in Event #2: Low-risk event. (a) Uncertain ellipses in the sequence of CDMs. Green ellipses correspond to earlier CDMs, and red ellipses to later CDMs. (b) Evolution of the PoC in the CDMs with the time to the TCA. Blue solid line: PoC; orange dashed line: PoC threshold.

Fig. 12. Fitting law to weight the CDMs after having received the whole sequence in Event #2: Low-risk event. (a) Solid black line: value of the determinant from the CDMs, dashed red line: fitting law of the covariance matrix determinant. (b) Weight of the CDMs as a function of the time to the TCA. (For interpretation of the references to colour in this figure legend, the reader is referred to the web version of this article.)
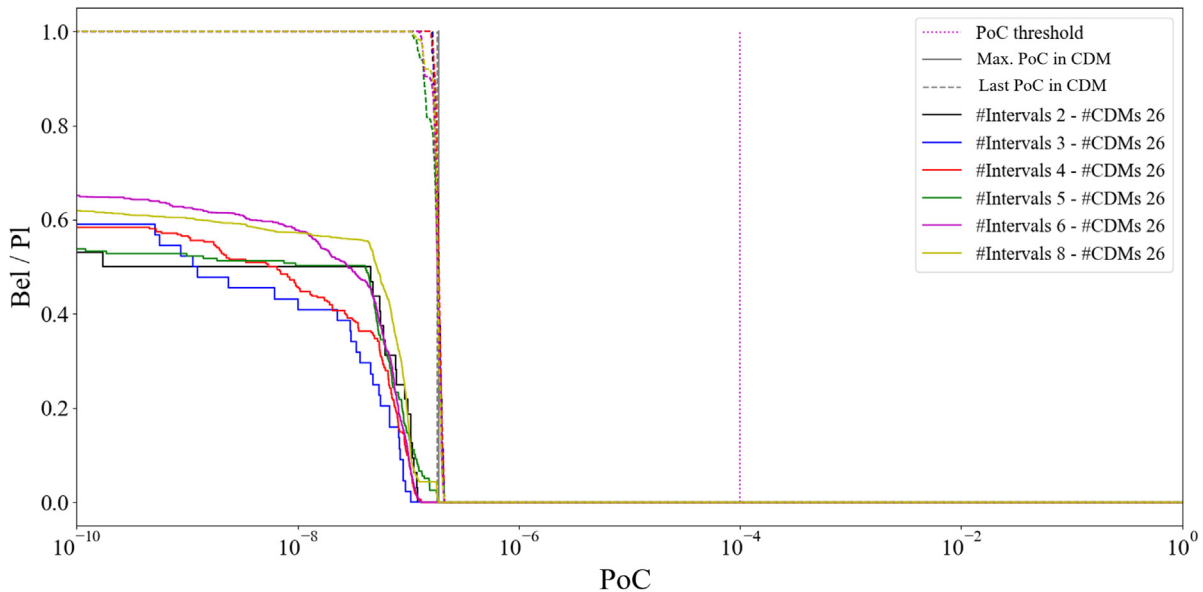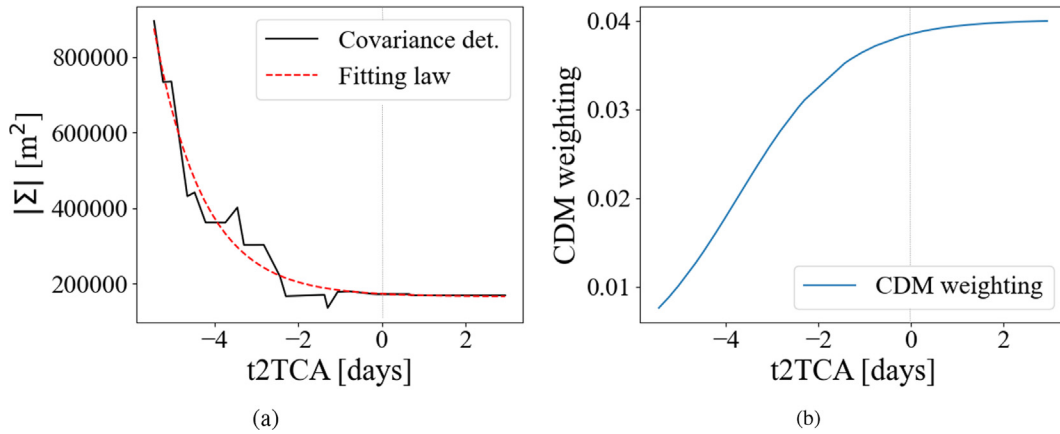

Fig. 13. *Pl* and *Bel* of the PoC after having received the whole sequence of CDMs Event #2: Low-risk event. Solid vertical grey line: maximum PoC in the sequence, dashed vertical grey line: PoC of last CDM, pointed purple line: PoC threshold. For the rest of the colours: Belief in solid lines and Plausibility in dashed lines. Black: 1 α-cut per variable (2 intervals per variable, 32 FEs), blue: 2 α-cuts, red: 3 α-cuts, green: 4 α-cuts, purple: 5 α-cuts, yellow: 7α-cuts. (For interpretation of the references to colour in this figure legend, the reader is referred to the web version of this article.)

evidence is well below the threshold, indicating that the event can be deemed to be safe. However, the left-most part of the *Bel* and *Pl* curves shows a significant gap. This can be explained by the fact that the ellipses are not too different from each other (Fig. 13, and they tend to converge to a single ellipse for the later CDMs, as shown in Fig. 11b. Thus, the initial information content in each CDM tends to support lower values of PoC, which explains the lower value of *Bel* on the left of the graph. However, due to the concentration of information around the later CDMs, the big drop both in *Pl* and *Bel* occurs at PoC∼ 10^{-7}.

Finally, the conjunction assessment for the whole sequence is shown in Fig. 14. This event displays a greater

uncertainty with respect to the previous scenario, but values of the PoC greater than 10^{-7} have no supporting evidence and *Pl* = *Bel* = 0. Thus, the event is initially classified as *Class 4* (*t2TCA* > T_1) and then dropped to *Class 5* (*t2TCA* ⩽ T_1) for the whole sequence, meaning that no further action should be taken by the operator. This is the same decision made by the SDO.

4.2.1.3. Event #3. This last event is affected by a significant level of uncertainty. The encounter geometry and the evolution of the PoC in the CDMs are shown in Fig. 15. Despite the initial high risk, with values of PoC close to the threshold, the final decision of the SDO was
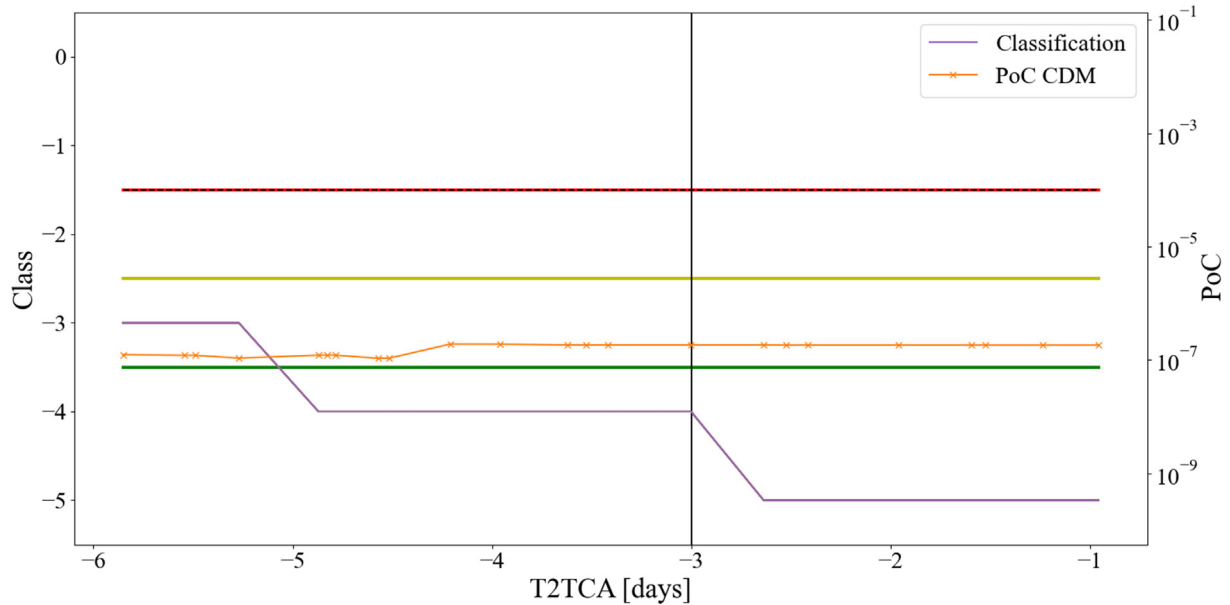
Fig. 14. Collision risk assessment for Event #2: Low-risk event. Solid narrow lines: evidence-based classification with different number of α-cuts: $\#\alpha - \text{cuts} = \{1, 2, 3, 4, 5, 7\}$ (note that they overlap each other, so only $\#\alpha - \text{cuts} = 7$ is visible in solid purple). Crossed-solid line: PoC in the CDMs used by SDO for assessment. Horizontal thick lines: evidence approach safety bands: green, low risk-uncertain boundary; yellow, uncertain–high risk boundary; red, mid term high risk-long term high risk boundary. Dashed black line: Risk threshold (overlapping evidence-based high-risk boundary). Vertical black line: decision time threshold.
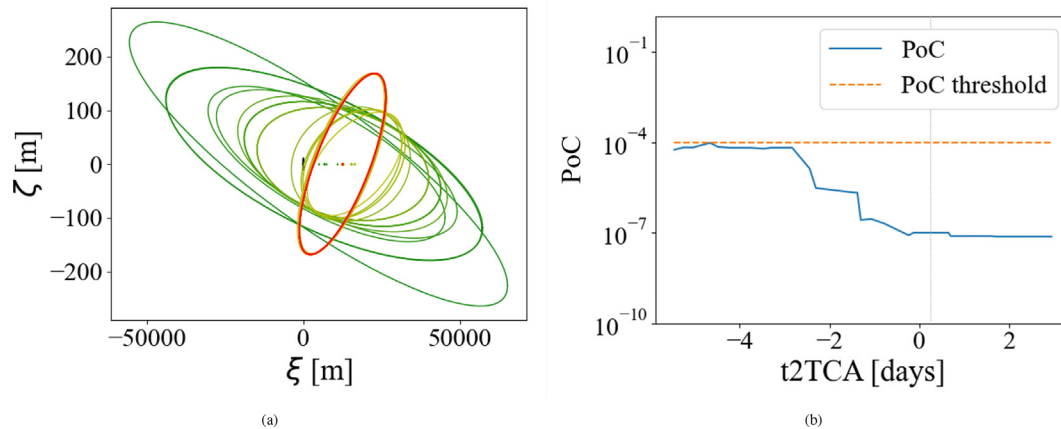
Fig. 15. CDM information for example in Event #3: Uncertain event. (a) Uncertain ellipses in the sequence of CDMs. Green ellipses correspond to earlier CDMs, and red ellipses to later CDMs. (b) Evolution of the PoC in the CDMs with the time to the TCA. Blue solid line: PoC; orange dashed line: PoC threshold, vertical dashed grey line: TCA. (For interpretation of the references to colour in this figure legend, the reader is referred to the web version of this article.)

not to take any further action. This decision was dictated by the later values of the PoC, that were all consistently lower than the initial ones, and considerably below PoC_0. Section A include figures for the whole sequence, no only for the last CDM.

The evidence-based analysis was performed with the same parameters as before: $\delta = 0.5$ for the DKW bands. The exponential fitting law Eq. (9b) to weight the CDMs, after having received the whole sequence, had the following parameters $A = 0.7917, B = 7.1471, C = 0.1858$ and is shown in Fig. 16 (red line) along with the covariance matrix determinant (black line).

The *Pl* and *Bel* curves for the PoC were computed for different α-cuts: $\#\alpha - \text{cuts} = \{1, 2, 3, 4, 5, 7\}$. The curves are shown in Fig. 17. In this case, there is a significant gap between *Pl* and *Bel* for all the values of PoC for which $Pl > 0$. This uncertainty (or level of disagreement between CDMs) can be seen in Fig. 15a, which shows the variety of the uncertainty ellipses from the beginning of the sequence to the last CDMs. In this case the supporting evidence that a value of $PoC > PoC_0$ is plausible does not go to zero but the gap between the *Pl* and *Bel* curves suggests that a further analysis is required although the value of *Pl* is low and *Bel* is zero.

Fig. 16. Fitting law to weight the CDMs after having received the whole sequence in Event #3: Uncertain event. (a) Solid black line: value of the determinant from the CDMs, dashed red line: fitting law of the covariance matrix determinant. Vertical dashed grey line: TCA. (b) Weight of the CDMs as a function of the time to the TCA. Vertical dashed grey line: TCA.
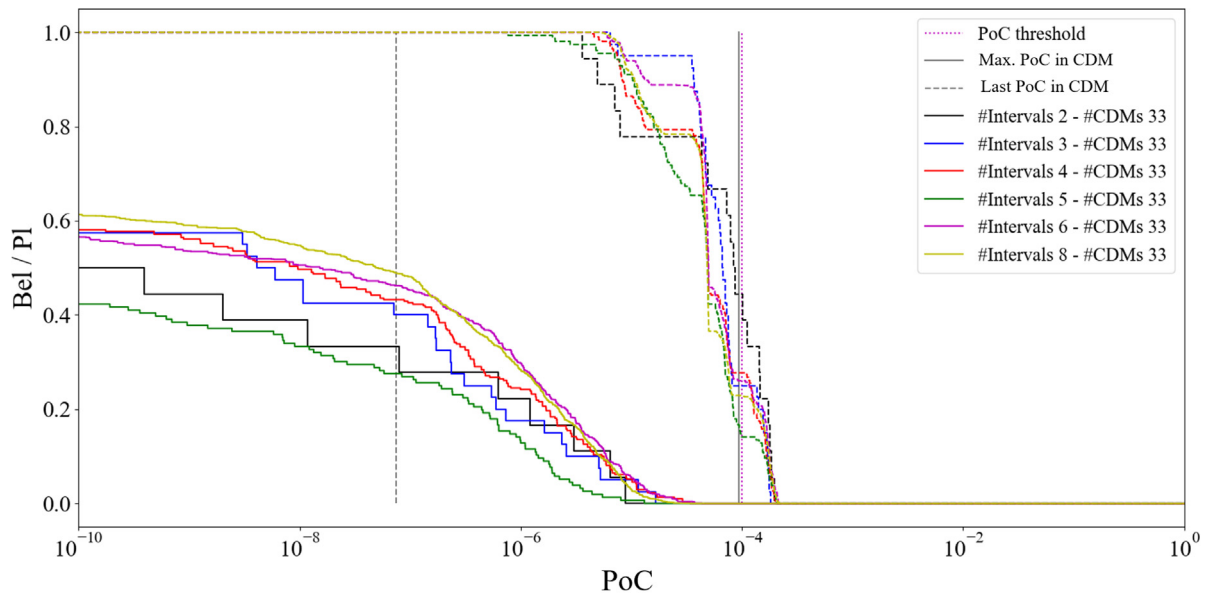

Fig. 17. *Pl* and *Bel* of the PoC after having received the whole sequence of CDMs Event #3: Uncertain event. Solid vertical grey line: maximum PoC in the sequence, dashed vertical grey line: PoC of last CDM, pointed purple line: PoC threshold. For the rest of the colours: Belief in solid lines and Plausibility in dashed lines. Black: 1 α-cut per variable (2 intervals per variable, 32 FEs), blue: 2 α-cuts, red: 3 α-cuts, green: 4 α-cuts, purple: 5 α-cuts, yellow: 7α-cuts. (For interpretation of the references to colour in this figure legend, the reader is referred to the web version of this article.)

Fig. 18 shows the result of the classification: the event starts at *Class 2*, given the potential high risk suggested by the initial CDMs but quickly drops to *Class 3* (*t2TCA > T_1*) because of the level of uncertainty and is finally classified as *Class 0*(for *t2TCA $\leqslant T_1$*). In this case, our approach would suggest a further analysis due to the non-zero plausibility of a high PoC and a high difference between *Pl* and *Bel*, while the decision made by the SDO was to take no further action. The more prudent recommendation coming from our classification system would lead to a further inspection of the *Pl* curve with the realisation that the supporting evidence is small, albeit not zero.

4.2.2. CNES conjunction risk assessment

In order to compensate for the possible lack of realism of the covariance matrix at TCA, CNES re-scales both the covariance matrix of the primary and secondary body with two factors, respectively $k_p \in K_P$ and $k_s \in K_S$. A scaled PoC, called scaled Probability of Collision (sPoC), is obtained by solving the following PoC maximisation problem (see Laporte (2014a,b)):

$$\begin{cases} sPoC = \max_{k_p \in K_P, k_s \in K_S} PoC(\Sigma) \\ \text{s.t.} \Sigma = k_p^2 \Sigma_p + k_s^2 \Sigma_s \end{cases}, \qquad (12)$$
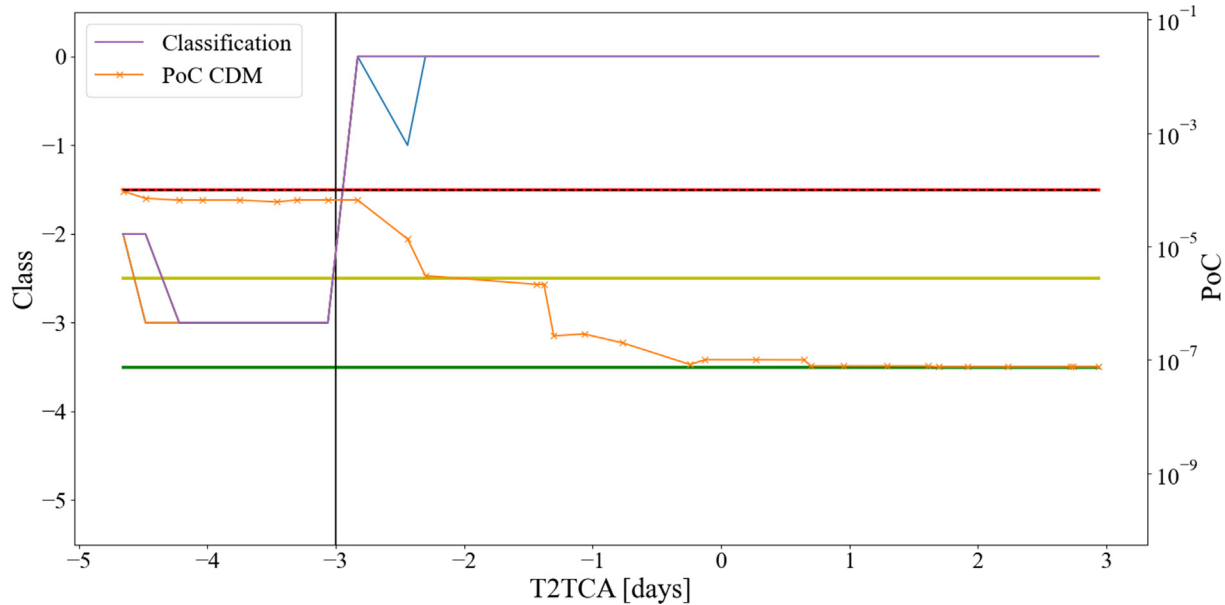
Fig. 18. Collision risk assessment for Event #3: Uncertain event. Solid narrow lines: evidence-based classification with different number of α-cuts: $\#\alpha - \text{cuts} = \{1, 2, 3, 4, 5, 7\}$ (note that they overlap each other, so only $\#\alpha - \text{cuts} = 7$ is visible for all t2TCA in solid purple; $\#\alpha - \text{cuts} = 1$ in solid blue and $\#\alpha - \text{cuts} = 2$ in solid orange are visible at one t2TCA each). Crossed-solid line: PoC in the CDMs used by SDO for assessment. Horizontal thick lines: evidence approach safety bands: green, low risk-uncertain boundary; yellow, uncertain–high risk boundary; red, mid term high risk-long term high risk boundary. Dashed black line: Risk threshold (overlapping evidence-based high-risk boundary). Vertical black line: decision time threshold T_1. Vertical dashed grey line: TCA.

where Σ_p and Σ_s are, respectively, the primary and secondary covariance matrices in a given CDM associated to the conjunction event under consideration.

The two sets K_P and K_S are derived, for each sequence of CDMs, under the assumption that CDMs are samples drawn from an underlying distribution, and the last CDM contains the most reliable estimation of the position of the two objects. Thus, by using the last CDMs as a reference, it is possible to compute the Mahalanobis distance of all previous CDMs from the last one. If one assumes that the uncertainty in position is Gaussian, the Mahalanobis distance should follow a X^2 distribution with 3 degrees of freedom. By performing a Kolmogorov–Smirnov (KS) test between the distribution of the computed Mahalanobis distances and the theoretical one, and setting a desired level of realism, one can define the sets K_P and K_S. More details can be found in Stroe et al. (2021).

CNES decision-making is based on both the value of sPoC and a number of geometric considerations. Events with values of $sPoC > 5 \cdot 10^{-4}$ are classified as *High-Interest Event*, the more risky classification level (red level). For values of $10^{-4} < sPoC < 5 \cdot 10^{-4}$, the event is classified as an *Interest Event*, the second level of risk (orange level). If the value of the sPoC is below those thresholds, caution geometric criteria are applied: miss distance below 1 km or radial distance below 200 m. Note that these threshold values are the default ones and may differ from mission to mission. If the CDMs are received 4–5 days before the encounter or earlier, no alerts are raised independently of the value of sPoC, although the event is placed under study

if some of the above criteria are violated. For later CDMs, alerts may be raised according to the value of sPoC. Finally, if the high risk continues after the decision time (usually 2 days before the encounter), a final decision is made before the TCA.

In the following, we will test our approach on a real close encounter faced by CNES and compare our classification against the one of CNES.

4.2.2.1. Event #4. This scenario presents a high-risk collision case for a real close encounter where CNES had to implement a manoeuvre to reduce the risk.

Fig. 19a shows the geometry of the event, where the earlier CDMs (green ellipses) suggested a low PoC, while later CDMs (red and amber ellipses) suggest a high PoC. Fig. 19b shows the PoC and the sPoC. The latter is above the threshold 10^{-4} from the start and progressively increases while the PoC displays a large variability till about a day before TCA. CNES classified the event as *High-Interest Event*, meaning that careful monitoring was required, starting from the 12th CDM (2.96 days before the TCA). The final decision to perform a manoeuvre was taken 30 h before the encounter. Note that the CDM received about a 1.2 days from TCA indicates a PoC $< 10^{-5}$, well below the risk threshold, while the sPoC indicates a risk above 10^{-3}, which aligns better with the last three CDMs received between the decision time and the CAM execution time).

The evidence-based analysis was performed following the same approach as for the SDO cases, with
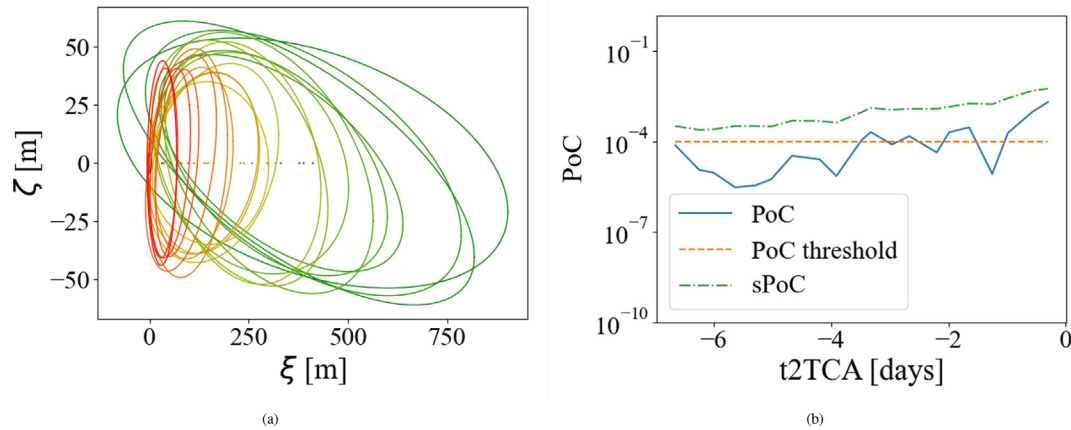
Fig. 19. CDM information for example in Event #4. (a) Uncertain ellipses in the sequence of CDMs. Green ellipses correspond to earlier CDMs, and red ellipses to later CDMs. (b) Evolution of the PoC in the CDMs with the time to the TCA. Blue solid line: PoC; dashed-dotted line: sPoC; orange dashed line: PoC threshold. (For interpretation of the references to colour in this figure legend, the reader is referred to the web version of this article.)
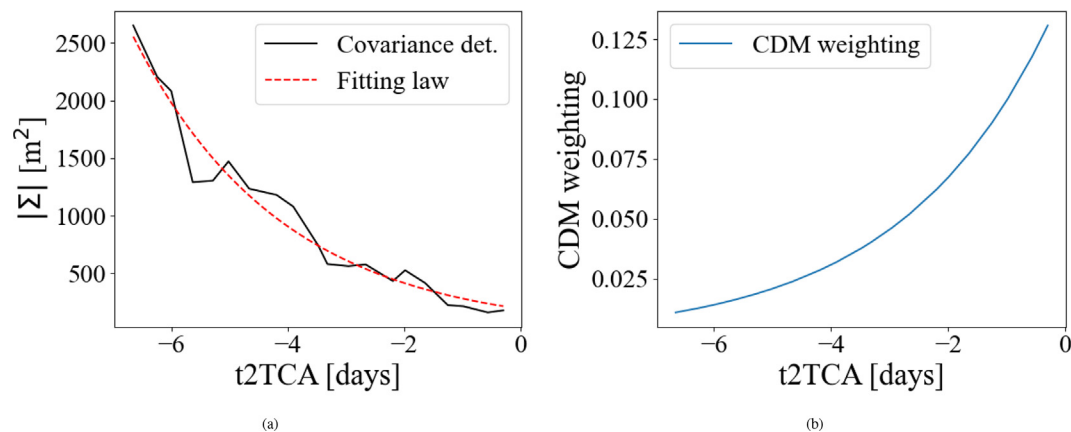

Fig. 20. Fitting law to weight the CDMs after having received the whole sequence in Event #4. (a) Solid black line: value of the determinant from the CDMs, dashed red line: fitting law of the covariance matrix determinant. (b) Weight of the CDMs as a function of the time to the TCA.

$\#intervals = \{2, 3, 4, 5, 6, 8\}$ intervals per variable and CDM weighted according to the exponential law in Fig. 20.

The *Pl* and *Bel* corresponding to the whole sequence of CDM are shown in Fig. 21, and the classification sequence for different numbers of intervals is shown in Fig. 22. In Fig. 21 one can see that $Pl(PoC_0)$ is nearly 1, and $Pl(sPoC) > 0$ along the whole time series. In fact, $Pl = 0$ at $PoC \sim 10^{-2}$, while $\max(sPoC) = 5 \cdot 10^{-3}$. However, the gap between the *Pl* and *Bel* curves is very high, indicating a degree of uncertainty in the sequence of CDMs. This is due to the variability in the CDMs. Thus the event is classified as *Class 0*.

Although this event is placed in the same class as Event 3, the supporting evidence is quite different. Event 4 has a $Pl \approx 1$ and *Bel* different from zero at PoC_0 while Event 3 has $Bel = 0$ and $Pl < 0.2$ at PoC_0. This means that, although in this paper we opted for a very conservative classification of the events such that both Events 3 and 4 fall in the same uncertainty class, a simple analysis of the *Bel* and *Pl* curves would suggests that the available evidence for Event 4 supports a high probability of collision,

up to 10^{-2} in fact, while for Event 3 the supporting evidence at PoC_0 is quite low.

4.3. Statistical analysis of CAM executions

After having compared the proposed evidence-based conjunction assessment approach against real operations on specific cases, in this section we compare the number CAMs that our evidence-based approach would recommend over a large number of real conjunctions experienced by a single mission.

The selected mission is the ESA SWARM-A satellite, orbiting in the LEO regime (circular polar orbit of 87.7 deg at 511 km of altitude), dedicated to studying the Earth's magnetic field as part of a constellation of three satellites. The mission thresholds to trigger conjunction alerts are $PoC_0 = 10^{-4}$ and $T_1 = 72$ hours. Thus, any satellite with a PoC above the threshold in the last 3 days would escalate and would require further analysis, and eventually, a possible CAM design or execution. Nevertheless, encounters presenting a higher risk or an increasing trend before
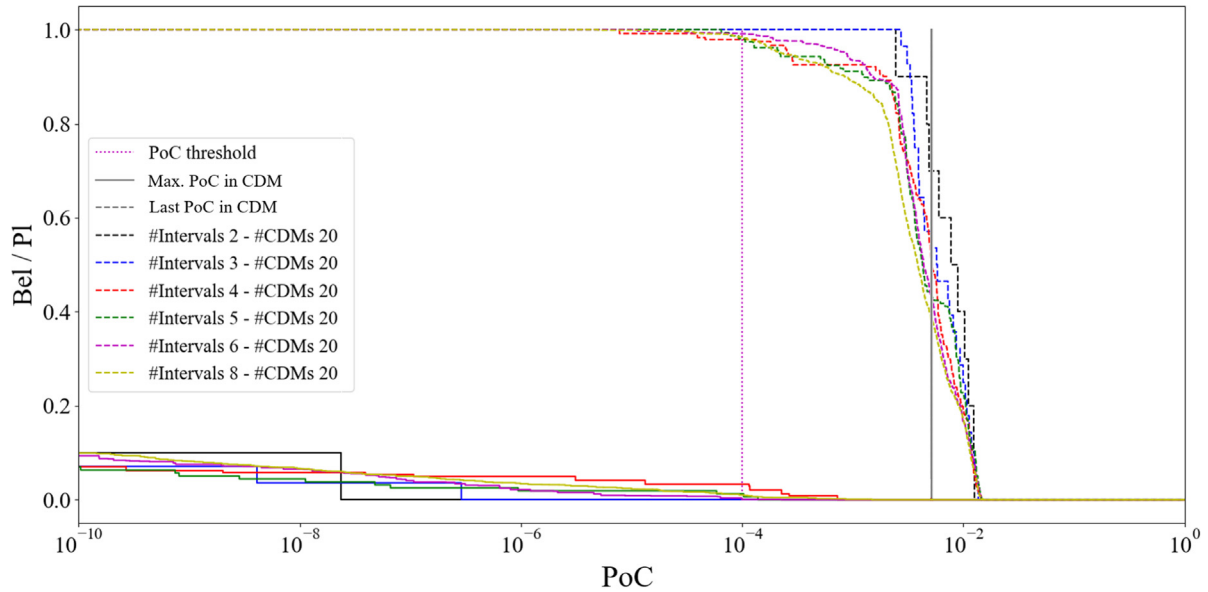
Fig. 21. *Pl* and *Bel* of the PoC after having received the whole sequence of CDMs Event #4. Solid vertical grey line: maximum PoC in the sequence, dashed vertical grey line: PoC of last CDM, pointed purple line: PoC threshold. For the rest of the colours: Belief in solid lines and Plausibility in dashed lines. Black: 1 α-cut per variable (2 intervals per variable, 32 FEs), blue: 2 α-cuts, red: 3 α-cuts, green: 4 α-cuts, purple: 5 α-cuts, yellow: 7 α-cuts. (For interpretation of the references to colour in this figure legend, the reader is referred to the web version of this article.)
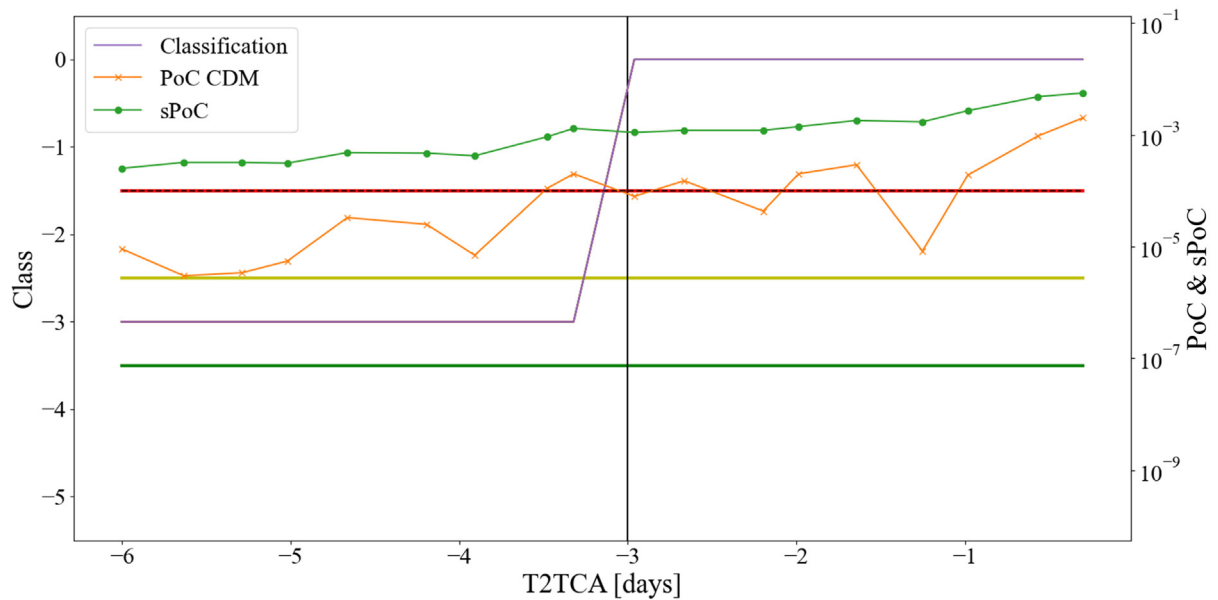
Fig. 22. Collision risk assessment for Event #4. Solid narrow lines: evidence-based classification with different number of α-cuts: $\#\alpha - \text{cuts} = \{1, 2, 3, 4, 5, 7\}$ (note that they overlap each other, so only $\#\alpha - \text{cuts} = 7$ is visible in solid purple). Crossed-solid line: PoC in the CDMs used by SDO for assessment. Horizontal thick lines: evidence approach safety bands: green, low risk-uncertain boundary; yellow, uncertain–high risk boundary; red, mid-term high risk-long term high risk boundary. Dashed black line: Risk threshold (overlapping evidence-based high-risk boundary). Vertical black line: decision time threshold T_1. (For interpretation of the references to colour in this figure legend, the reader is referred to the web version of this article.)

T_1 may be escalated if the operator considers that there is a potential risk for the mission. Finally, the go/no-go decision is subject to operational constraints: the time required to design a CAM after receiving the triggering manoeuvre, the possibility to upload and check the design manoeuvre and the ground station availability.

The database of CDMs includes alerts from 2015 to 2022, with a total of 36,072 events. Overall, most of the events in the database did not represent a threat to the satellite, with only 20 representing escalated events. As explained before, an escalated event is an encounter where the PoC, or the PoC trend, suggests that the conjunction

may be high risk. From those escalated events, only 2 required a CAM to be executed.

The evidence-based analysis was performed with the same thresholds as the previous study cases (Table 3): $PoC_0 = 10^{-4}$, $T_1 = 3$ days, $T_2 = 5$ days, $Pl_0 = 1/243$, $A_0^* = 0.1$, with $\underline{PoC} = 10^{-30}$, and $A_0 = 3$. The DKW bands were obtained assuming a confidence interval of $\delta = 0.5$. As shown before, a higher number of α-cuts would refine the Pl and Bel curves, providing closer curves that better represent the actual epistemic uncertainty. However, this is at the expense of increasing the computational cost and with limited impact on the final classification. Thus 2 α-cuts (3 intervals) per variable, with a total of 243 FEs per analysis were used.

Since the evidence-based analysis lacks the real information available in the actual operation of the satellite that may have affected the operator decision (for example, the ground station availability or the mission constraints), the statistics were computed at four decision times: $T_d = 3$ days to the TCA, corresponding with the mission time threshold, T_1; $T_d = 2$ days to the TCA, allowing for more data to arrive; $T_d = 1$ day to the encounter, the usual go-no go decision time in ESA's missions, Merz et al. (2017); and the epoch of the last CDM in the sequence, $T_d = 0$. For simplicity, we assume that there is no operational constraint that prevents or modifies the final decision and all information is, thus, available.

Table 4 includes the results from the analysis, compared with the actual statistics provided by the SDO. It is important to bear in mind the differences between the approaches. An event classified as *Class 3* or *Class 0* (labelled as *Uncertain*), with the evidence-based approach, would not correspond, necessarily, to an escalated event, since the meaning is different: while an escalated event assumes a certain level of risk, a *Class 0* or *3*, suggests a degree of uncertainty that requires further investigation before making a final decision. This further investigation might be simply limited to an inspection of the *Bel* and *Pl* curves as in cases 3 and 4 above or might require additional observations. On the other hand, for all *Class 1* events, the recommendation is to perform a CAM.

From the upper tier in Table 4 (with $A_0^* = 0.1$), one can observe that: i) the total number of events increases with

the delay in the decision time because more CDMs are available for a decision; ii) the number of manoeuvres proposed by the evidence-based approach is similar to the number of CAMs proposed by the SDO operators; iii) the evidence-based classification system found many more uncertain cases than the SDO. The Table shows also the number of CAMs and uncertain events for A_0^* equal to 0.5 and 0.8. As expected, an increase in the values of A_0^* increases the number of CAMs and reduces the number of uncertain cases because a good portion of all uncertain cases is now *Class 1*.

Even if the Pl_0 threshold is quite low, for A_0^* low, the number of events escalating to *Class 1* remains small. Thus, in this test case, the system is robust enough to remove FN (collision/high-risk collision scenarios overlooked) without introducing false alerts (no collision/low-risk encounters wrongly identified as dangerous or FP). Also, the number of CAMs remains roughly constant independently of the decision time, for $A_0^* = 0.1$. On the other hand, the number of *Class 0* events is between 6 and 15 times higher than the number of escalated events proposed by ESOC. It is here where the evidence-based system differentiates from the probabilistic approach used by ESOC. *Class 0* events are those with $Pl(PoC_0) > Pl_0$, but are still deemed uncertain because $A_{Pl,Bel} > A_0$. Pl captures all realisations, within each Focal Element, that correspond to extreme cases, extreme low or extreme high PoC, compatible with the observed sequence of CDMs. Hence, a large $A_{Pl,Bel}$ with high Pl signifies that there is the evidence that a high PoC event can occur but is uncertain. As in the case of Event 3, many of these cases display a low Pl and zero Bel. Others present conflicting CDM, that cannot be resolved without further observations, or a high Pl for high PoC values, as in Event 4 but with a low Bel. An example can be seen in Fig. 23. The evolution of the combined covariance shows a radical rotation of nearly 90 degrees at −4 days from TCA. The evolution of the PoC does not provide any evidence that the covariance had a step change, but remains close to the threshold limit. The evidence-based approach, instead. shows quite some uncertainty and maintains a high Pl till the end of the sequence, suggesting that the event cannot be discarded and requires further analysis.

Table 4
Results from the statistical analysis on the SWARM-A mission, with the SDO approach and the evidence-based approach. Threshold: $PoC_0 = 10^{-4}$, $T_1 = 3$ days, $T_2 = 5$ days, $Pl_0 = 1/243$. Partition with 2 α-cuts per variable. Upper tier: $A_0^* = 0.1$ ($A_0 = 3$); middle tier: $A_0^* = 0.5$ ($A_0 = 15$); lower tier: $A_0^* = 0.8$ ($A_0 = 24$).

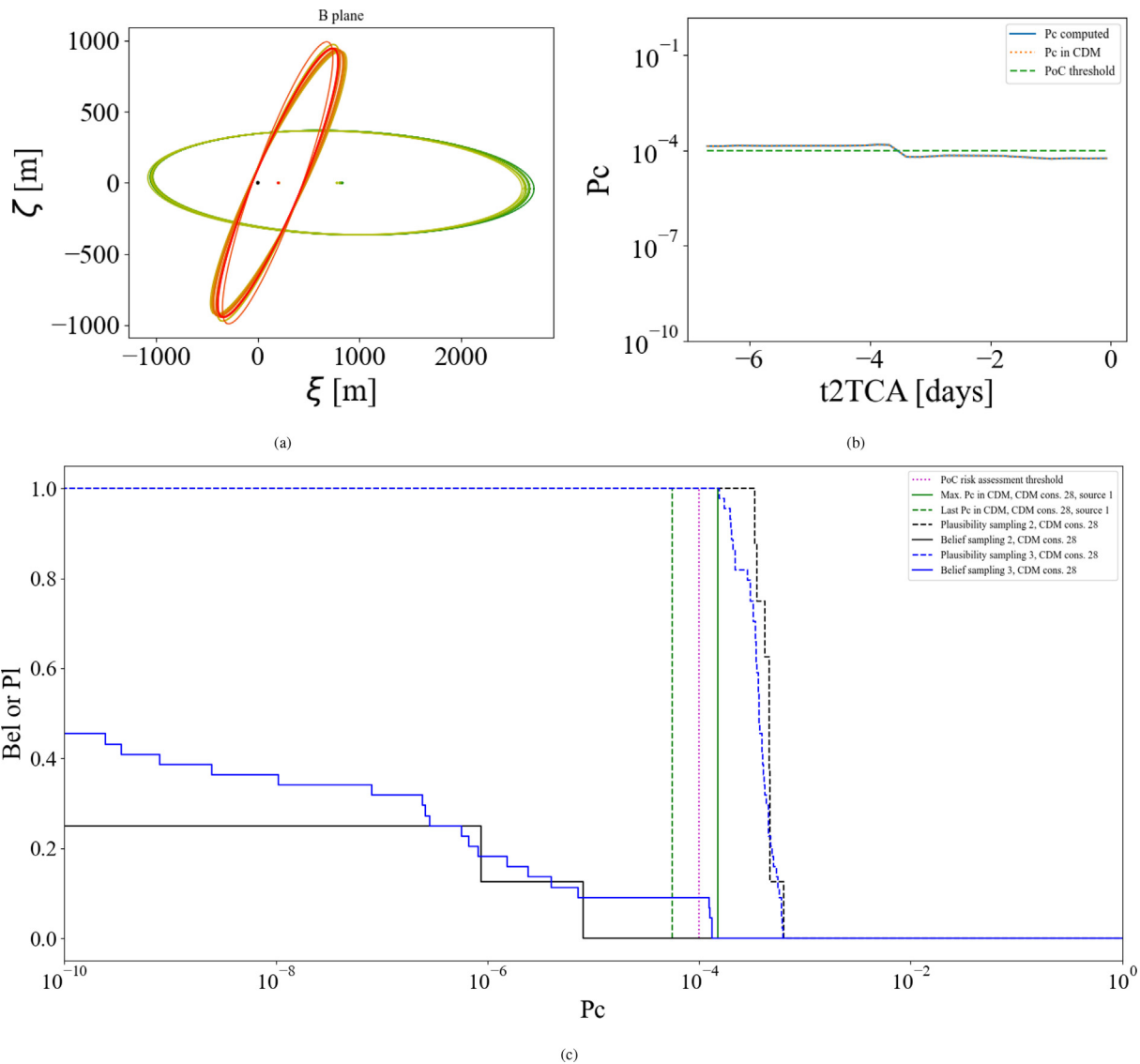| SDO		Evidence-based					
# events		A_0^*	# events	$T_d = 3$	$T_d = 2$	$T_d = 2$	$T_d = 0$
Total	36,072		Total	24,296	27,918	32,108	36,072
Escalated	20	0.1	Unc.	120	130	172	293
CAM	2		CAM	1	2	3	2
		0.5	Unc.	102	98	107	154
			CAM	19	34	68	141
		0.8	Unc.	95	83	77	75
			CAM	26	49	98	220

Fig. 23. Conjunction event with conflicting CDMs: (a) evolution of the relative position distribution on the impact place, (b) evolution of the PoC, (c) Pl and Bel curves of the whole CDMs sequence.

Note that the percentage of events in this category increases when delaying the decision. This indicates a growing disagreement among CDMs in the sequence as the time approaches TCA, an aspect usually overlooked by probabilistic-based approaches.

4.4. Treatment of uncertain cases

The approach proposed in this paper provides operators with a quantification of the uncertainty on the value of the PoC. In doing so it enables the operators to make decisions under uncertainty rather than under complete ignorance or false confidence in the correctness of the PoC. On the other hand the two uncertain cases, class 0 and 3, require additional information to lead to an action by the operator.

For class 3 the recommended course of action is to acquire additional information. If the sequence of CDMs so far has led to a class 3 the new information would need

to be of better quality to reduce the level of uncertainty. If the additional CDMs do not reduce the uncertainty the class escalates to 0. If in both class 0 and 3 additional information is not available one can rely on a trade-off between CAM cost and consequences of a collision. In Hejduk (2017) a methodology is suggested to quantify the possible consequences. This trade-off should include operational constraints and availability of new observations. An approach to come to an optimal decision with multi-criteria decision making (MCDM) was proposed in Sánchez and Vasile (2021) and can be applied in cascade to the approach proposed in this paper to come to a final decision in all uncertain cases.

Furthermore, as noted in one of the test cases presented in this paper, for both class 0 and 3 the $Pl(PoC_0)$ can be significantly higher than Pl_0 and reach 1 with a non-zero Bel, albeit with a large $A_{Pl,Bel}$. Both class 0 and 3 do not differentiate between cases in which $Pl(PoC_0)$ is marginally

above Pl_0 and cases in which $Pl(PoC_0) = 1$. Hence, in all uncertain cases, operators are advised to check the degree of supporting evidence by inspecting the Pl/Bel curves. Furthermore, the value of $Pl(PoC_0)$ and $Bel(PoC_0)$ can be included in the MCDM approach mentioned above. This point will be the subject of future developments.

5. Conclusions

This work presented a methodology to model and quantify the epistemic uncertainty in a sequence of CDMs, and exploit this quantification to make robust decisions about conjunction events. The method was tested against real operations on a number of real scenarios. The key working assumption was that the value of the miss distance and covariance matrix in each CDM were drawn from a set of unknown distributions. The DKW inequality was used to build bounds on this set and derive a set of focal elements, with associated probability mass supporting a given value of the probability of collision.

The collection of focal elements was used to compute the Pl and Bel on a given value of the PoC. The Pl at PoC_0, or Pl_0 was proposed as a further criterion to make a decision on the actual severity of a conjunction event, while the difference between Pl and Bel, or $A_{Pl,Bel}$, was proposed as a measure of the uncertainty in the quantification of the PoC.

It was found that when the set of CDMs contains coherent information over the whole time series, the proposed classification system suggests the same decisions normally made by the ESA SDO. When the sequence of CDMs presents a higher degree of variability or a degree of inconsistency the proposed evidence-based approach recommends more conservative decisions compared to the SDO but also provides the operator with a quantification of the related uncertainty.

A comparison with the approach used at CNES, based on the concept of sPoC, showed that the proposed evidence-based approach returns decisions that are less conservative but, at the same time, provides a higher level of information on the uncertainty in the decision. By comparing the ESA and CNES uncertain cases, it was also found that a further inspection of the Pl and Bel curves offers a way to disambiguate the events as the different evolution of PoC over time is reflected in a lower or higher value of Pl and Bel.

Finally, a statistical analysis on a database of real encounters of an ESA mission showed that the number of recommended CAMs is similar but the evidence-based approach tends to detect a higher number of uncertain cases that require further analysis.

Although in our analysis no operational constraints were considered, the number of detected uncertain cases suggests that relying only on the last CDM may be too optimistic while the scaled PoC approach might be too pessimistic without a further uncertainty quantification. In relation to the uncertain cases, different situations can be found which

may lead the operator to take different actions. Further analysis on the treatment of these scenarios should be taken and a threshold tuning analysis using virtual datasets or a mixed dataset of real and virtual CDMs may help with this task. The approach proposed in this paper assumes that no additional information on the CDMs is available nor that information on the uncertainty in the propagation model or individual observations can be used. However, if additional information was available one could improve the quantification of uncertainty of each CDMs and build better defined p-boxes with tighter bounds.

Future work will need to consider the correlation and interdependence among variables during the construction of the focal elements and build a more refined model. Furthermore, the current databases of real CDMs do not represent a controlled set of events, because the actual outcome is unknown. A representative synthetic database would greatly help in improving the classification system. Last but not least, machine learning can be used to directly classify events from the time series of CDMs. This approach represents an extension of what was already proposed by the authors and would improve on current efforts to predict the last CDM with machine learning as it would embed a quantification of uncertainty in the prediction.

Declaration of Competing Interest

The authors declare that they have no known competing financial interests or personal relationships that could have appeared to influence the work reported in this paper.

Acknowledgements

Appendix A. Appendix

This appendix includes the sequence of CDMs for *Event #3*. It includes the geometry, the covariance determinant evolution and fit, the intervals weighting law and the Pl and Bel curves for 3, 4 and 5 α-cuts (or intervals per dimension).
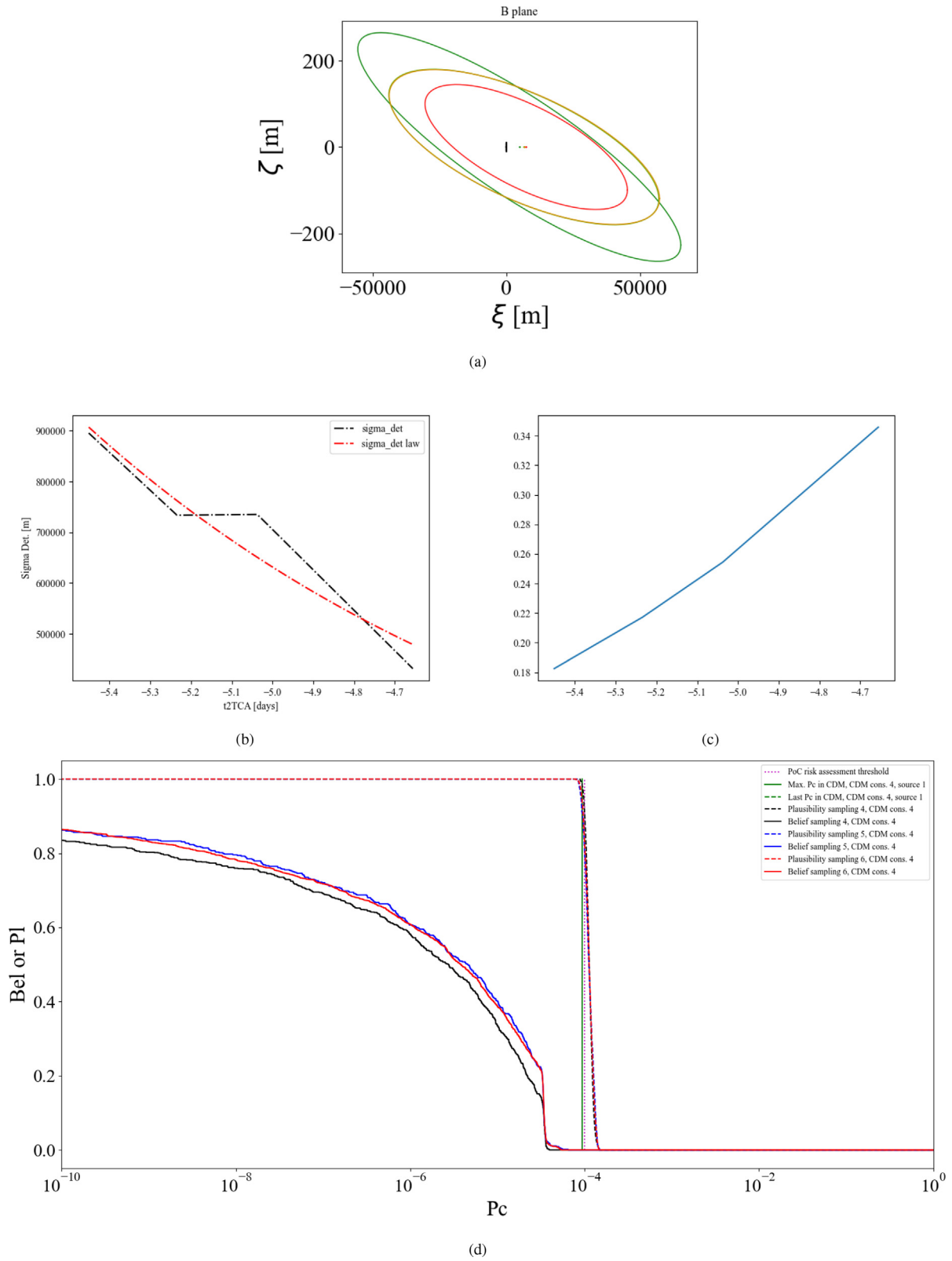
(a)

(b)

(c)

(d)

Fig. 24: Sequence for Event #3. Number of CDM 4. (a) Encounter geometry, (b) Covariance determinant (CDM in black, fit in red), (c) Weighting law, (d) Bel (solid) and Pl (dashed) curve for 3 (blue), 4 (black),and 5 (red) intervals.
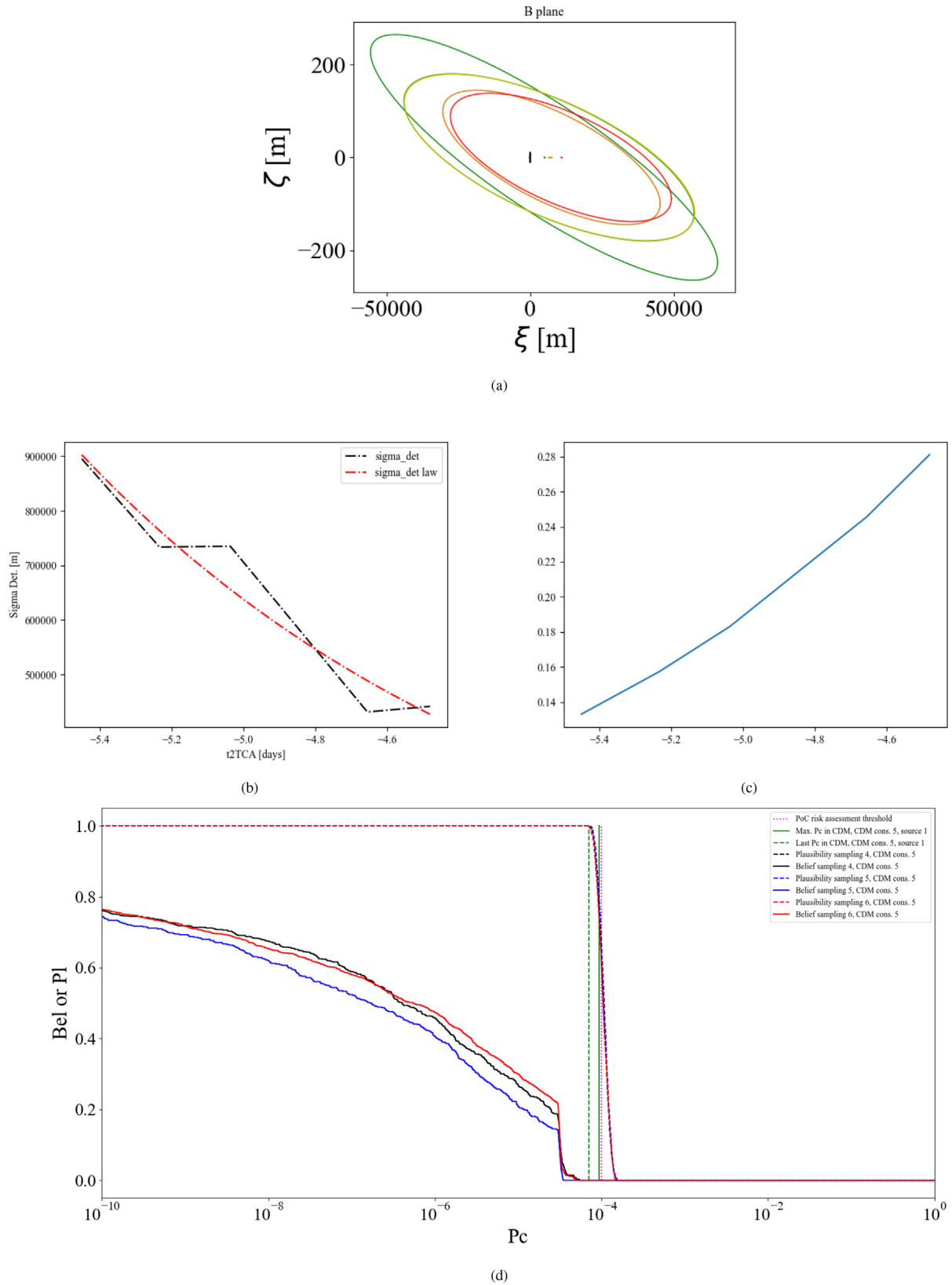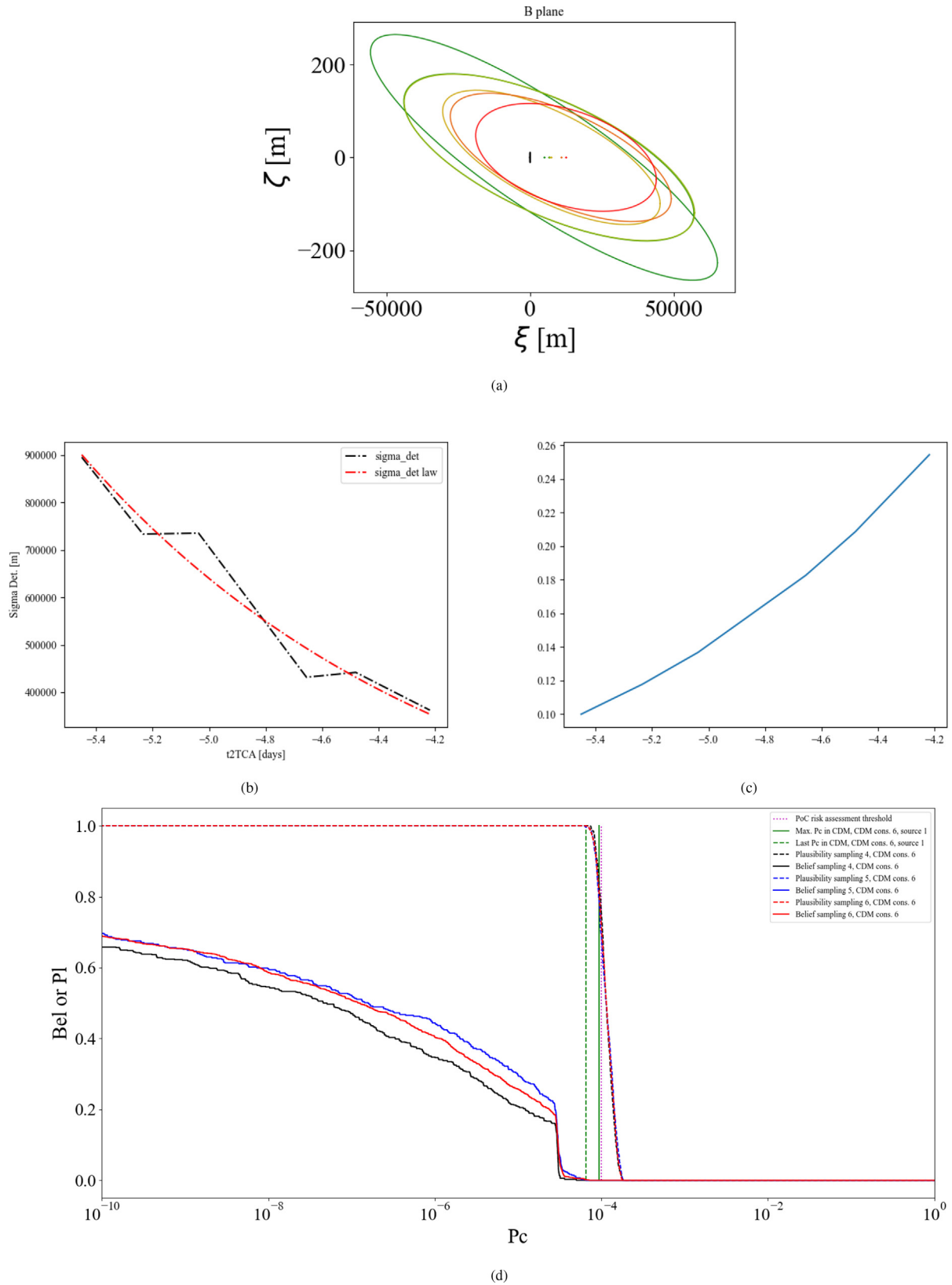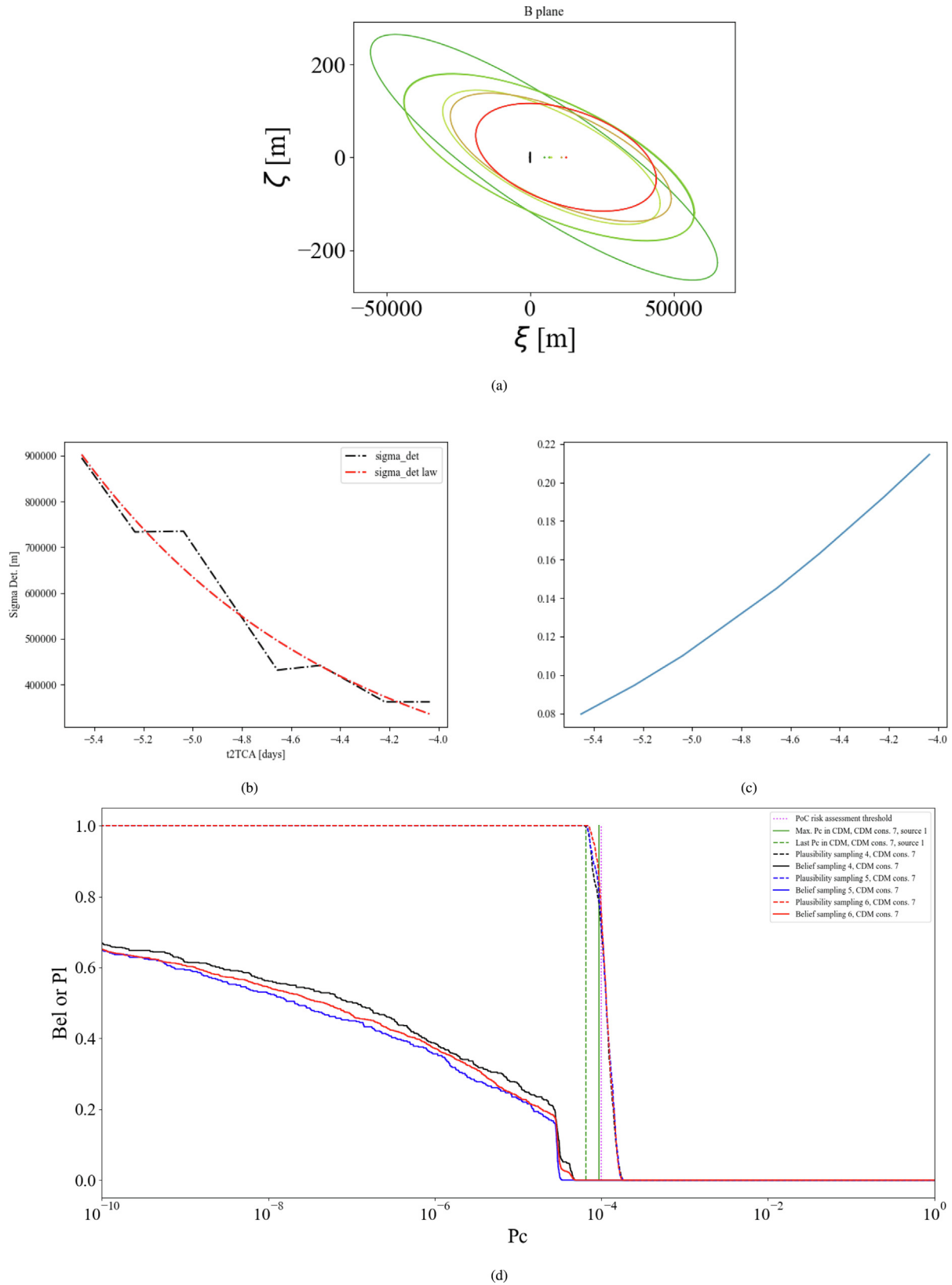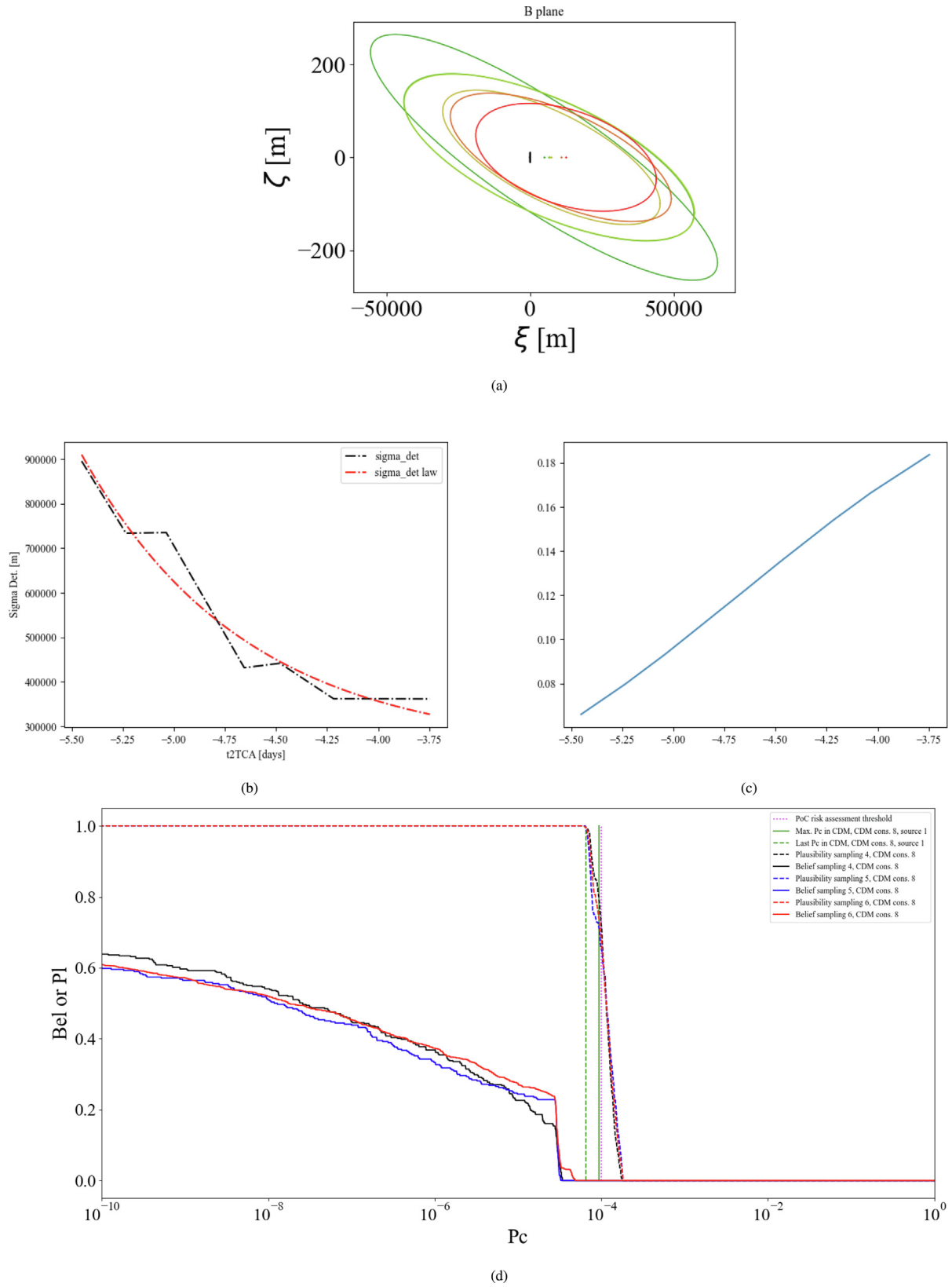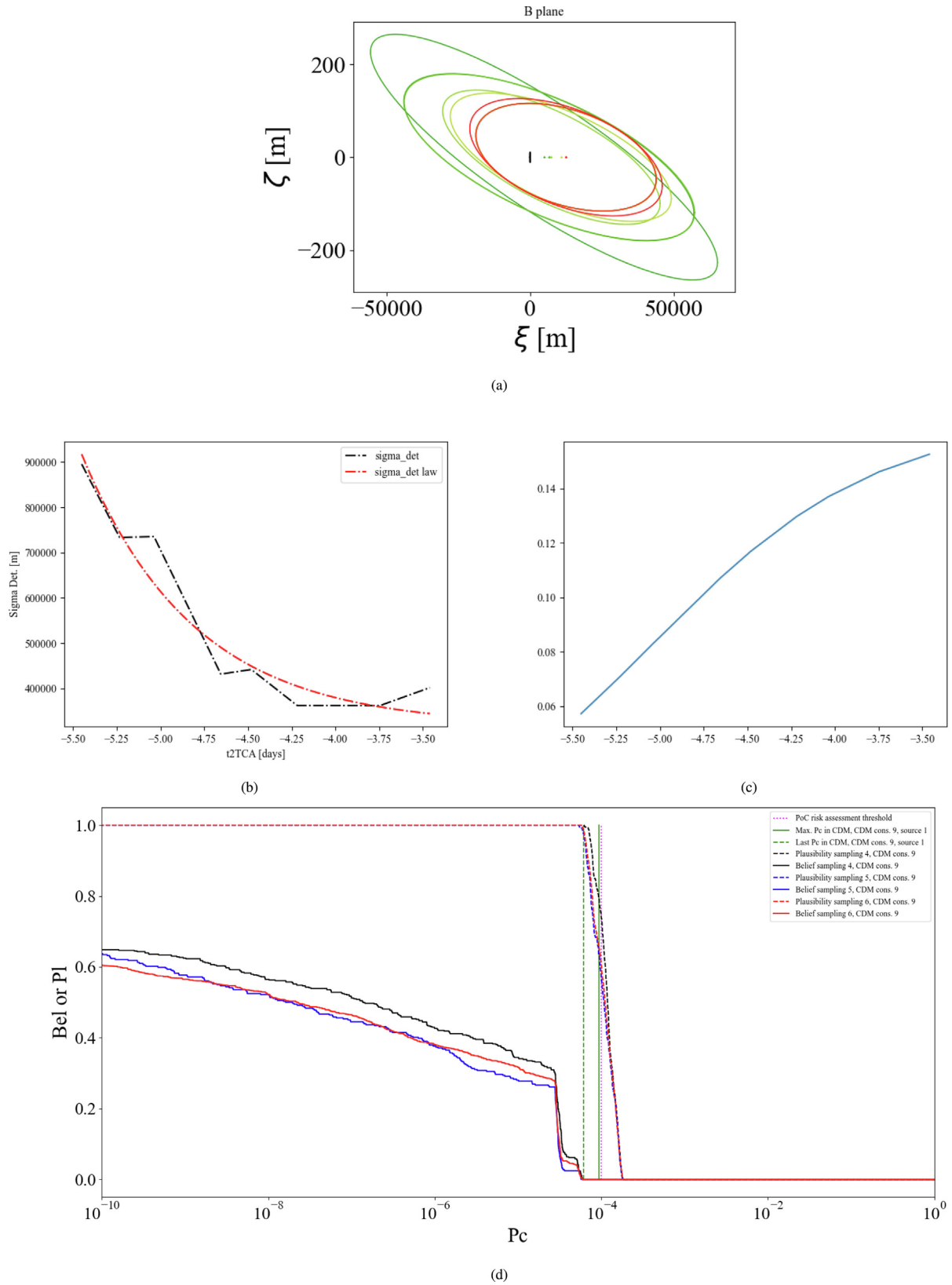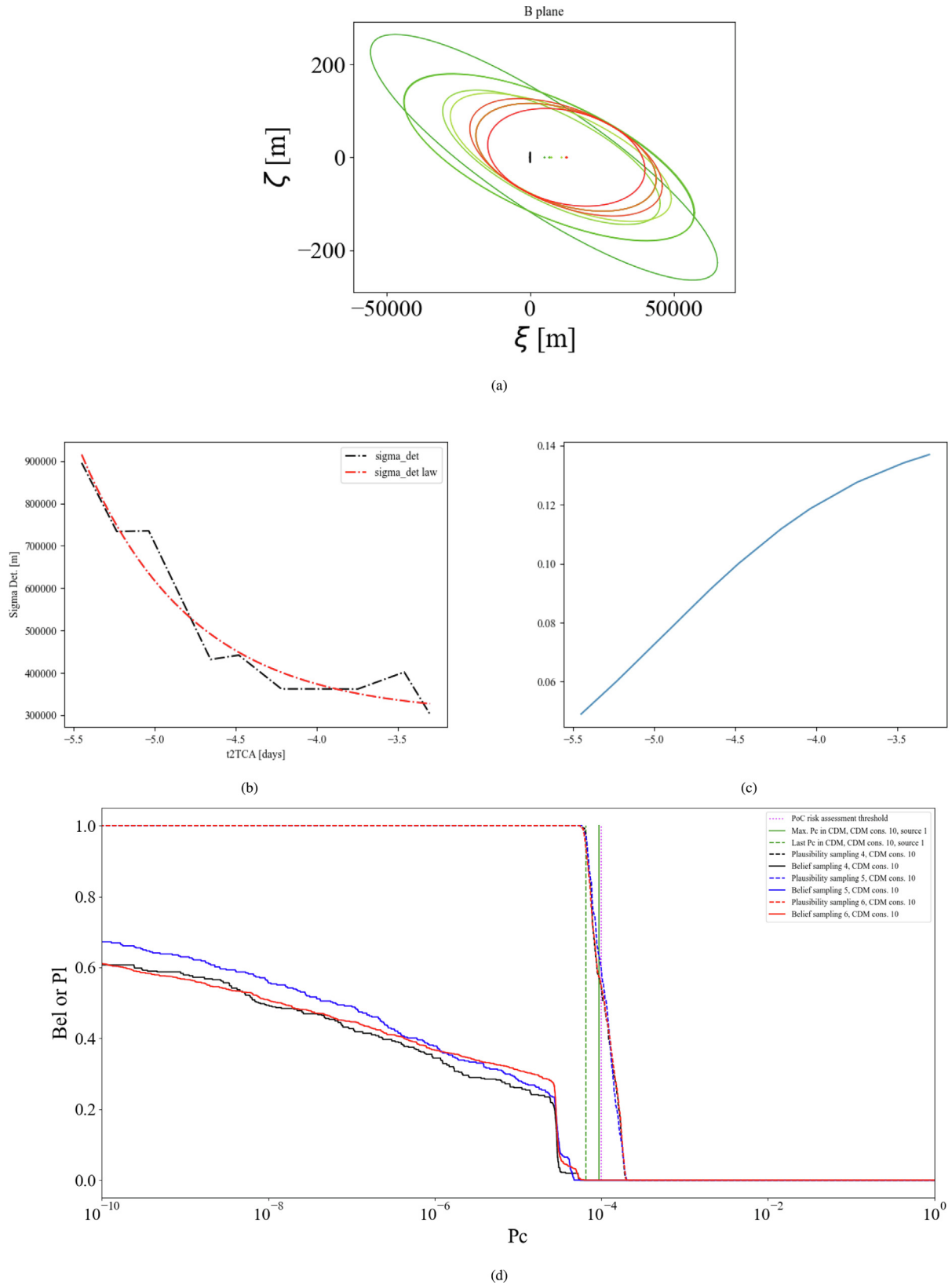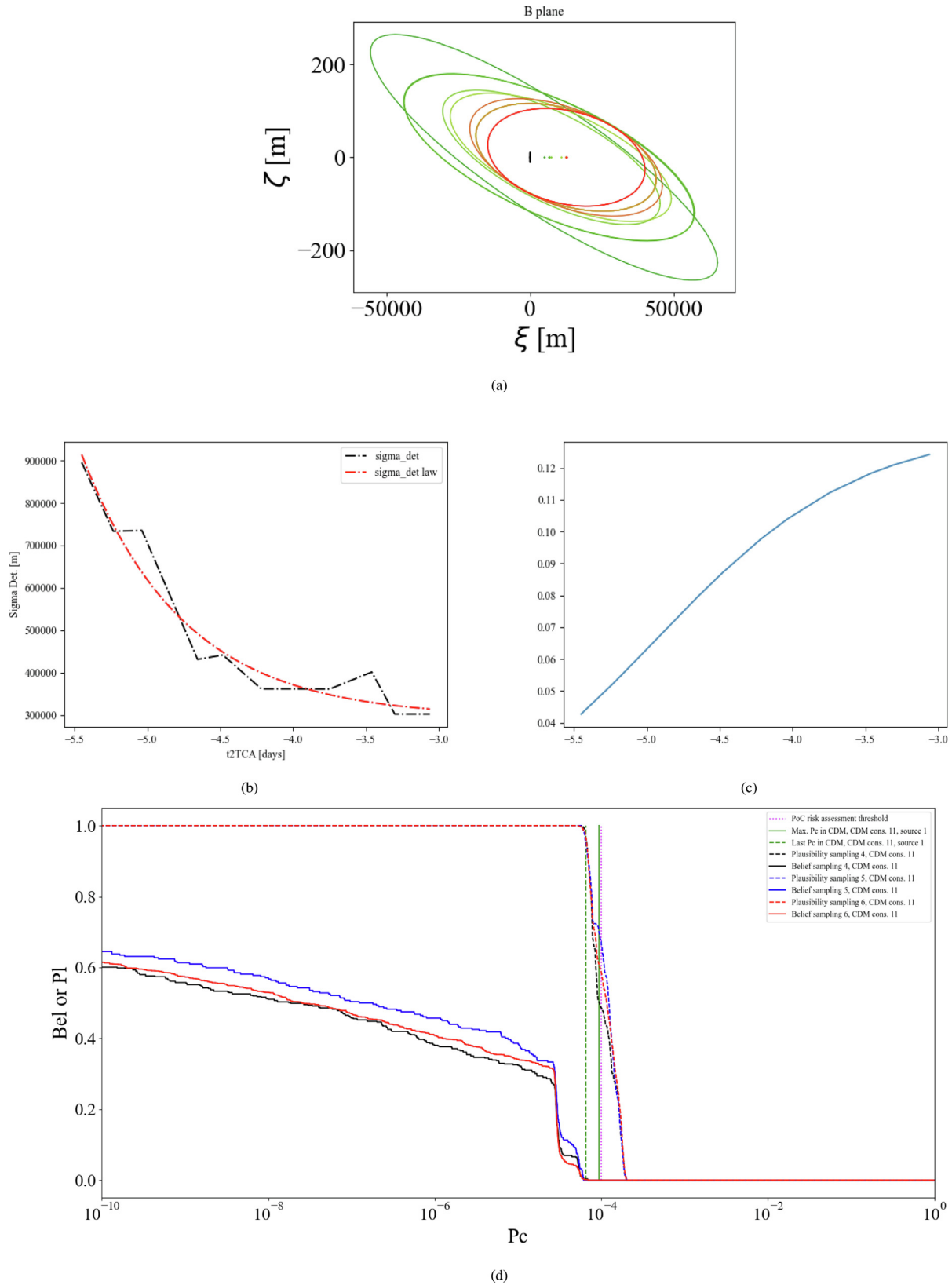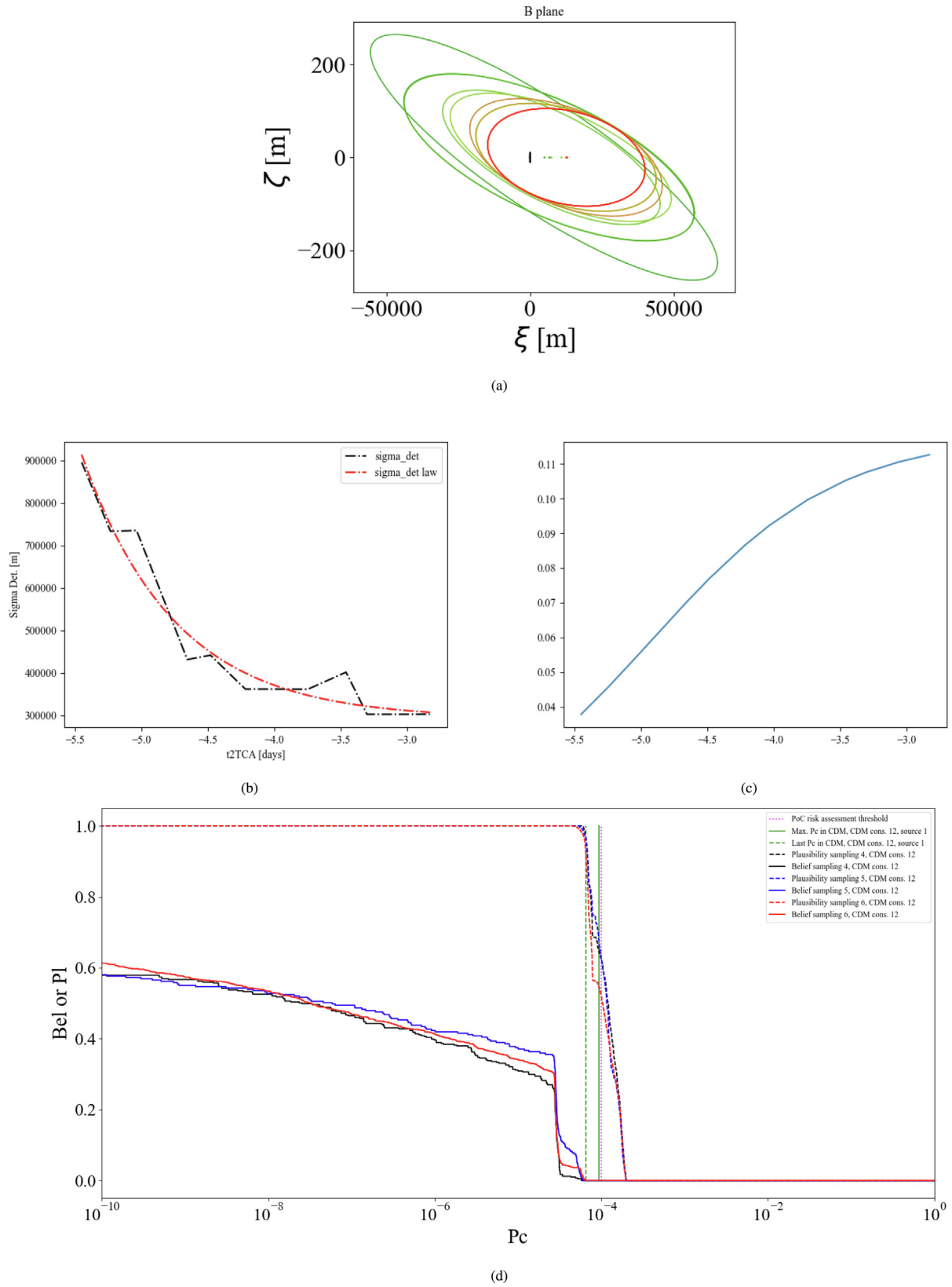
Fig. 25: Sequence for Event #3. Number of CDM 5. (a) Encounter geometry, (b) Covariance determinant (CDM in black, fit in red), (c) Weighting law, (d) Bel (solid) and Pl (dashed) curve for 3 (blue), 4 (black), and 5 (red) intervals.
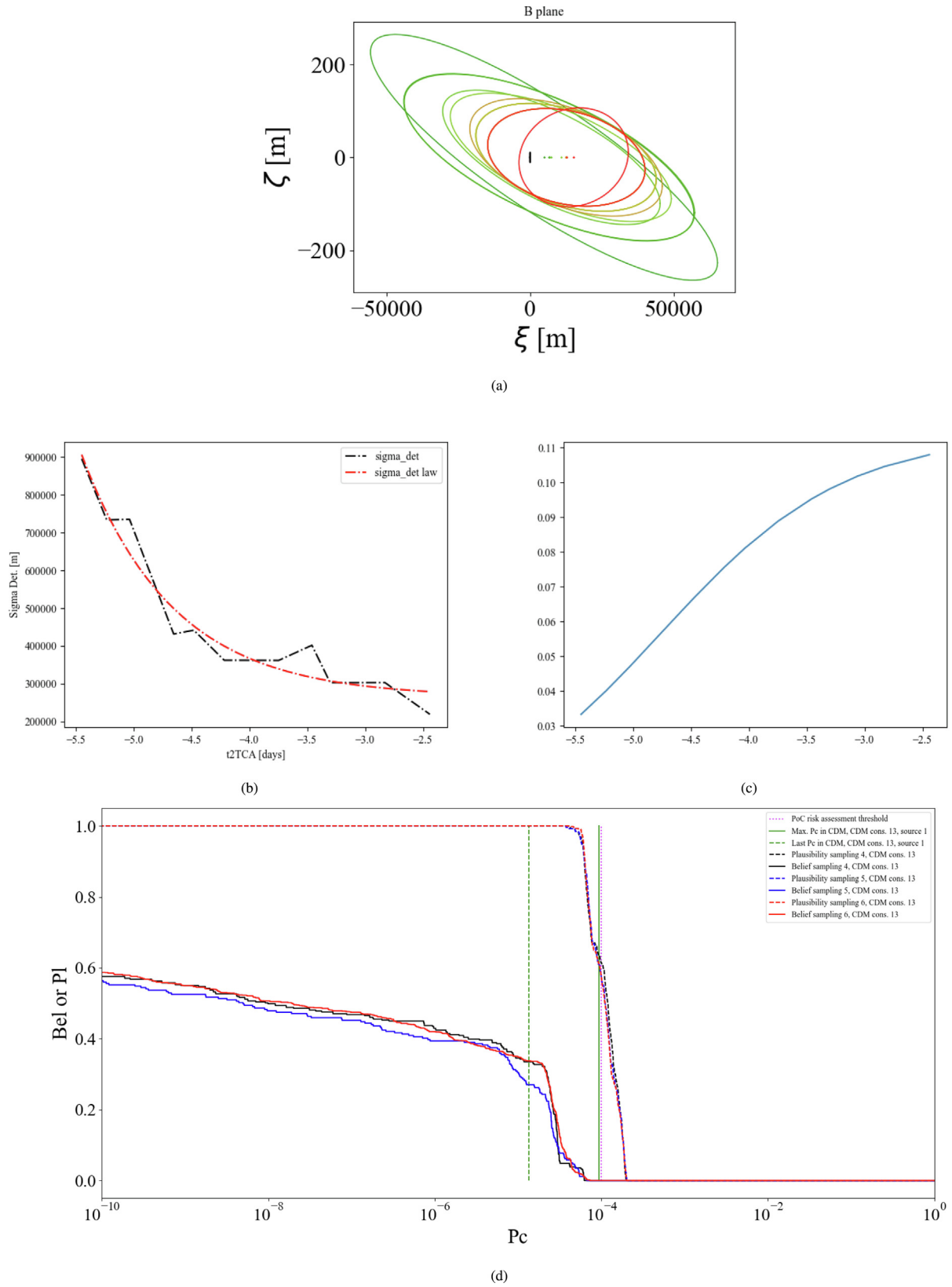
(a)

(b)

(c)

(d)

Fig. 26: Sequence for Event #3. Number of CDM 6. (a) Encounter geometry, (b) Covariance determinant (CDM in black, fit in red), (c) Weighting law, (d) Bel (solid) and Pl (dashed) curve for 3 (blue),4 (black),and 5 (red) intervals.

Fig. 27: Sequence for Event #3. Number of CDM 7. (a) Encounter geometry, (b) Covariance determinant (CDM in black, fit in red), (c) Weighting law, (d) Bel (solid) and Pl (dashed) curve for 3 (blue),4 (black),and 5 (red) intervals.
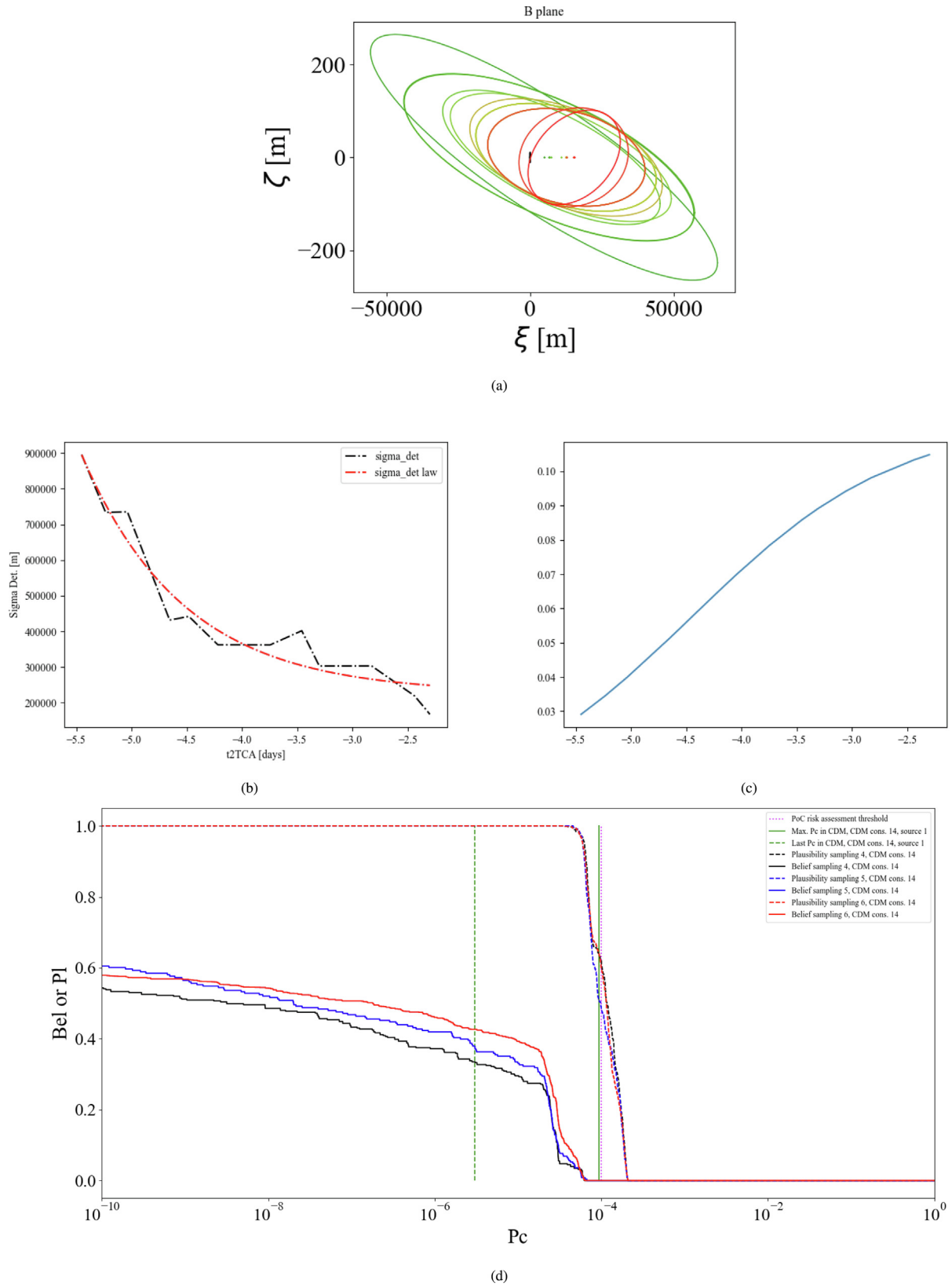
Fig. 28: Sequence for Event #3. Number of CDM 8. (a) Encounter geometry, (b) Covariance determinant (CDM in black, fit in red), (c) Weighting law, (d) Bel (solid) and Pl (dashed) curve for 3 (blue),4 (black),and 5 (red) intervals.

Fig. 29: Sequence for Event #3. Number of CDM 9. (a) Encounter geometry, (b) Covariance determinant (CDM in black, fit in red), (c) Weighting law, (d) Bel (solid) and Pl (dashed) curve for 3 (blue),4 (black),and 5 (red) intervals.
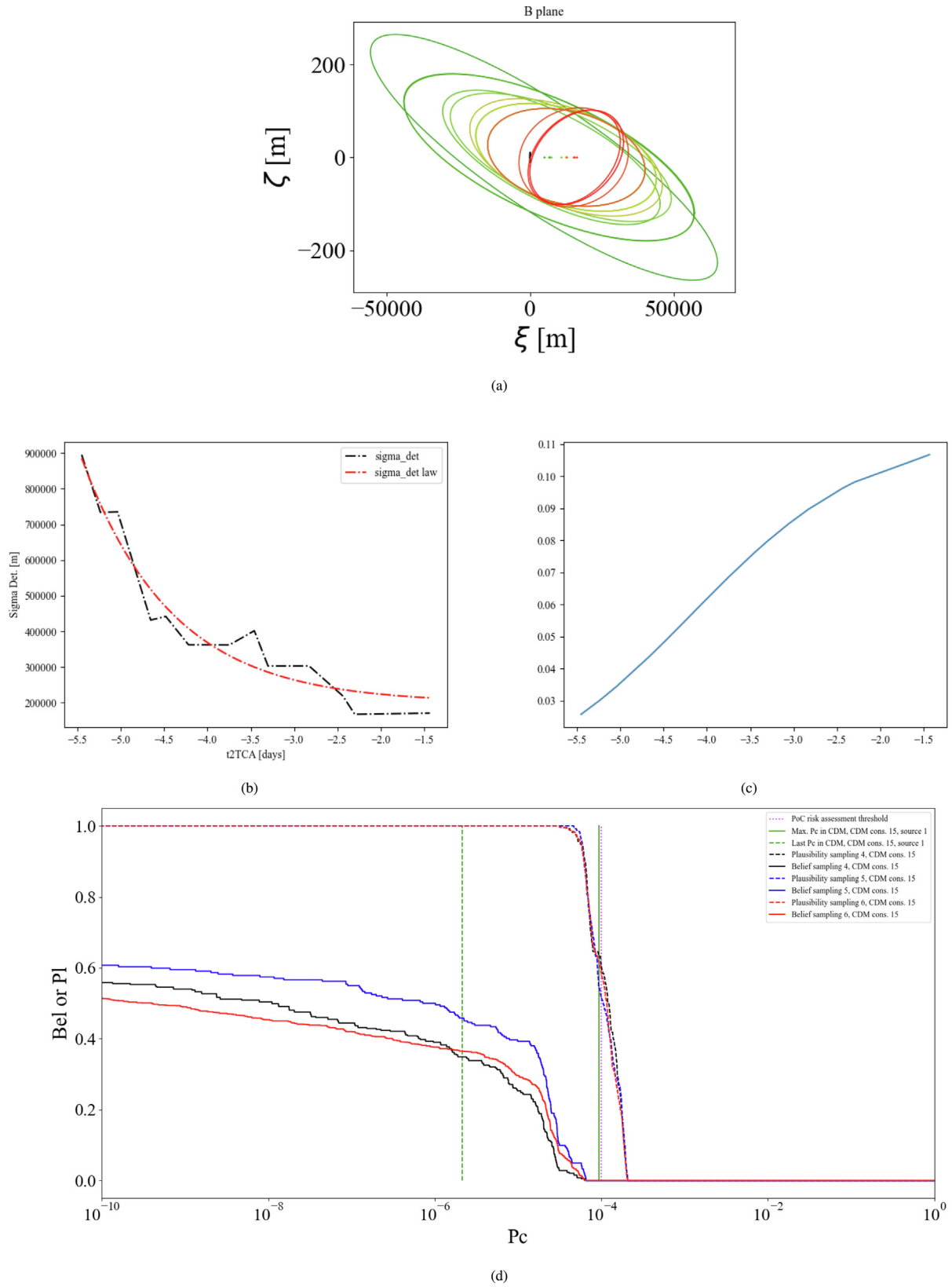
Fig. 30: Sequence for Event #3. Number of CDM 10. (a) Encounter geometry, (b) Covariance determinant (CDM in black, fit in red), (c) Weighting law, (d) Bel (solid) and Pl (dashed) curve for 3 (blue),4 (black),and 5 (red) intervals.
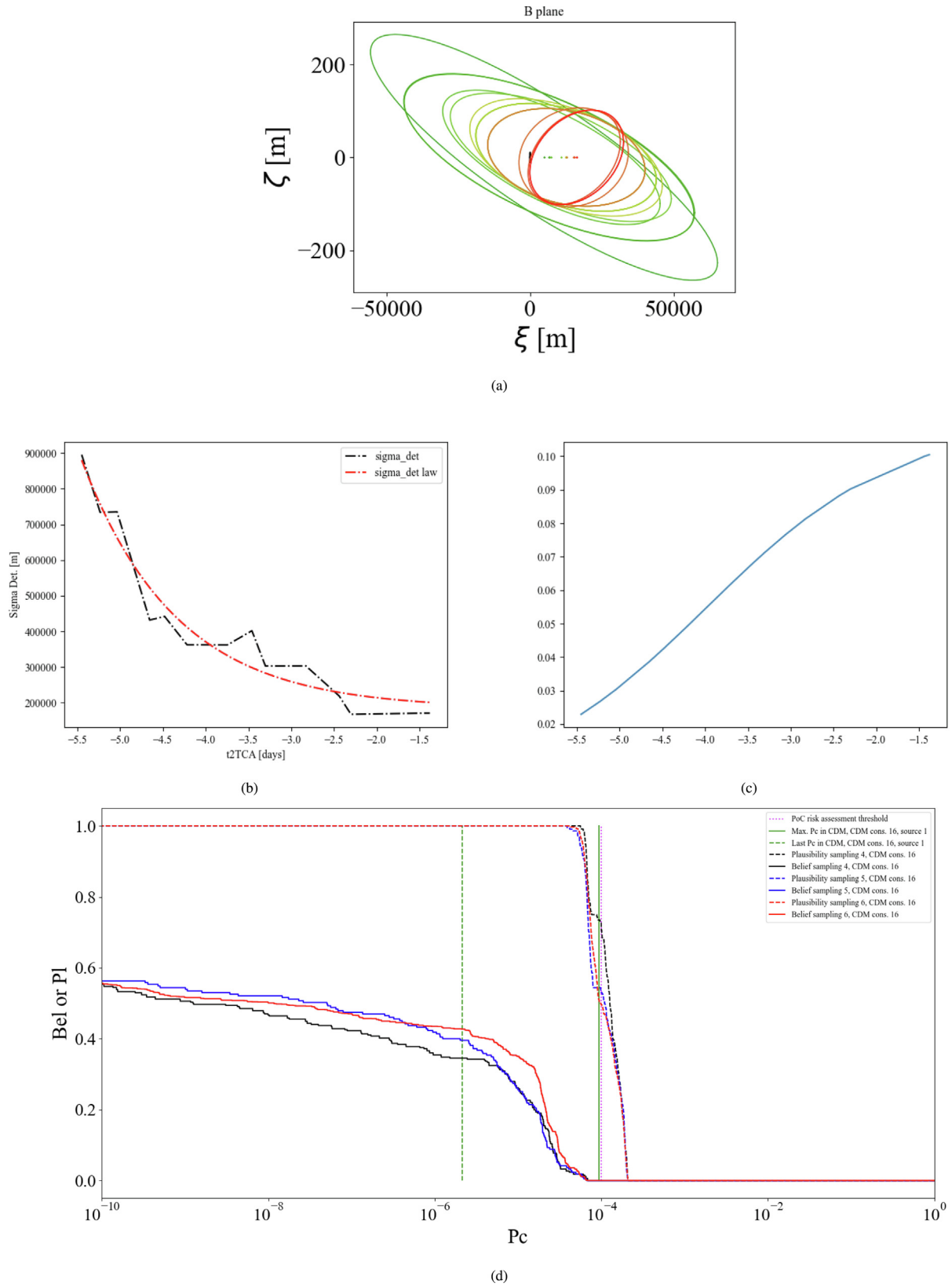
Fig. 31: Sequence for Event #3. Number of CDM 11. (a) Encounter geometry, (b) Covariance determinant (CDM in black, fit in red), (c) Weighting law, (d) Bel (solid) and Pl (dashed) curve for 3 (blue),4 (black),and 5 (red) intervals.

Fig. 32: Sequence for Event #3. Number of CDM 12. (a) Encounter geometry, (b) Covariance determinant (CDM in black, fit in red), (c) Weighting law, (d) Bel (solid) and Pl (dashed) curve for 3 (blue),4 (black),and 5 (red) intervals.
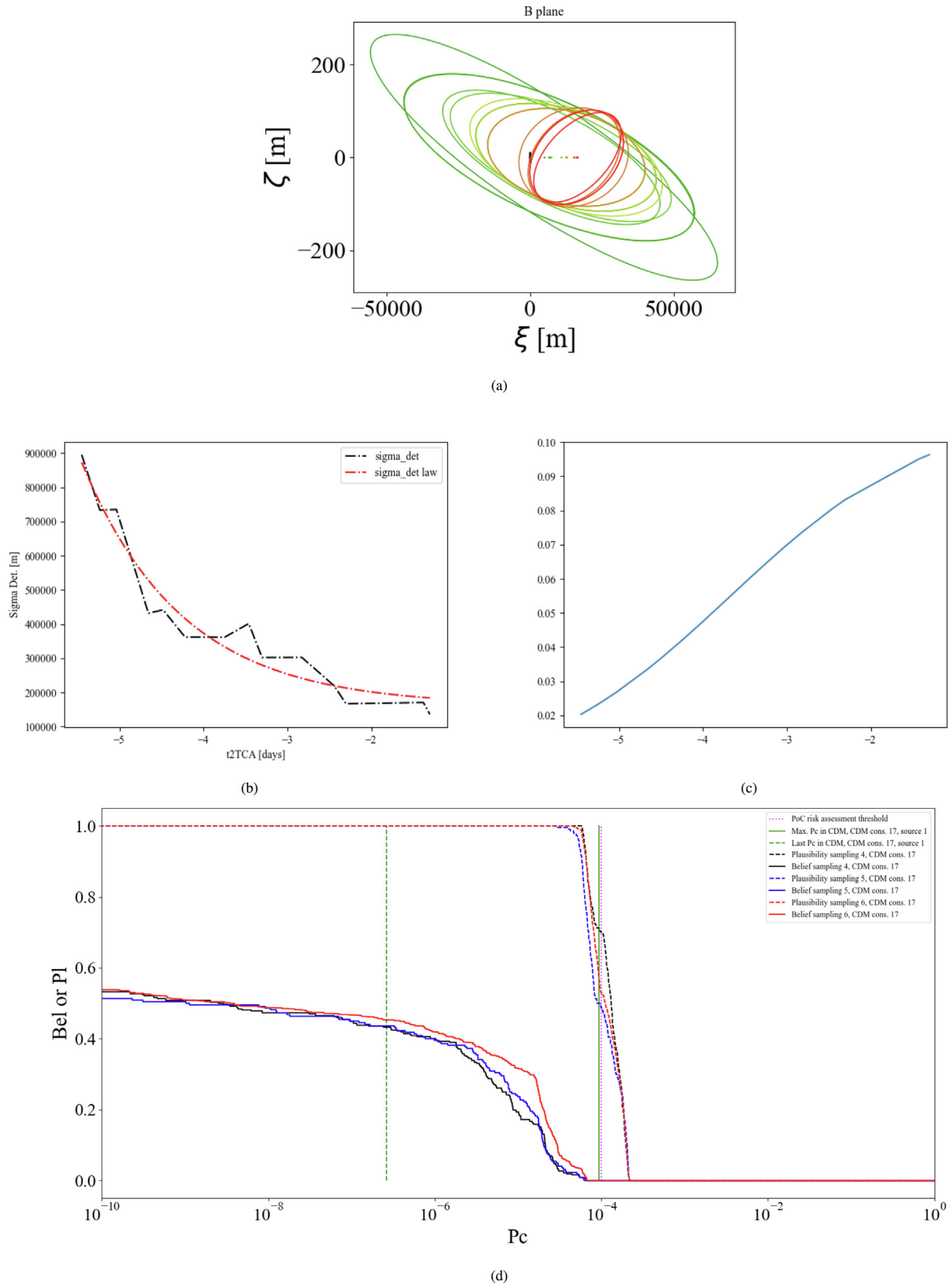
(a)

(b)   (c)

(d)

Fig. 33: Sequence for Event #3. Number of CDM 13. (a) Encounter geometry, (b) Covariance determinant (CDM in black, fit in red), (c) Weighting law, (d) Bel (solid) and Pl (dashed) curve for 3 (blue),4 (black),and 5 (red) intervals.
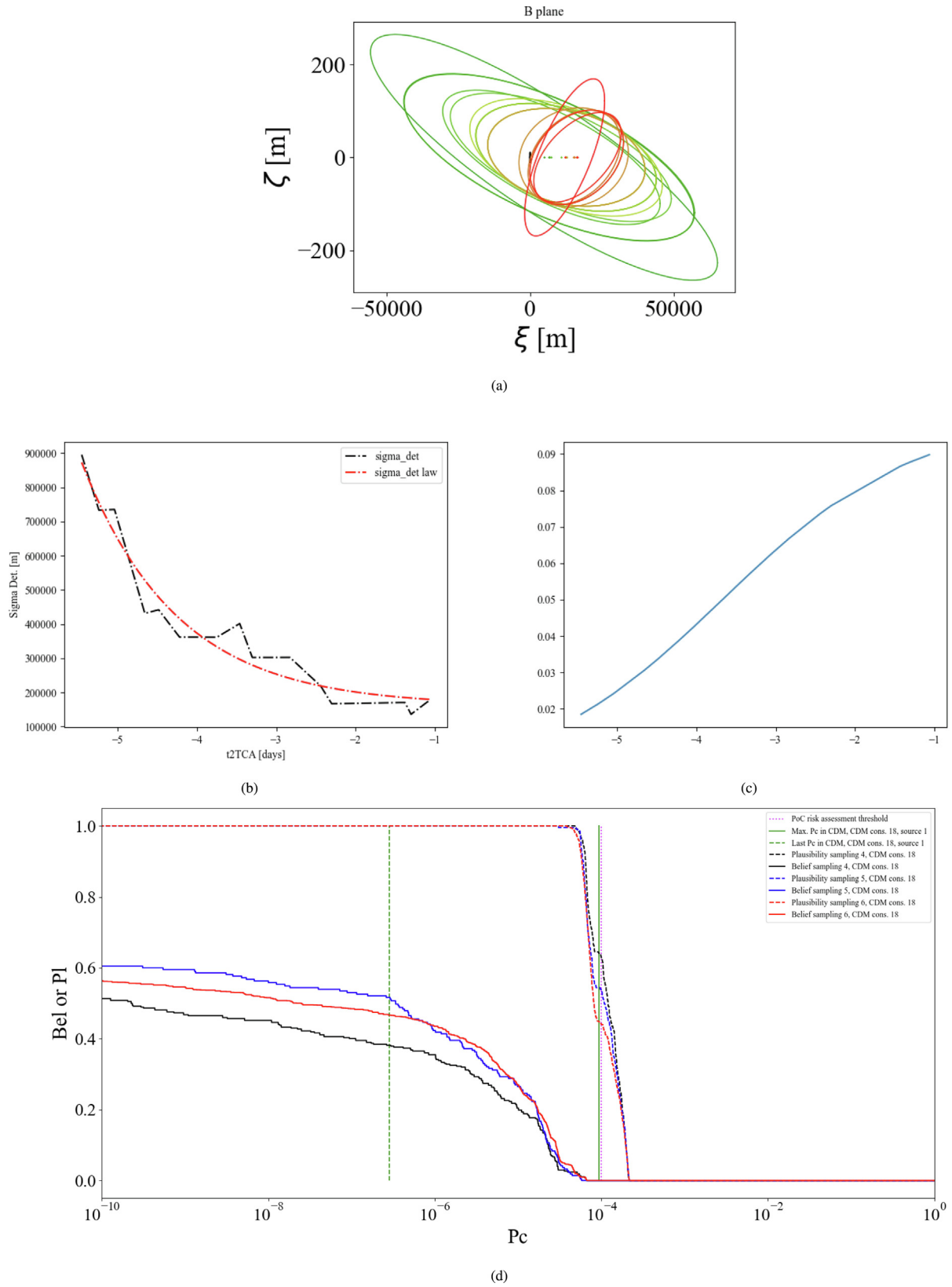
(a)

(b)

(c)

(d)

Fig. 34: Sequence for Event #3. Number of CDM 14. (a) Encounter geometry, (b) Covariance determinant (CDM in black, fit in red), (c) Weighting law, (d) Bel (solid) and Pl (dashed) curve for 3 (blue),4 (black),and 5 (red) intervals.

Fig. 35: Sequence for Event #3. Number of CDM 15. (a) Encounter geometry, (b) Covariance determinant (CDM in black, fit in red), (c) Weighting law, (d) Bel (solid) and Pl (dashed) curve for 3 (blue),4 (black),and 5 (red) intervals.
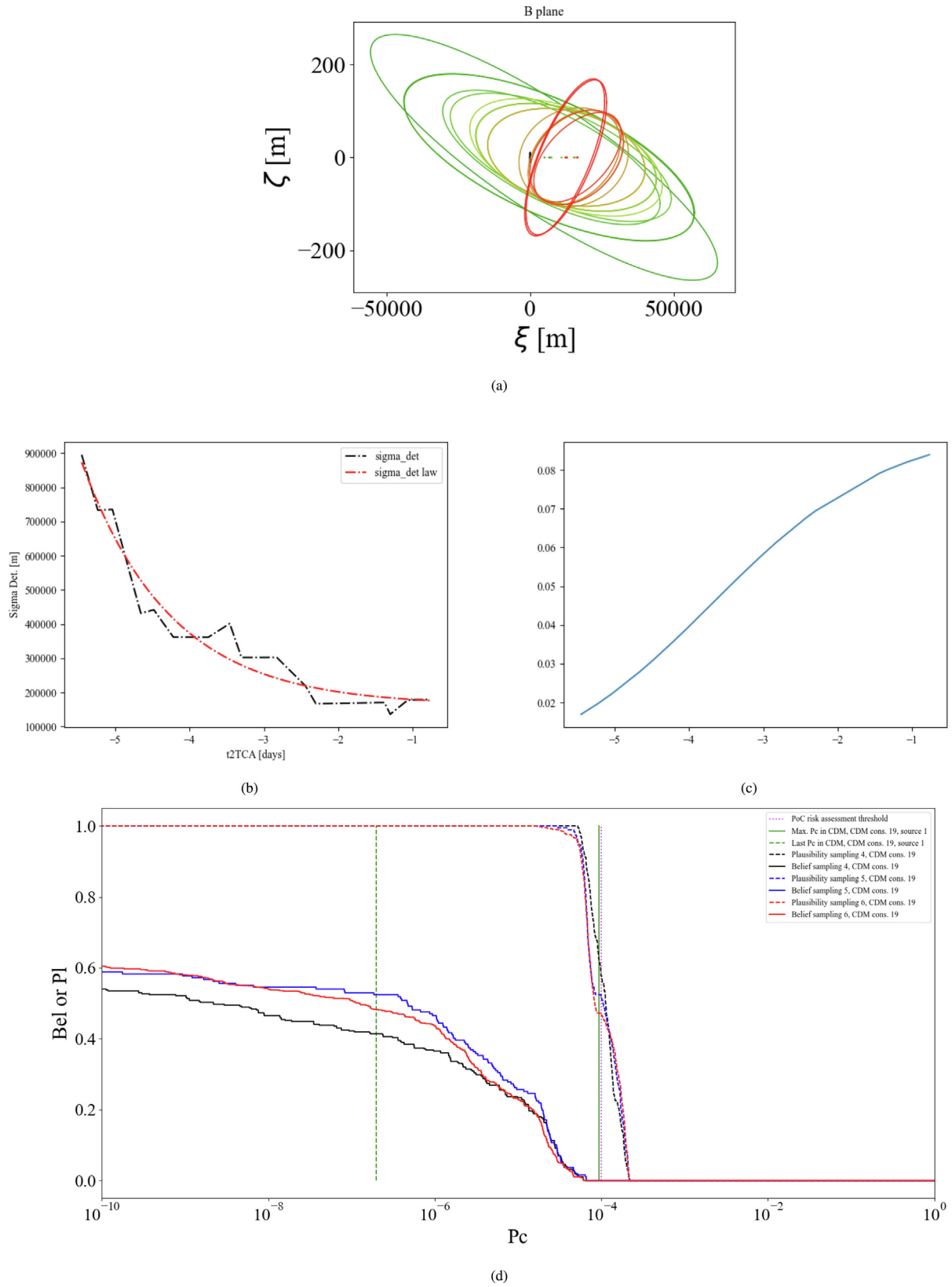
(a)

(b)

(c)

(d)

Fig. 36: Sequence for Event #3. Number of CDM 16. (a) Encounter geometry, (b) Covariance determinant (CDM in black, fit in red), (c) Weighting law, (d) Bel (solid) and Pl (dashed) curve for 3 (blue),4 (black),and 5 (red) intervals.
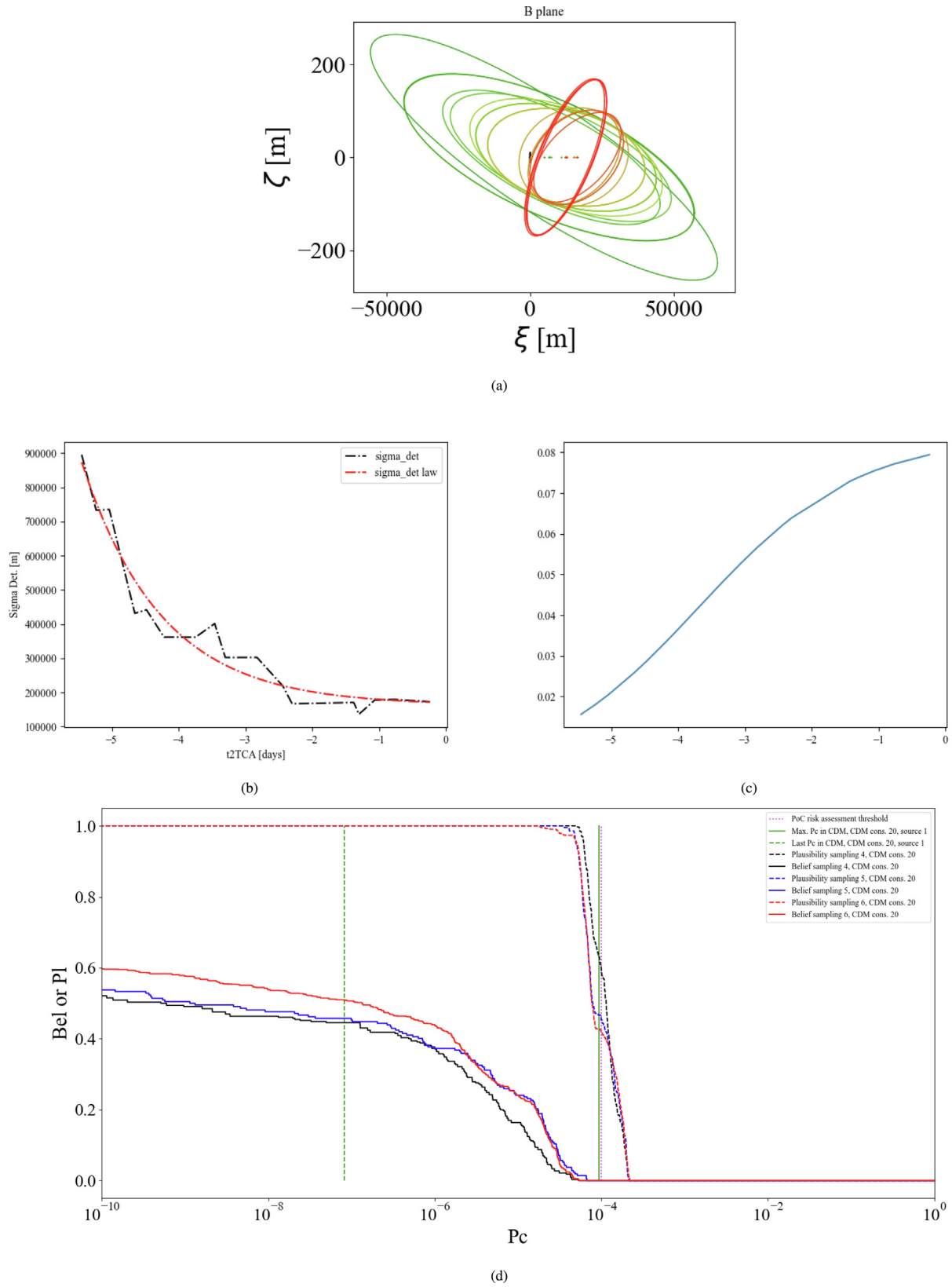
Fig. 37: Sequence for Event #3. Number of CDM 17. (a) Encounter geometry, (b) Covariance determinant (CDM in black, fit in red), (c) Weighting law, (d) Bel (solid) and Pl (dashed) curve for 3 (blue),4 (black),and 5 (red) intervals.

Fig. 38: Sequence for Event #3. Number of CDM 18. (a) Encounter geometry, (b) Covariance determinant (CDM in black, fit in red), (c) Weighting law, (d) Bel (solid) and Pl (dashed) curve for 3 (blue),4 (black),and 5 (red) intervals.
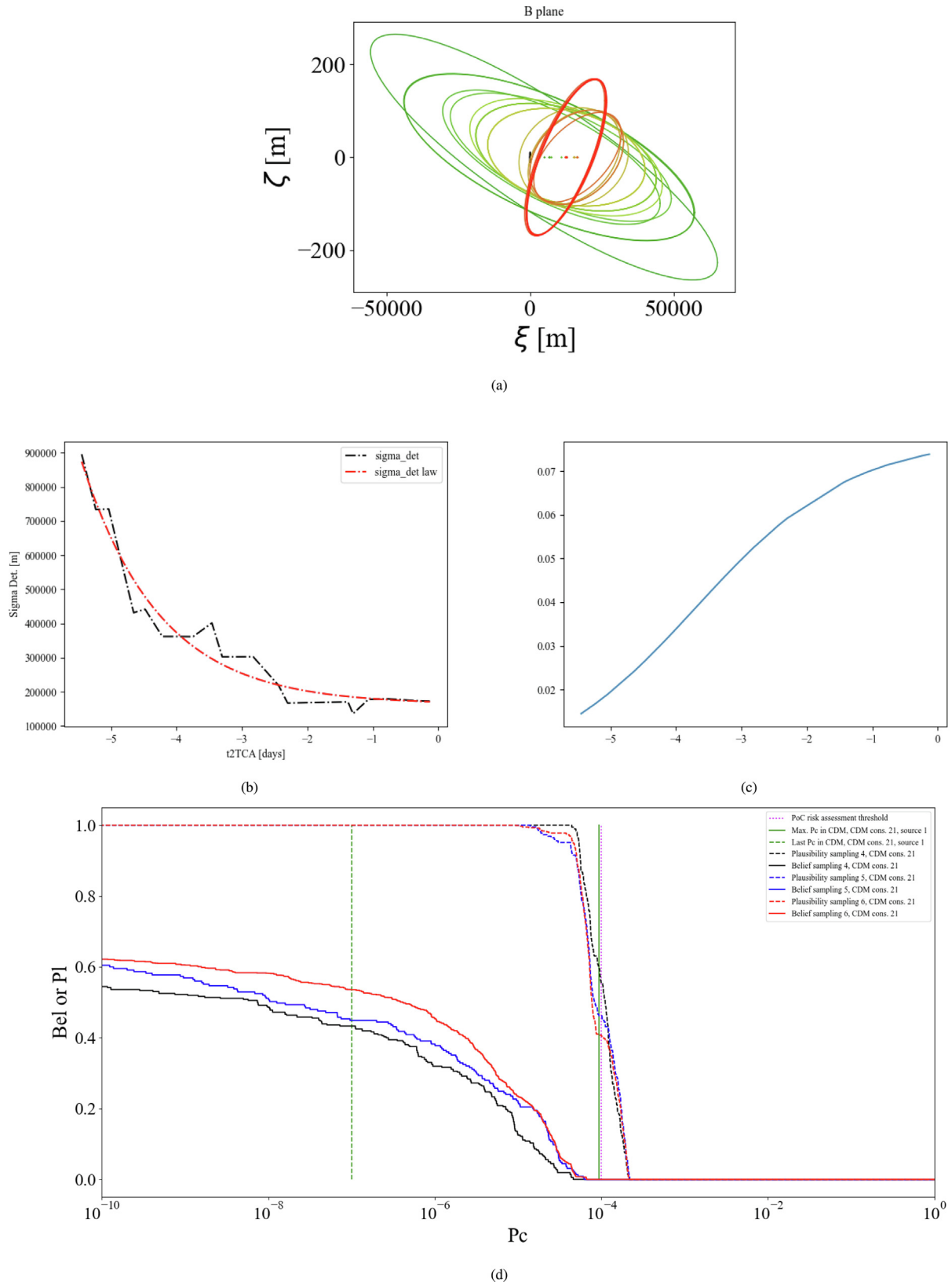
Fig. 39: Sequence for Event #3. Number of CDM 19. (a) Encounter geometry, (b) Covariance determinant (CDM in black, fit in red), (c) Weighting law, (d) Bel (solid) and Pl (dashed) curve for 3 (blue),4 (black),and 5 (red) intervals.
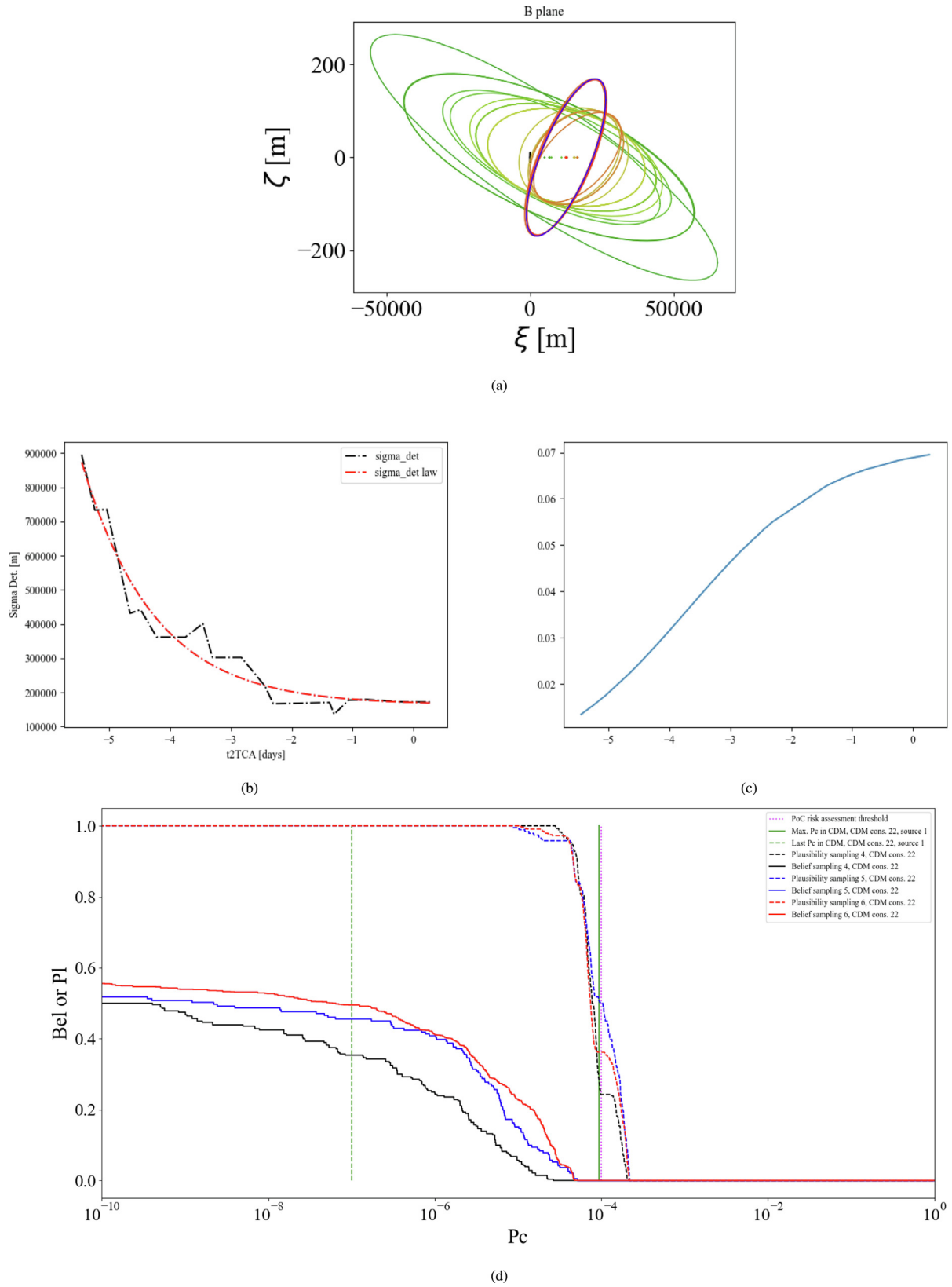
Fig. 40: Sequence for Event #3. Number of CDM 20. (a) Encounter geometry, (b) Covariance determinant (CDM in black, fit in red), (c) Weighting law, (d) Bel (solid) and Pl (dashed) curve for 3 (blue),4 (black),and 5 (red) intervals.

Fig. 41: Sequence for Event #3. Number of CDM 21. (a) Encounter geometry, (b) Covariance determinant (CDM in black, fit in red), (c) Weighting law, (d) Bel (solid) and Pl (dashed) curve for 3 (blue),4 (black),and 5 (red) intervals.
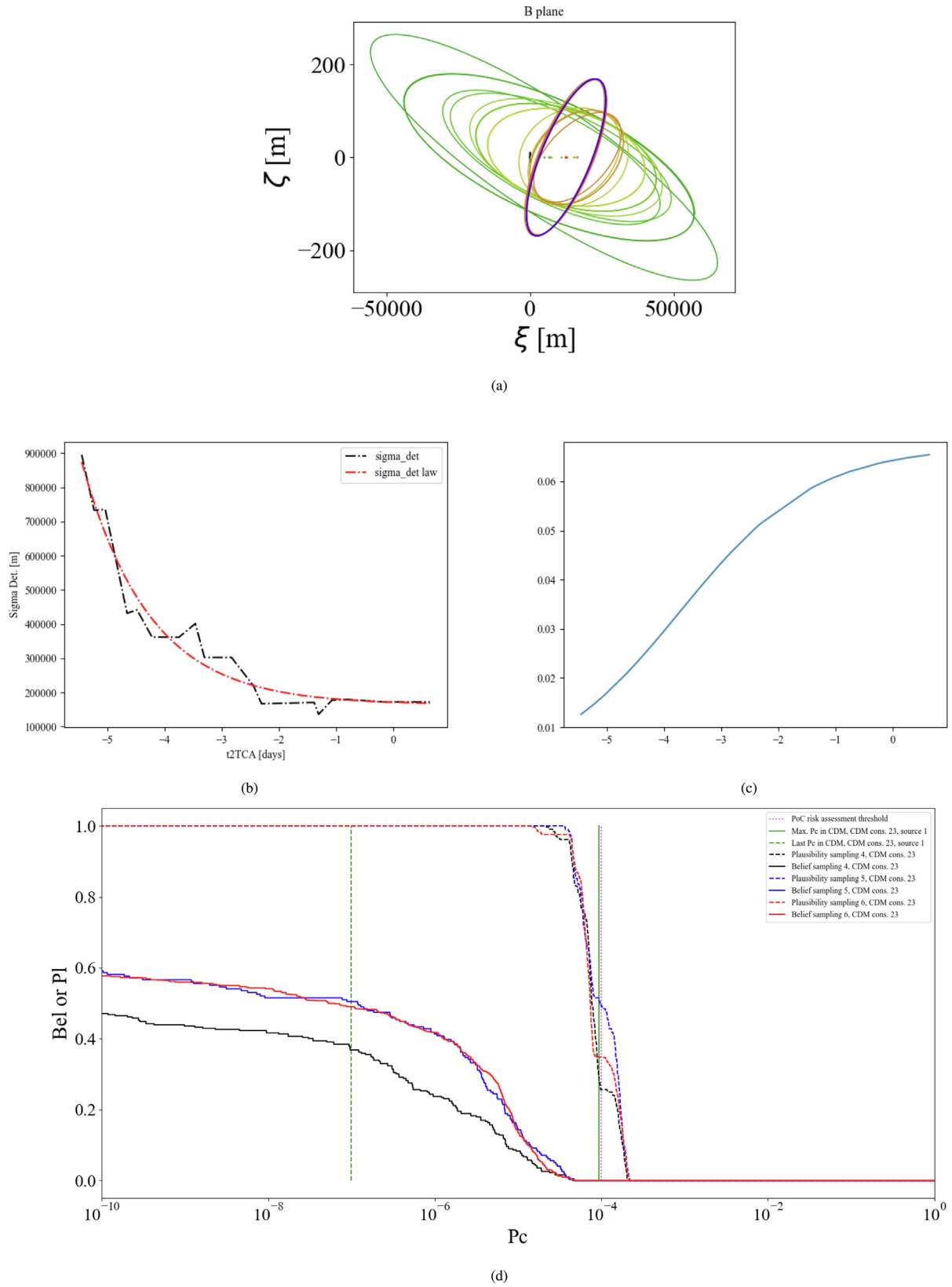
Fig. 42: Sequence for Event #3. Number of CDM 22. (a) Encounter geometry, (b) Covariance determinant (CDM in black, fit in red), (c) Weighting law, (d) Bel (solid) and Pl (dashed) curve for 3 (blue),4 (black),and 5 (red) intervals.

Fig. 43: Sequence for Event #3. Number of CDM 23. (a) Encounter geometry, (b) Covariance determinant (CDM in black, fit in red), (c) Weighting law, (d) Bel (solid) and Pl (dashed) curve for 3 (blue),4 (black),and 5 (red) intervals.
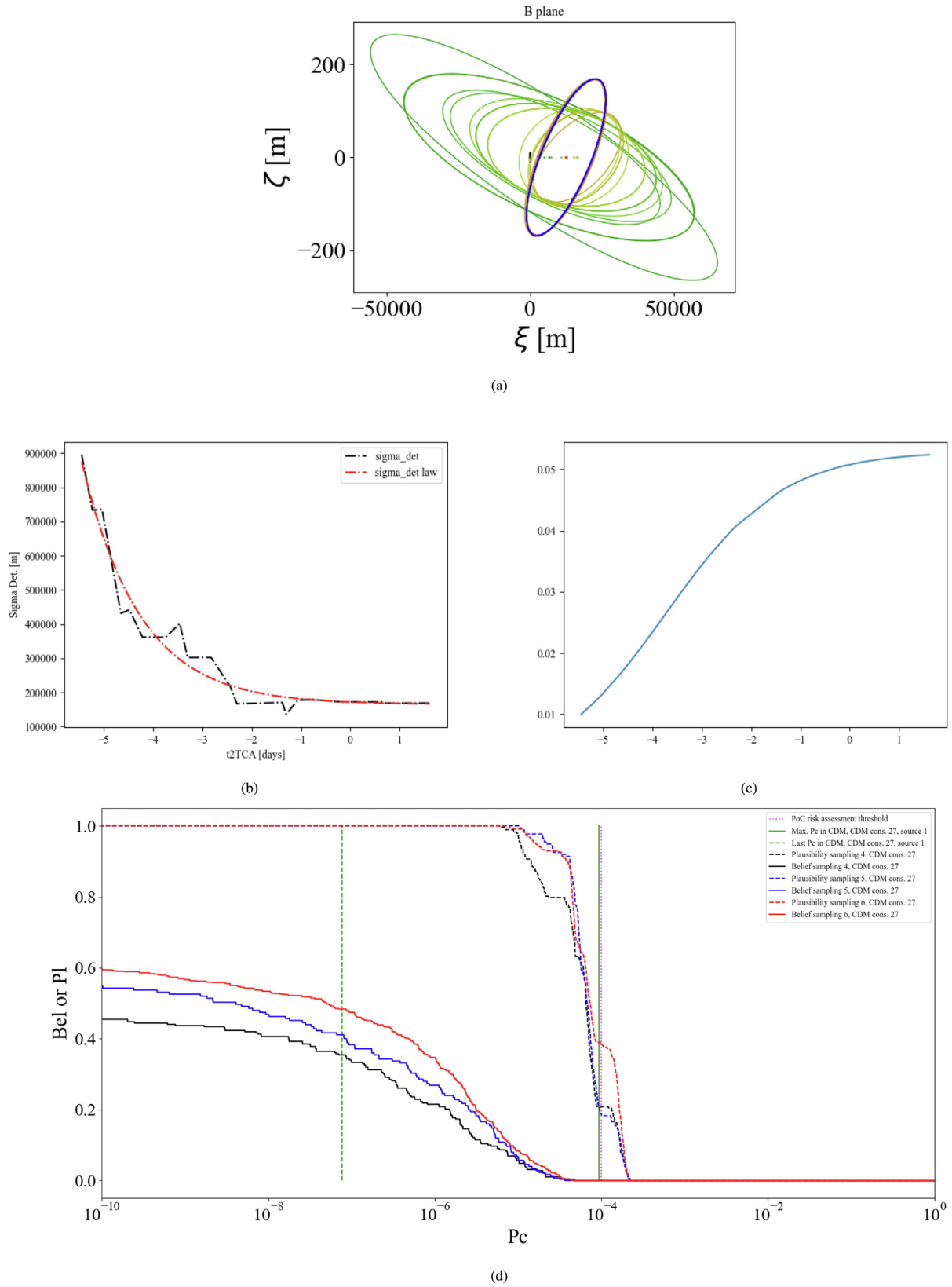
Fig. 44: Sequence for Event #3. Number of CDM 27. (a) Encounter geometry, (b) Covariance determinant (CDM in black, fit in red), (c) Weighting law, (d) Bel (solid) and Pl (dashed) curve for 3 (blue),4 (black),and 5 (red) intervals.
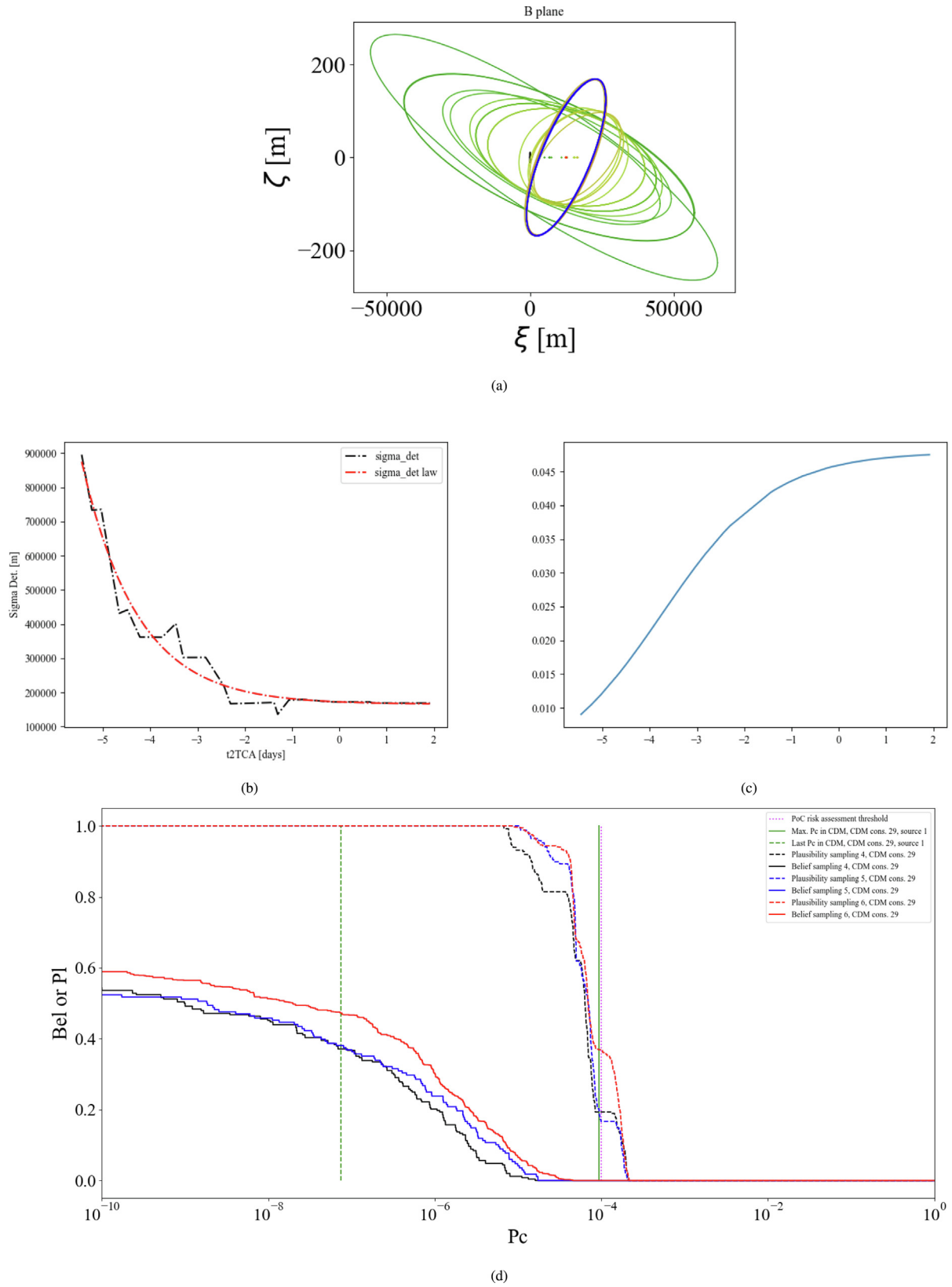
Fig. 45: Sequence for Event #3. Number of CDM 29. (a) Encounter geometry, (b) Covariance determinant (CDM in black, fit in red), (c) Weighting law, (d) Bel (solid) and Pl (dashed) curve for 3 (blue),4 (black),and 5 (red) intervals.
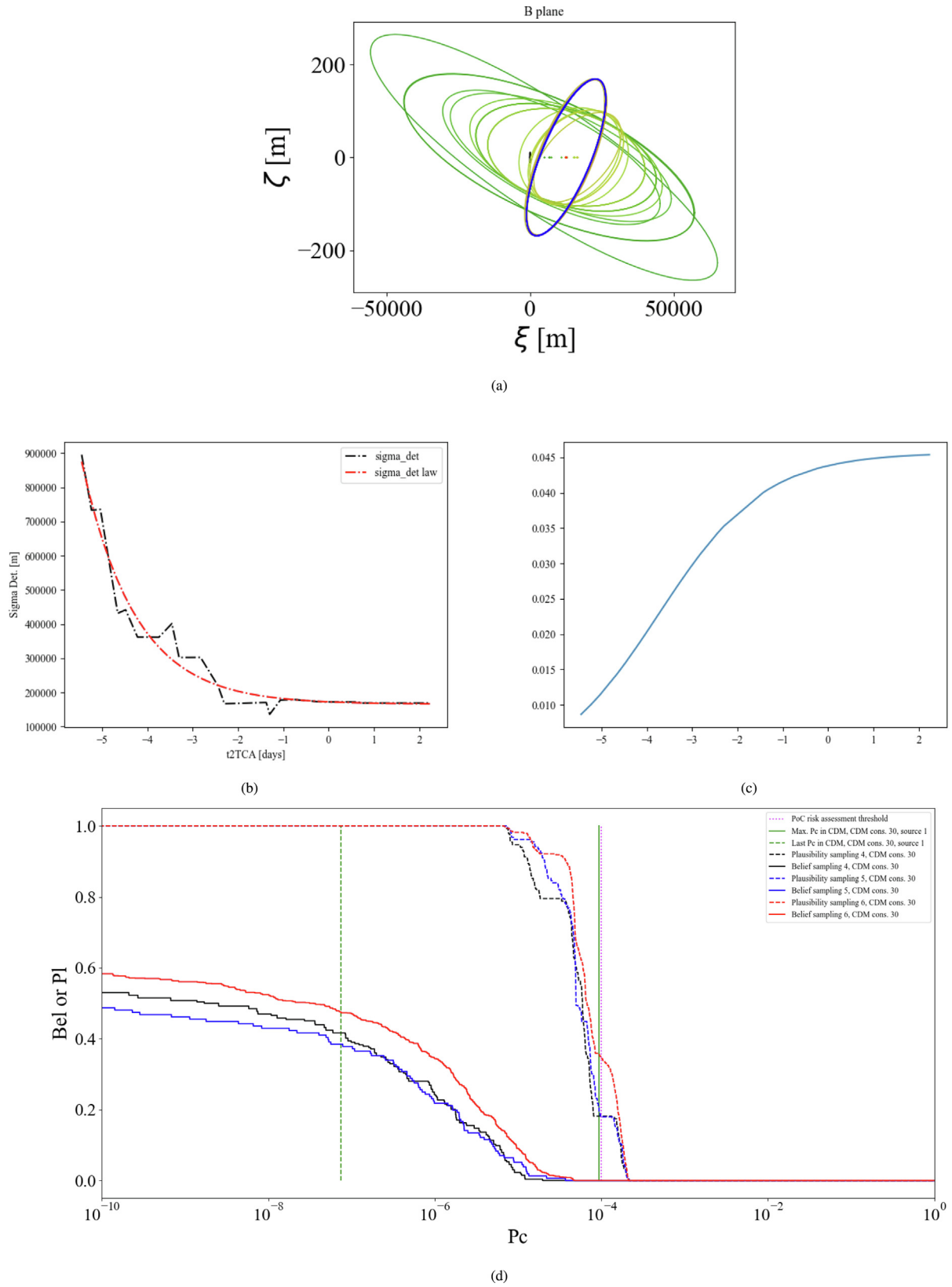
Fig. 46: Sequence for Event #3. Number of CDM 30. (a) Encounter geometry, (b) Covariance determinant (CDM in black, fit in red), (c) Weighting law, (d) Bel (solid) and Pl (dashed) curve for 3 (blue),4 (black),and 5 (red) intervals.

Fig. 47: Sequence for Event #3. Number of CDM 31. (a) Encounter geometry, (b) Covariance determinant (CDM in black, fit in red), (c) Weighting law, (d) Bel (solid) and Pl (dashed) curve for 3 (blue),4 (black),and 5 (red) intervals.
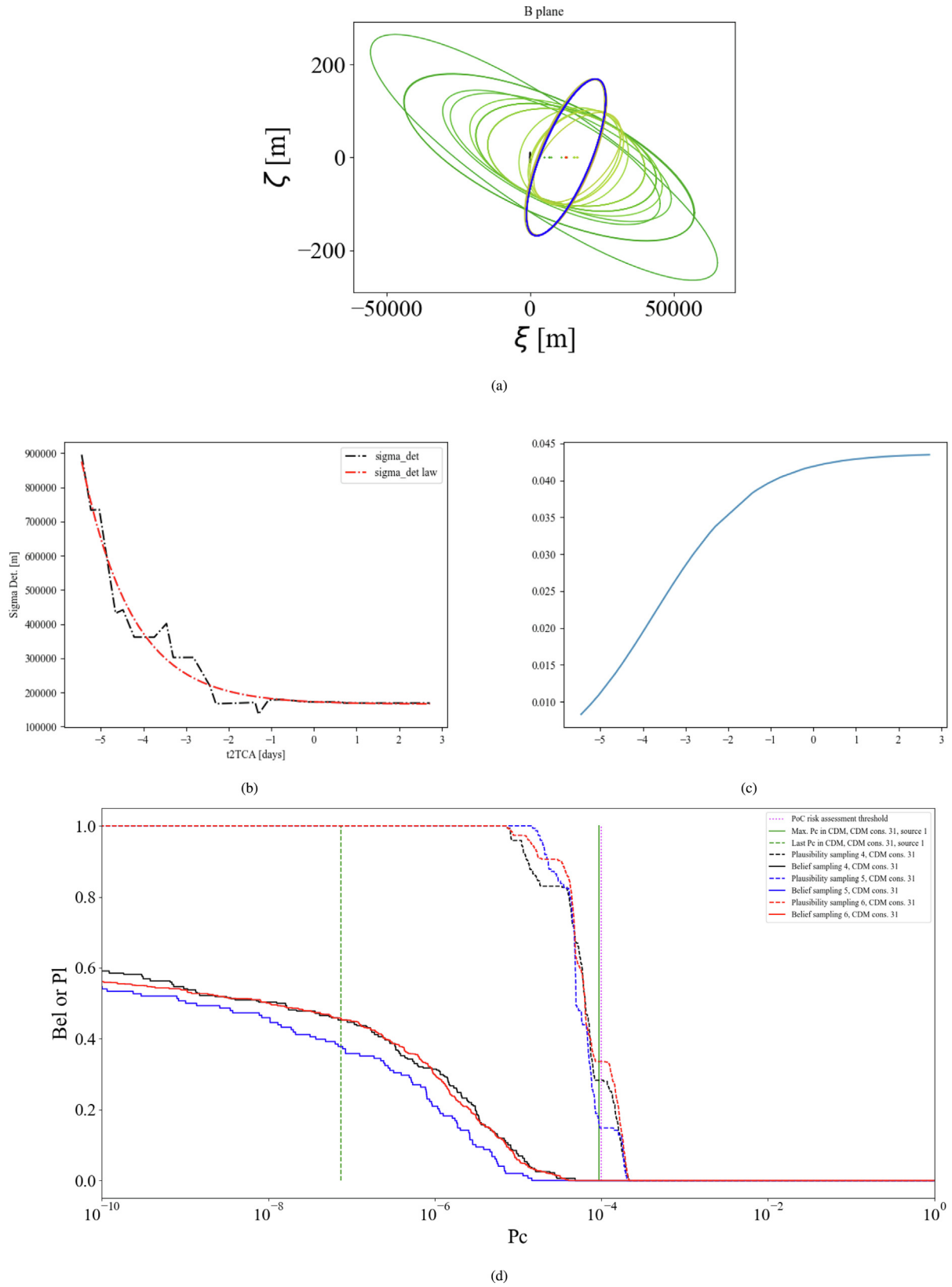
Fig. 48: Sequence for Event #3. Number of CDM 32. (a) Encounter geometry, (b) Covariance determinant (CDM in black, fit in red), (c) Weighting law, (d) Bel (solid) and Pl (dashed) curve for 3 (blue),4 (black),and 5 (red) intervals.
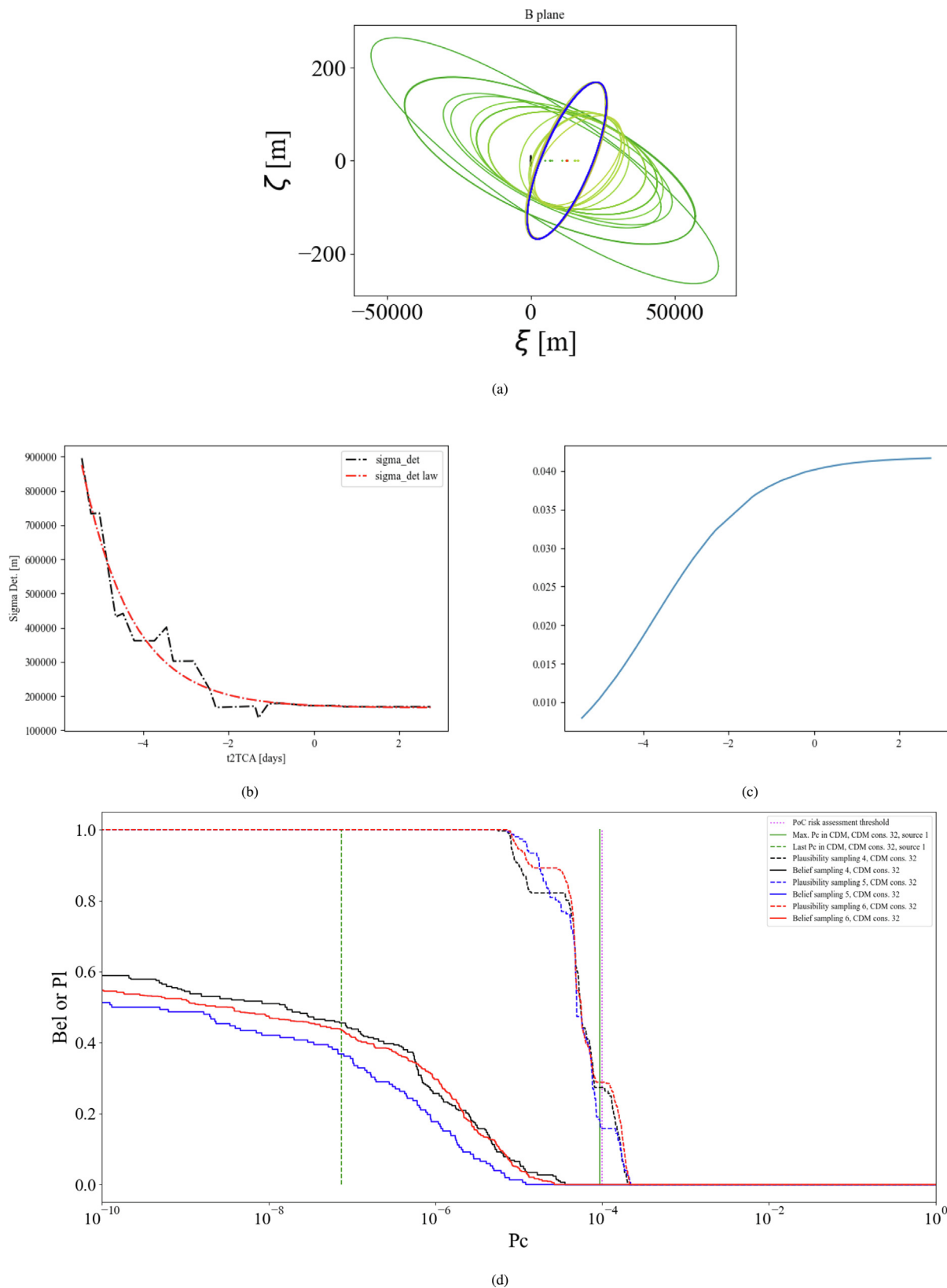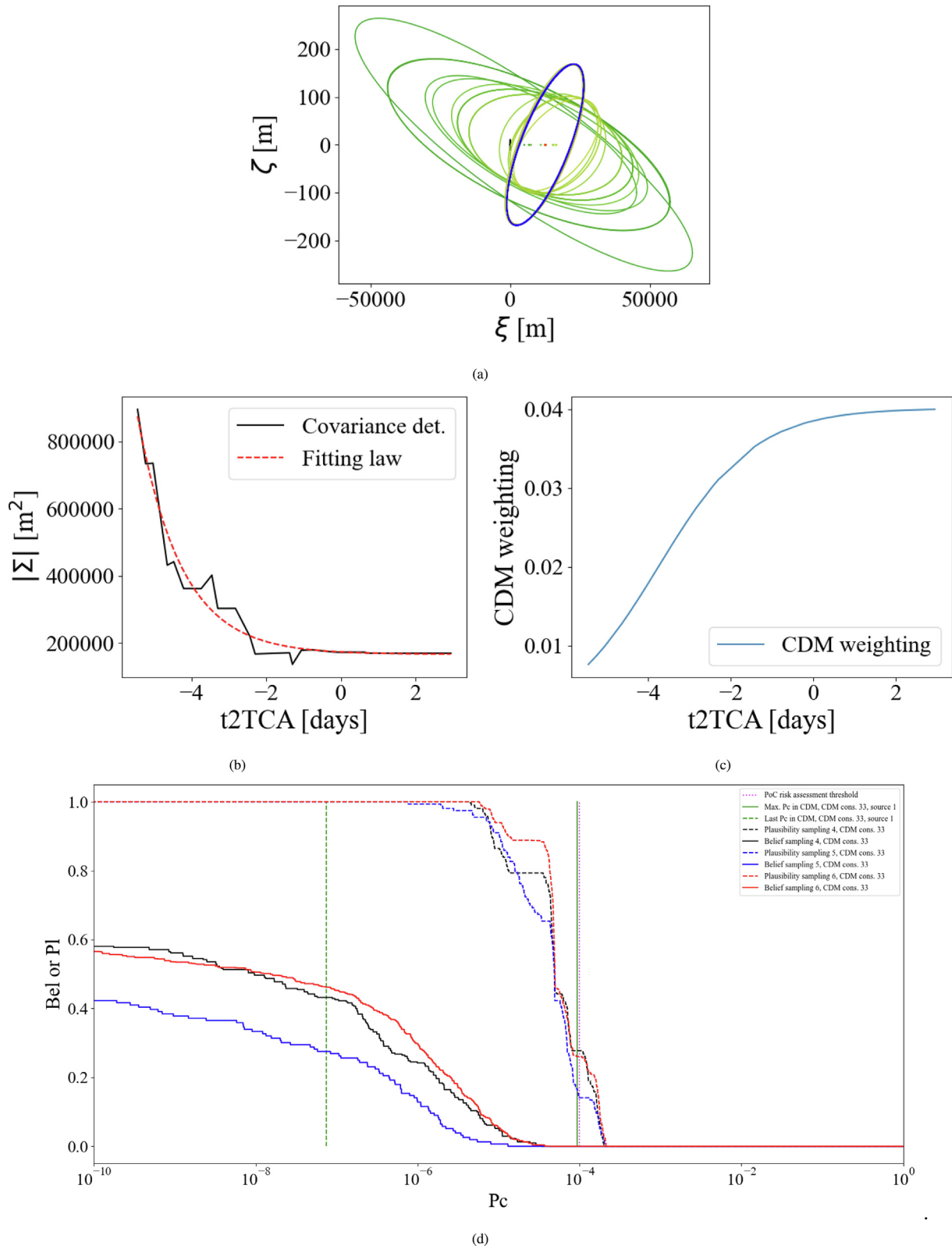
(a)

(b)

(c)

(d)

Fig. 49: Sequence for Event #3. Number of CDM 33. (a) Encounter geometry, (b) Covariance determinant (CDM in black, fit in red), (c) Weighting law, (d) Bel (solid) and Pl (dashed) curve for 3 (blue),4 (black),and 5 (red) intervals.

References

Acciarini, G., Pinto, F., Letizia, F., et al., 2021. Kessler: a machine learning library for spacecraft collision avoidance. In: In 8th European Conference on Space Debris. ESA/ESOC, Darmstadt, Germany.

Aristoff, J.M., Horwood, J.T., Singh, N., et al., 2014. Nonlinear uncertainty propagation in orbital elements and transformation to Cartesian space without loss of realism. In: AAS/AIAA Astrodynamics Specialist Conference. San Diego, CA, US.

Balch, M., Martin, R., Ferson, S., 2019. Satellite conjunction analysis and the false confidence theorem. Proc. Roy. Soc. A: Math., Phys. Eng. Sci. 475 (20180565). https://doi.org/10.1098/rspa.2018.0565.

Caldas, F., Soares, C., Nunes, C., et al., 2023. Conjunction Data Messages for space collision behave as a Poisson process. In: In 31st European Signal Processing Conference (EUSIPCO). Hesinki, Finland.

Cano, A., Pastor, A., Escobar, D., et al., 2023. Covariance determination for improving uncertainty realism in orbit determination and propagation. Adv. Space Res. Space Environment Management and Space Sustainability 72 (7), 2759–2777. https://doi.org/10.1016/j.asr.2022.08.001.

CCSDS (2013). Recommended Standard: CCSDS 508.0-B-1. Recommendation for space data system standards. Conjunction data message. Technical Report CCSDS Washington, DC, USA. https://public.ccsds.org/Pubs/508x0b1e2s.pdf.

Chojnacki, E., Baccou, J., Destercke, D., 2007. Numerical sensitivity and efficiency in the treatment of epistemic and aleatory uncertainty. In: In 5th International Conference on Sensitivity Analysis of Model Output. Budapest, Hungary. https://doi.org/10.1016/j.ijar.2015.07.002.

Delande, E., Houssineau, J., & Jah, M. (2018). A New Representation of uncertainty for data fusion in SSA Detection and Tracking Problems. In 2018 21st International Conference on Information Fusion (FUSION). Cambridge, United Kingdom. DOI: https://doi.org/10.23919/ICIF.2018.8455540.

Dvoretzky, A., Kiefer, J., Wolfowitz, J., 1956. Asymptotic minimax character of the sample distribution function and of the classical multinomial estimator. Annals Math. Stat. 27 (3), 642–669. https://doi.org/10.1214/aoms/1177728174.

ESA (2019). European Space Agency: Kelvins collision avoidance challenge. https://kelvins.esa.int/collision-avoidance-challenge/home/.

Ferson, S., Kreinovich, V., Ginzburg, L., et al., 2023. Constructing probability boxes and Dempster-Shafer structures. Technical Report Sandia National Lab. Albuquerque, NM, United States. https://doi.org/10.2172/809606.

Ferson, S., Kreinovich, V., Hajagos, J., et al., 2007. Experimental uncertainty estimation and statistics for data having interval uncertainty. chapter 4: Descriptive statistics for interval data. In: Sandia National Laboratories (SNL). Princeton University Press, Albuquerque, NM, and Livermore, CA (United States), pp. 28–87. https://doi.org/10.2172/910198.

Ferson, S., Nelsen, R.B., Hajagos, J., et al., 2004. Dependence in probabilistic modeling, Dempster-Shafer theory, and probability bounds analysis. Technical Report Sandia National Lab. United States. https://doi.org/10.2172/919189.

Greco, C., Sánchez, L., Vasile, M., 2021. A robust Bayesian agent for optimal collision avoidance manoeuvre planning. In: In 8th European Conference on Space Debris. ESA/ESOC, Darmstadt, Germany.

Greco, C., Vasile, M., 2021. Robust Bayesian particle filter for space object tracking under severe uncertainty. J. Guid., Control, Dynam. 45 (3), 481–498. https://doi.org/10.2514/1.G006157.

He, Y., Mirzargar, M., Kirby, R.M., 2015. Mixed aleatory and epistemic uncertainty quantification using fuzzy set theory. Int. J. Approximate Reasoning 66, 1–15. https://doi.org/10.1016/j.ijar.2015.07.002.

He, Y., Mirzargar, M., Kirby, R.M., 2017. An efficient reliability analysis approach for structure based on probability and probability box models. Structural and Multidisciplinary Optimization 56, 167–181. https://doi.org/10.1007/s00158-017-1659-7.

Hejduk, L.F.M.M.N.L.S.R., M. (2017). Consideration of collision consequence in satellite conjunction assessment and risk analysis. In International Symposium on Space Flight Dynamics. Matsuyama, Japan.

Helton, J.C., Oberkampf, W.L., Johnson, J.D., 2005. Competing failure risk analysis using evidence theory. Risk Anal. 25 (4), 973–995. https://doi.org/10.1111/j.1539-6924.2005.00644.x.

Laporte, F., 2014a. JAC Software, dedicated to the analysis of conjunction messages. In: SpaceOps 2014 Conference. Pasadena, CA, US. https://doi.org/10.2514/6.2014-1774.

Laporte, F. (2014b). JAC Software, solving conjunction assessment issues. In Proceedings of the Advanced Maui Optical and Space Surveillance Technologies Conference (AMOS). Maui, Hawaii, US.

Merz, K., Braun, V., Benjamin Bastida, V., et al., 2017. Current collision avoidance service by ESA's Space Debris Office. In: In 7th European Conference on Space Debris. ESA/ESOC, Darmstadt, Germany.

Newman, L.K., Mashiku, A.K., Hejduk, M.D., et al., 2019. NASA Conjunction Assessment Risk Analysis (CARA) updated requirements architecture. In: AAS/AIAA Astrodynamics Specialist Conference. Portland, Maine, US.

Pinto, F., Acciarini, G., Metz, S. et al. (2020). Towards automated satellite conjunction management with bayesian deep learning. In AI for Earth Sciences Workshop at NeurIPS. URL: https://nips.cc/virtual/2020/public/workshop_16105.html.

Sánchez, L., Vasile, M., 2021. Constrained optimal collision avoidance manoeuvre allocation under uncertainty for subsequent conjunction events. In: In 72nd International Astronautical Congress (IAC). Dubai, EAU, 25–29 October.

Serra, R., Arzelier, D., Joldes, M., et al., 2016. Fast and accurate computation of orbital collision probability for short-term encounters. J. Guid., Control, Dynam. 39, 1–13. https://doi.org/10.2514/1.G001353.

Shafer, G., 1976. A Mathematical theory of evidence, 1st ed. Princeton University Press, Princeton, NJ, ISBN 9780691100425.

Stroe, I.F., Stanculescu, A.D., Ilioaica, P.B., et al., 2021. AUTOCA autonomous collision avoidance system. In: In 8th European Conference on Space Debris. ESA/ESOC, Darmstadt, Germany.

Sánchez, L., Stevenson, E., Vasile, M., et al., 2022. An intelligent system for robust decision-making in the all-vs-all conjunction screening problem. In: In 3rd IAA Conference on Space Situational Awareness (ICSSA). Tres Cantos. Madrid, Spain.

Sánchez, L., Vasile, M., 2021. On the use of machine learning and evidence theory to improve collision risk management. Acta Astronaut. 181, 694–706. https://doi.org/10.1016/j.actaastro.2020.08.004.

Sánchez, L., & Vasile, M. (2022). Intelligent agent for decision-making support and collision avoidance manoeuvre design on space traffic management. Advances in Space Research. In press, doi: 10.1016/j.asr.2022.09.023.

Tardioli, C., Vasile, M., 2015. Collision and re-entry analysis under aleatory and epistemic uncertainty. Advances in Astronautical Sciences 156, 4205–4220.

Uriot, T., Izzo, D., Simões, L.F., et al., 2022. Spacecraft collision avoidance challenge: design and results of a machine learning competition. Astrodynamics 6 (2), 121–140. https://doi.org/10.1007/s42064-021-0101-5.